NAVAL POSTGRADUATE SCHOOL

MONTEREY, CALIFORNIA

THESIS

VARIABLE SPEED HYDRODYNAMIC MODEL OF AN AUV UTILIZING CROSS TUNNEL THRUSTERS

by

Ian Taylor

September 2017

Thesis Advisor:	Douglas Horner
Second Reader:	Sean Kragelund

THIS PAGE INTENTIONALLY LEFT BLANK

REPORT DOCUMENTATION PAGE

Form Approved OMB No. 0704–0188

1. AGENCY USE ONLY *(Leave Blank)*	2. REPORT DATE	3. REPORT TYPE AND DATES COVERED
	September 2017	Master's Thesis 10-01-2015 to 09-21-2017

4. TITLE AND SUBTITLE

VARIABLE SPEED HYDRODYNAMIC MODEL OF AN AUV UTILIZING CROSS TUNNEL THRUSTERS

5. FUNDING NUMBERS

6. AUTHOR(S)

Ian Taylor

7. PERFORMING ORGANIZATION NAME(S) AND ADDRESS(ES)

Naval Postgraduate School
Monterey, CA 93943

8. PERFORMING ORGANIZATION REPORT NUMBER

9. SPONSORING / MONITORING AGENCY NAME(S) AND ADDRESS(ES)

N/A

10. SPONSORING / MONITORING AGENCY REPORT NUMBER

11. SUPPLEMENTARY NOTES

The views expressed in this document are those of the author and do not reflect the official policy or position of the Department of Defense or the U.S. Government. IRB Protocol Number: N/A.

12a. DISTRIBUTION / AVAILABILITY STATEMENT

Approved for public release. Distribution is unlimited.

12b. DISTRIBUTION CODE

13. ABSTRACT *(maximum 200 words)*

This research presents the first accurate three and six Degree of Freedom (DOF) models of the small diameter REMUS 100 with cross-tunnel thrusters (CTT). These are the first known hydrodynamic models to explicitly consider the impact on navigation of forward and aft CTTs. The models presented in this research provide an alternative method to test new docking strategies and provide a better understanding of a torpedo-shaped Autonomous Underwater Vehicle's (AUV) dynamics.

Future AUV missions will have AUVs operating in cluttered and dynamic areas using CTTs. This sort of operating environment requires torpedo-shaped vehicles, such as the REMUS 100, to maneuver efficiently at slow speeds. The variable-speed CTT models in this thesis were originally developed to improve the understanding of vehicle control during docking missions. Sub-sea docking stations provide AUVs the ability to remain on station for extended periods of time. The extended missions allowed by an AUV with docking capabilities greatly improve and increase AUVs' civilian and military applications by decreasing operational costs and increasing on-station time.

This thesis provides the first variable speed models with CTTs that can be used to develop and critique new docking strategies. Installing and extracting a docking system for testing is time consuming and expensive. The models created are valuable because they save time and resources. These models also provide a cost-effective method for validating control strategies and vehicle dynamics. This thesis provides experimental verification of the new models and a discussion of the models' capabilities and limitations.

14. SUBJECT TERMS	15. NUMBER OF PAGES
Autonomous Underwater Vehicles (AUV), Terminal Homing Docking, REMUS, Cross-Tunnel Thrusters (CTT), Hydrodynamic Coefficients, Hydrodynamic Model, Variable Speed Model	119
	16. PRICE CODE

17. SECURITY CLASSIFICATION OF REPORT	18. SECURITY CLASSIFICATION OF THIS PAGE	19. SECURITY CLASSIFICATION OF ABSTRACT	20. LIMITATION OF ABSTRACT
Unclassified	Unclassified	Unclassified	UU

NSN 7540-01-280-5500

Standard Form 298 (Rev. 2–89)
Prescribed by ANSI Std. 239–18

THIS PAGE INTENTIONALLY LEFT BLANK

Approved for public release. Distribution is unlimited.

VARIABLE SPEED HYDRODYNAMIC MODEL OF AN AUV UTILIZING CROSS TUNNEL THRUSTERS

Ian Taylor
Lieutenant, United States Navy
B.S., University of Texas, 2009

Submitted in partial fulfillment of the
requirements for the degree of

MASTER OF SCIENCE IN MECHANICAL ENGINEERING

from the

NAVAL POSTGRADUATE SCHOOL
September 2017

Approved by: Douglas Horner
Thesis Advisor

Sean Kragelund
Second Reader

Garth Hobson
Chair, Department of Mechanical and Aerospace Engineering

THIS PAGE INTENTIONALLY LEFT BLANK

ABSTRACT

This research presents the first accurate three and six Degree of Freedom (DOF) models of the small diameter REMUS 100 with cross-tunnel thrusters (CTT). These are the first known hydrodynamic models to explicitly consider the impact on navigation of forward and aft CTTs. The models presented in this research provide an alternative method to test new docking strategies and provide a better understanding of a torpedo-shaped Autonomous Underwater Vehicle's (AUV) dynamics.

Future AUV missions will have AUVs operating in cluttered and dynamic areas using CTTs. This sort of operating environment requires torpedo-shaped vehicles, such as the REMUS 100, to maneuver efficiently at slow speeds. The variable-speed CTT models in this thesis were originally developed to improve the understanding of vehicle control during docking missions. Sub-sea docking stations provide AUVs the ability to remain on station for extended periods of time. The extended missions allowed by an AUV with docking capabilities greatly improve and increase AUVs' civilian and military applications by decreasing operational costs and increasing on-station time.

This thesis provides the first variable speed models with CTTs that can be used to develop and critique new docking strategies. Installing and extracting a docking system for testing is time consuming and expensive. The models created are valuable because they save time and resources. These models also provide a cost-effective method for validating control strategies and vehicle dynamics. This thesis provides experimental verification of the new models and a discussion of the models' capabilities and limitations.

THIS PAGE INTENTIONALLY LEFT BLANK

Table of Contents

List of Figures

THIS PAGE INTENTIONALLY LEFT BLANK

List of Tables

List of Acronyms and Abbreviations

3DOF	Three Degrees of Freedom
6DOF	Six Degrees Of Freedom
ADCP	Acoustic Doppler Current Profiler
AUV	Autonomous Underwater Vehicle
CAVR	Center for Autonomous Vehicle Research
CTT	Cross Tunnel Thrusters
DOF	Degree Of Freedom
GPS	Global Positioning System
HCTT	Horizontal Cross Tunnel Thrusters
INS	Inertial Navigation System
KF	Kalman Filter
LBL	Long Baseline
MBARI	Monterey Bay Aquarium Research Institute
NED	North East Down
NPS	Naval Postgraduate School
ODE	Ordinary Differential Equation
PUC	Positional Uncertainty
REMUS	Remote Environmental Measuring Units
RPM	Rotations Per Minute

USBL Ultra-short Baseline

UUV Unmanned Underwater Vehicle

VCTT Vertical Cross Tunnel Thrusters

WHOI Woods Hole Oceanographic Institute

Acknowledgments

First, I would like to thank my advisor, Dr. Douglas Horner, for mentoring me through the thesis process here at NPS. Thank you also to Sean Kragelund and Aurelio Monarrez for your help and guidance over the last year. Last, but certainly not least, I would like to thank my wife, Stevie, for providing her support. I could not have done it without all of you!

THIS PAGE INTENTIONALLY LEFT BLANK

CHAPTER 1:
Introduction

1.1 Motivation

Autonomous Underwater Vehicles (AUV) represent a paradigm shift in U.S. Naval underwater operations. The world's oceans represent an extreme environment that makes the use of autonomous systems highly enticing for all actors that strive to perform operations in its depths. Rising autonomous systems such as the Remote Environmental Measuring Unit (REMUS) 100 vehicle represents not only a feat of engineering prowess but a modern platform that can further human exploration and warfare. By furthering the capabilities of AUVs, such as the REMUS 100, the Naval Postgraduate School (NPS) furthers the scope of modern science and engineering, as well as the Navy's maritime capacity.

Work on the REMUS 100 vehicle and its predecessors has been ongoing at civilian and military institutions around the globe for the past 20 years. There has been a multitude of research into the capabilities of the REMUS vehicle and in producing a simulated model that mimics the vehicle's motion in the underwater environment with high fidelity. Docking a REMUS vehicle safely and effectively has been a coveted goal for all parties who operate these vehicles. Docking an AUV provides longer on station times and reduces human interaction with the vehicle, which in turn increases mission effectiveness and operational costs. Research conducted on previous REMUS variants, which had no cross tunnel thruster (CTT) capabilities, proved that the vehicle lacked the controllability at low speeds to safely and effectively dock the vehicle in a subsea environment. Kongsberg, REMUS's production company, has released a REMUS variant that now implements CTTs in the lateral and vertical directions to sustain control of the REMUS vehicle at low speeds. A picture of the NPS Center for Autonomous Vehicle Research (CAVR) REMUS 100 with CTTs can be seen in Figure 1.1.

Figure 1.1. Naval Postgraduate School Center for Autonomous Vehicle Research (CAVR) REMUS 100 Vehicle with CTTs. Source: [1].

The REMUS vehicles used in the CAVR have two vertical and two horizontal CTTs. The four CTTs generate force on the REMUS using a small propeller at one end of their associated tunnels shown in Figure 1.2. The propellers used by the CTTs can operate in both directions, however there is a dominant direction of operation where the generated force is slightly greater than in the opposite direction.

The addition of vertical and lateral CTTs to the physical vehicle presents an opportunity for new hydrodynamic modeling for small diameter AUVs. Previous models did not provide a high-fidelity model of the vehicle's motion during variable speed operations. The reason for the lack of a variable speed model of the REMUS vehicle was twofold:

1. In previous REMUS variants (no CTTs), the vehicle needed to maintain higher speeds to maintain control of the vehicle's pose. At higher speeds, the control surfaces of the REMUS vehicle are effective; allowing for vehicle controllability and system modeling.
2. The software available for the development of a high-fidelity REMUS model that handled variable speeds, especially lower speeds where the vehicle is difficult to control and hydrodynamic behavior is non-linear, was not available during the creation of the original simulated REMUS MATLAB models.

Figure 1.2. Location of CTTs on a REMUS Vehicle. Source: [1].

This research presents new models of the REMUS vehicle that simulate it's behavior at lower speeds while utilizing CTTs. These models provide the ability to simulate a REMUS vehicle performing low speed surveys, CTT maneuvering in confined areas, and hover missions at optimal depths for tactical/oceanographic sonar data collection. Also, the models presented in this paper bring the goal of reliable autonomous docking of a REMUS AUV closer to realization. Using these models to simulate missions prior to deploying the REMUS vehicle will provide insight to the vehicle's capabilities, limitations, and efficient utilization.

1.2 Problem Description

Undersea docking stations provide AUVs the ability to remain on station for extended periods of time. Extended AUV missions greatly improve and increase widespread applications for these vehicles. However, docking stations are not currently in wide spread use due to the challenges of consistently and safely docking an AUV. Before consistent docking can occur, an accurate hydrodynamic model that can simulate an AUV operating at various speeds with CTTs should be produced. This model can provide an accurate simulation of a docking maneuver and increase the spectrum of control options available to the vehicle. CTTs allow an AUV to hover and perform precise movements at slow speeds. Variable speed modeling and CTT functionality is investigated and analyzed in this research. This thesis furthers the understanding of AUV hydrodynamic behavior during future docking missions. The added capability provided by CTTs will insure damage to both the AUV and the docking station can be avoided.

Several docking missions were attempted in Monterey Bay by the Center for Autonomous Vehicle Research (CAVR). These missions used a REMUS variant that did not have a CTT capability enabled. The REMUS vehicle was required to maintain a 2-3 knot speed when docking to ensure control over the vehicle's dynamics. At the required speed, the docking attempts caused damage to both the vehicle and the docking station, seen in Figure 1.3, and were largely unsuccessful. With the results of these missions, it was determined that a CTT capability and an accurate hydrodynamic model of the REMUS vehicle with this new CTT capability could be used to more reliably dock a REMUS vehicle. The new models provide a more concrete understanding of the capabilities of a REMUS vehicle with CTTs. They can also be used to better examine the impact of the environment to the vehicle's behavior and help in determining the best control strategy for a docking mission.

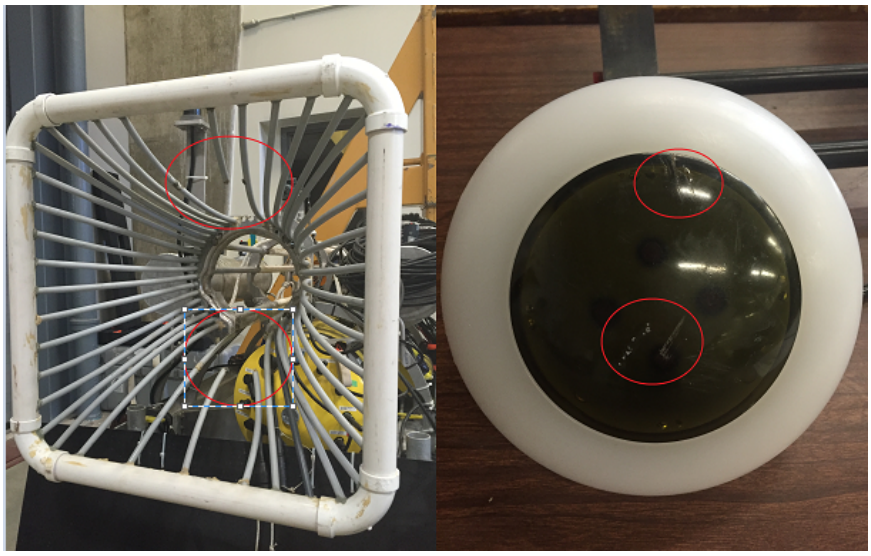

Figure 1.3. Damage Caused by Unsuccessful Docking Attempts with the REMUS at 2-3 Knots. Damage Indicated by Red Circles. Source: [1].

To more reliably dock an AUV with CTTs, accurate hydrodynamic models were developed. These models allow for accurate simulation and control of the REMUS vehicle. Accurate models can be used to help determine optimal trajectories and vehicle limitations under various oceanographic conditions. The models presented in this research are:

1. a three degree of freedom (3DOF) model which represents a REMUS vehicle's behavior when operating two vertical CTTs while at various speeds,
2. a six degree of freedom (6DOF) model which simulates a vehicle with vertical and horizontal CTTs while at various speeds.

This thesis also provides experimental verification of the new 3DOF and 6DOF models and a discussion of their capabilities and limitations. It is distinctive from previous research because, while previous work on the REMUS presented hydrodynamic models of the vehicle, these models could not accurately reflect the REMUS vehicle's hydrodynamic behaviors while operating at variable velocities and while utilizing CTTs. The new hydrodynamic model presented in this thesis is important for accurately representing a vehicle transitioning into a hover mode as it slowly approaches a docking station.

The current docking techniques have an AUV approaching the terminal objective using an

Ultra Short Baseline (USBL) transponder to determine range and bearing to an acoustic transponder mounted on the docking station. Due to a lack of attitude data and low periodicity (approximately 1Hz), the USBL does not provide the required resolution of position at close range which are necessary for the final portion of a docking maneuver. Docking performance could be improved if control algorithms utilize different sensors and actuators for precise alignment and positioning at close range, namely a forward-looking camera and CTTs. At close range, the REMUS's control sensor could transition from USBL to a forward-looking camera for final alignment and positioning. A combination of the main aft thruster and CTTs may be used to position the AUV in front of the docking station. An accurate hydrodynamic model that can represent the vehicle's motion at various speeds and with CTTs is needed to develop control algorithms that allow a REMUS vehicle to execute a precise, slow-speed approach to a docking station.

The 3DOF model presented in this thesis focuses on the vertical plane. This research investigates the relationships between hydrodynamic coefficients and control surface forces with the vehicle's forward velocity, and the relationship between propeller forces and propeller speed (RPM). By coalescing previous research on AUV behavior into 3DOF and 6DOF variable speed models, high-fidelity simulations of a REMUS AUV were demonstrated.

1.3 Literature Review

Work on AUV hydrodynamic models has been ongoing at civilian and military institutions around the globe for over 20 years [2]. There has been a multitude of research into producing a model that simulates the REMUS vehicle's motion in the underwater environment. Previous research developed and investigated the following topics:

1. hydrodynamic models that handle single speed dynamics of a REMUS AUV,
2. reduction of cross tunnel thruster efficiency as vehicle speed increases,
3. identification and verification of an AUVs' hydrodynamic coefficients,
4. accurate simulation of the forces generated by an AUV's propeller at various RPMs,
5. accurate simulation of the forces on the control surfaces of an AUV at certain speeds.

1.3.1 Hydrodynamic Models

There have been several researchers that have developed models of undersea vehicles. [2] is a known expert in this field of study and his work developed an accurate and widely accepted six degree of freedom model for undersea vehicles. Many of the equations used to develop the three degree of freedom model presented in this paper are simplified equations from the six degree of freedom model developed by [2]. CTT research has been conducted by [1], [3], and [4]. AUV modeling research was pursued by [4], [5], and [6]. All these researchers and their work have contributed or influenced the models presented in this thesis.

The hydrodynamic coefficients used in this thesis are adapted from the coefficients developed by [7] and the coefficients that were further developed by other researchers. [8] created models for a REMUS 100 vehicle in a standard configuration, a REMUS with no CTTs. In [1] and [9], hydrodynamic coefficients were further tuned to more accurately reflect a REMUS configuration used by the CAVR. The CAVR owns REMUS vehicles that are configured to utilize cross tunnel thrusters and house a USBL in the end cap of the vehicle. AUV thruster behavior and controllability for a three-state thruster model was analyzed by [10] and applied to the REMUS 100 by [8], and then verified by [1]. Further work on reduced cross tunnel thruster efficiency as an AUV speed increased was published by [3], which was built upon an earlier study by [11], who developed a cross tunnel thruster behavioral model at zero speed of advance in 2007.

None of the prior AUV hydrodynamic models accurately simulated REMUS behavior at various speeds while utilizing CTTs. The aim of this thesis was to build off the previous work conducted by these researchers and create a hydrodynamic model that could accurately reflect an AUV's behavior in the vertical channel at various speeds. The 3DOF and 6DOF models presented account for reduced control surface efficiency at low speeds and build an accurate representation of a REMUS AUV's behavior while operating at slow/variable speeds with CTTs.

1.4 Thesis Organization

The thesis is organized by the following chapters:

1. Developing the 3DOF Model for a REMUS - Provides the mathematical derivation

of the equations of motion for a 3DOF Model.

2. Programming the REMUS 3DOF Model- An overview of the programming required to implement the 3DOF equations of motion for constructing an accurate model of a REMUS vehicle.
3. Verification of the 3DOF Model - Results from experiments that were conducted in Monterey Bay, CA used to test and validate the 3DOF Model.
4. Developing the 6DOF Model for a REMUS- Provides the mathematical derivation of the equations of motion for a 6DOF Model.
5. Programming the REMUS 6DOF Model - An overview of the programming required to implement the 6DOF equations of motion for constructing an accurate and more detailed model of a REMUS vehicle. This chapter shows the added complexity of modeling extra degrees of freedom.
6. Verification of the 6DOF Model - Results from experiments that were conducted in Monterey Bay, CA used to test and validate the 6DOF Model.
7. REMUS Controller Design - A discussion of the controllers used in the 3DOF and 6DOF models and the considerations that went into their design.
8. Behavior and Significance of the Coefficient of Drag (Cd) in a Variable Speed Hydrodynamic Model - Provides insight and modeling considerations specifically regarding the impact of slow speed operations
9. Conclusion and Future Work- An exploration of the future work and aspirations that the 3DOF and 6DOF models have revealed.

THIS PAGE INTENTIONALLY LEFT BLANK

CHAPTER 2:
3DOF Model Development

The focus of this chapter is to develop a vertical channel 3DOF model of a REMUS 100 AUV with CTTs enabled. A vertical channel model can simulate the vehicle's control in the Z-direction. Due to the constant buoyancy force acting on the vehicle, CTTs must be utilized to maintain depth control at slow speeds. The model developed provides insight into the behavior of vehicle at slow speeds and illuminates possible challenges to depth control while maneuvering a vehicle into a docking station.

A six degree of freedom (6DOF) model of the REMUS 100 was originally developed by [7] and refined by [8]. The 3DOF model in this paper is a simplified version of these 6DOF models. However, the previous 6DOF models did not simulate a REMUS 100 vehicle at various speeds and utilizing cross-tunnel thrusters. The 3DOF model developed in this thesis simulates the behavior of the REMUS 100 vehicle at various speeds and utilizing cross-tunnel thrusters. All REMUS 100 mathematical models have been developed using AUV equations of motion and kinematics developed by [2] and [12].

2.1 3DOF Model Design Considerations

The aim of this paper is to create a "useful" variable speed model of the new REMUS 100 variant that utilizes cross-tunnel thrusters. Even when limiting the model to heave, surge, and pitch, the 3DOF model is able to show critical vehicle behavior such as the speed at which cross-tunnel thrusters need to be utilized to maintain vehicle depth. The 3DOF model significantly reduces processing time to run a simulated mission allowing for faster tuning and comparison with data collected in the field. Also, a 3DOF model can accurately reflect situations in which the REMUS vehicle maintains its depth/altitude when implementing cross-tunnel thrusters. The model therefore allows for fast and accurate assessment of possible docking missions. External forces in the Z-direction are usually the most limiting factor for a successful autonomous docking of an AUV. The model provides the first step toward development of a variable speed cross-tunnel thruster 6DOF model.

The following assumtions for the 3DOF model were adapted from [7] and [8]:

1. No external current is acting on the vehicle. The modeled vehicle is operating in a benign operating environment. This assures that the only forces acting on the vehicle are from itself and the fluid interaction with the water.
2. No vehicle interaction with waves, external structures, or the sea floor is occurring. This assumption further defines benign operating environment and acknowledges that any experiments conducted in the field may have these factors acting on the vehicle.
3. Hydrodynamic coefficients of the model change only due to changes in the vehicle's velocity. Hydrodynamic coefficients may change due to salinity, pressure, or temperature of the water. This assumption is again enforcing the benign operating environment for modeling.
4. The vehicle's center of gravity is aligned with the center of buoyancy when the vehicle is at trim. This may not be the case with the real world REMUS, especially if the payload and ballasting of the vehicle changes. Often times the center of gravity is offset from the center of buoyancy during normal operations. This offset will induce a moment in the vehicle that will effect its pitch behavior. Also, if the center of gravity is offset from the center line, the vehicles roll behavior may be effected.
5. The vehicle has a slight positive buoyancy. Prior to any operation, the AUV is checked to ensure a slight positive buoyancy. The inherent positive buoyancy ensures that if the vehicle should loss power while submerged, it will return to the surface so that it may be recovered.
6. The vehicle is a rigid body with constant mass. This assumes that the flex inherent to the vehicle's construction and length has a minimal impact on the behavior and control of the vehicle.
7. The rudder and dive fins will not stall at any angle of attack. If the rudder and dive fins stall, the force equations used to describe forces acting on these control surfaces are no longer valid. A stall should not occur for the normal spectrum of vehicle operating velocities and the maximum angle of attack for these control surfaces.
8. The assuption that speed of the vehicle does not impact CTT efficiency is necessary due to the lack of information on how speed impacts a REMUS's CTTs. However, there has been research that has proven that vehicle velocity does impact CTT efficiency [3]. The force equations used in this research's models were developed by [1]. The CTT equations for the REMUS were created by measuring the force output of CTTs at various RPMs. These force measurements were recorded on a near stationary

vehicle. To use these equations to provide a direct force input to the equations of motion, the vehicle's velocity must be assumed to have a negligible impact on CTT efficiency.

9. The forces acting on the vehicle are limited to inertial, gravitational, hydrostatic, propulsive, lift, CTT, and hydrodynamic forces. This is a catch-all assumption for eliminating all other extraneous forces from impacting the model.
10. Coupled components of the equations of motion from sway, roll, and yaw are negligible in the 3DOF model. This allows for the simplifying of the REMUS vehicle's equations of motion and converts a 6DOF REMUS vehicle into a 3DOF REMUS vehicle simulation. In the full 6DOF model presented in Chapter 5, this assumption is no longer valid.

These assumptions provide a standard test setting where environmental and external factors, other than hydrodynamic, will have a negligible impact on the model.

2.2 Reference Frame and Degrees of Freedom

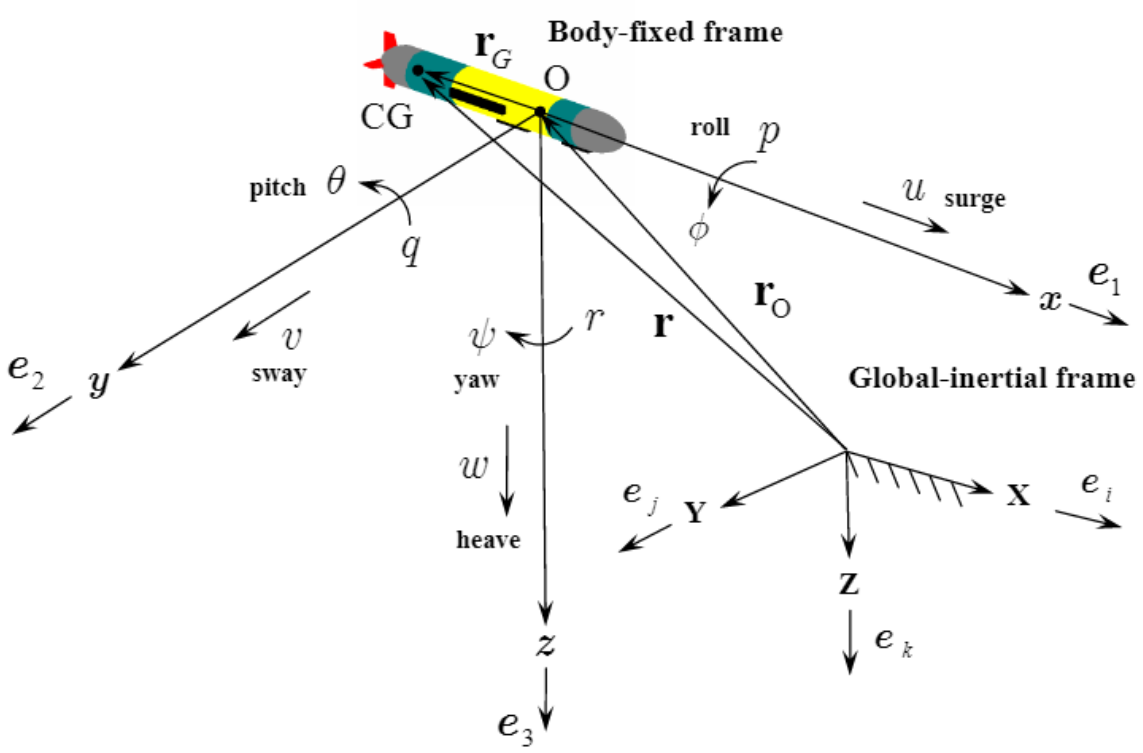

Figure 2.1. Reference Frame and Degrees of Freedom of a REMUS AUV. Source: [8].

Figure 2.1 shows the reference frames normally utilized when modeling an AUV. When representing the position, orientation, and motion of an AUV, two orthogonal reference frames are required. The first reference frame is the global-inertial frame which is a fixed frame with respect to the center of the earth. The second reference frame is a body-fixed frame with an origin fixed at the vehicle's center of buoyancy with the principle axes aligned with vehicle motion. This body reference frame allows for a more intuitive derivation of equations of motion. Both reference frames are right hand reference frames oriented in the North, East, and Down directions.

2.3 Equations of Motion

The equations of motion shown in this paper are provided for reference and to show the different components of each force and moment considered in the REMUS 100 3DOF model. For an in-depth derivation of these equations, please reference [2] and [12].

The equations derived in this section are developed in the body reference frame using Newton's second law and Euler's rigid body equations:

$$\sum F = m * a \tag{2.1}$$

$$\sum M = I * \omega \tag{2.2}$$

These forces and moments are a summation of hydrostatic (HS), added mass (A), hydrodynamic (HD), lift (L), CTT (CTT) and propeller (P) components.

$$\sum F = F_{HS} + F_A + F_{HD} + F_L + F_{CTT} + F_P \tag{2.3}$$

$$\sum M = M_{HS} + M_A + M_{HD} + M_L + M_{CTT} + M_P \tag{2.4}$$

With these equations, forces and moments for a 3DOF and 6DOF model of a AUV with CTTs can be derived.

Surge Equation

Table 2.1. Surge Equation Hydrodynamic Coefficients

Coefficients	Description	Value	Units
$X_{u\|u\|}$	Axial Flow Drag Coefficient	-12.4759	$\frac{kg}{m}$
$X_{\dot{u}}$	Added Mass Coefficient	-0.930	kg

The following equations derive the summation of forces acting in the X-direction on the vehicle. These forces are a summation of hydrostatic, added mass, hydrodynamic, and propeller forces.

$$\sum X = X_{HS} + X_A + X_{HD} + X_P \tag{2.5}$$

$$\sum X = -(W - B)\sin(\theta) + X_{u|u|}u|u| + X_{\dot{u}}\dot{u} + (1 - \tau_p)T_{n|n|}n|n| \tag{2.6}$$

The propeller force is simplified to a single variable, $F_{Propeller}$, which is a function of propeller RPM.

$$(1 - \tau_p)T_{n|n|}n|n| = F_{Propeller} \tag{2.7}$$

The alternate force equation is now:

$$\sum X = -(W - B)sin(\theta) + X_{u|u|}u|u| + X_{\dot{u}}\dot{u} + F_{Propeller} \tag{2.8}$$

Heave Equation

Table 2.2. Heave Equation Hydrodynamic Coefficients

Coefficients	Description	Value	Units
Z_{uw}	Body Lift Force and Fin Lift Coefficient	−28.6	$\frac{kg}{m}$
$Z_{w\|w\|}$	Cross Flow Drag Coefficient	−185.621	$\frac{kg}{m}$
$Z_{uu\delta_s}$	Fin Lift Force Coefficient	−21.37	$\frac{kg}{m \cdot rad}$

The following equations derive the summation of forces acting in the Z-direction on the vehicle. These forces are a summation of hydrostatic, added mass, hydrodynamic, lift, and CTT forces.

$$\sum Z = Z_{HS} + Z_A + Z_{HD} + Z_L + Z_{CTT} \tag{2.9}$$

$$\sum Z = (W - B)\cos\theta + Z_{\dot{w}}\dot{w} + Z_{w|w|}w|w| + Z_{uw}uw + Z_{uu\delta_s}u^2\delta_s + F_{vert-CTT,fwd} + F_{vert-CTT,aft} \tag{2.10}$$

It is assumed that the two vertical CTTs can be treated as a single force acting in the Z-Direction:

$$F_{vert-CTT,fwd} + F_{vert-CTT,aft} = F_{vert-CTT,Total} \tag{2.11}$$

The modified heave equation is now:

$$\sum Z = (W - B)\cos\theta + Z_{\dot{w}}\dot{w} + Z_{w|w|}w|w| + Z_{uw}uw + Z_{uu\delta_s}u^2\delta_s + F_{vert-CTT,Total} \tag{2.12}$$

Pitch Equation

Table 2.3. Pitch Equation Hydrodynamic Coefficients

Coefficients	Description	Value	Units
$M_{\dot{w}}$	Added Mass Coefficient	−4.16	$kg \cdot m$
M_{uw}	Body and Fin Lift and Munk Moment Coefficient	24.0	kg
M_{uq}	Add Mass Cross Term and Fin Lift Coefficient	−10.00	$\frac{kg \cdot m}{rad}$
$M_{w\|w\|}$	Cross Flow Drag Coefficient	4.00357	kg
$M_{uu\delta_s}$	Fin Lift Moment Coefficient	−22.3855	$\frac{kg}{rad}$

The following equations derive the summation of moments contributing to the pitch of the vehicle. These moments are a summation of hydrostatic, added mass, hydrodynamic, lift, and cross-tunnel thruster moments.

$$\sum M = M_{HS} + M_A + M_{HD} + M_L + M_{CTT} \tag{2.13}$$

$$\begin{aligned}\sum M = -z_G W \sin\theta + M_{\dot{w}}\dot{w} + M_{uw}uw + M_{uq}uq + M_{w|w|}w|w| \\ + M_{uu\delta_s}u^2\delta_s + T_{vert-CTT,aft} + T_{vert-CTT,fwd}\end{aligned} \tag{2.14}$$

The vertical thrusters are assumed to be equal distance from the center of buoyancy and are assumed to be receiving the same RPM command. Therefore,

$$T_{vert-CTT,aft} = -T_{vert-CTT,fwd} \tag{2.15}$$

This assumption was made to create a more simplified model of the REMUS 100 which still provides an accurate representation of the vehicle's motion in the Z-direction and pitch behavior. The pitch controller in the actual REMUS vehicle ensures that the moments acting on the REMUS from the VCTTs are near equal in magnitude. Assuming $T_{vert-CTT,aft}$ and $T_{vert-CTT,fwd}$ are equal in magnitude and opposite in direction while being equal distance from the center of buoyancy essentially provides the same behavior that is created by the pitch controller on the vehicle. This assumption reduces the programming and computational load of implementing a pitch controller in the model while providing an accurate representation of the vehicle's behavior.

The total vertical thruster torque is equal to a linear combination of the forward and aft vertical thrusters.

$$T_{vert-CTT,Total} = T_{vert-CTT,aft} + T_{vert-CTT,fwd} = 0 \tag{2.16}$$

This results in the final moment equation:

$$\sum M = -z_G W \sin\theta + M_{\dot{w}}\dot{w} + M_{uw}uw + M_{uq}uq + M_{w|w|}w|w| + M_{uu\delta_s}u^2\delta_s \quad (2.17)$$

2.4 Variables Used in the 3DOF Model

Table 2.4 provides the vehicle specific and environmental values required for coefficient calculations.

Table 2.4. Critical Values for Coefficient Calculations

Variable	**Value**	**Source**
Weight (W)	52.5 kg	Bermudez [1]
Buoyancy (B)	55.8362 N	Bermudez [1]
Length (L)	2.26 m	Bermudez [1]
Hull Frontal Area (A_f)	$2.85 * 10^{-2}$ m^2	Prestero [7]
Hull Projected Area (A_p)	0.430512 m^2	Taylor
Sea Water Density(ρ)	1030 kg/m^3	White [13]
Sea Water Viscosity (μ)[1]	0.00141 $kg/(m \cdot s)$	White [13]
Diameter of REMUS (D)	0.190492 m	Prestero [7]
Fin Taper Ratio (t)	0.654	Whicker-Fellner [14]
Fin Platform Area (S_fin)	$6.65 * 10^{-3}$ m^2	Prestero [7]
Moment Arm ($x_{finpost}$) [2]	-1.0475 m	Taylor
Fin Lift Slope ($c_L\alpha$)	3.12	Prestero [7]

2.5 Vehicle Hydrodynamics, Added Mass, and Thrust Coefficients

Through analysis of the 3DOF equations in regard to real world vehicle data, it was determined that the following coefficients are the major contributors to the equations of motion

in a variable speed cross-tunnel thruster model:

1. $X_{u|u|}$-Axial Flow Coefficient,
2. $T_{n|n|}$-REMUS Non-linear Thruster Coefficient,
3. $Z_{w|w|}$-Cross Flow Coefficient,
4. $M_{w|w|}$-Cross Flow Coefficient,
5. $Z_{uu\delta_s}$- Fin Lift Coefficient,
6. $M_{uu\delta_s}$-Fin Lift Coefficient.

The following sections provide the calculations and justifications for the 3DOF model's major coefficients.

The following equation defines the axial drag coefficient $X_{u|u|}$:

$$X_{u|u|} = -\frac{1}{2}\rho C_d A_f \tag{2.18}$$

ρ and A_f are both constants, however the coefficient of drag (C_d) will change with the vehicle's velocity depending on the Reynolds number. To better interpret how this C_d will be affected, the Reynolds number in the X-direction for the REMUS needs to be calculated over its entire operating regime [13]:

$$Re = \frac{\rho|U|D}{\mu} \tag{2.19}$$

Diameter (D) was used instead of the vehicle cross-sectional area to ensure that the smallest Reynolds number that could be seen by the vehicle was calculated. This calculation provided the most conservative analysis of the fluid dynamic properties of the REMUS vehicle operating at variable speeds.

The value of the Reynolds number determines turbulent or laminar flow by the relationships seen in Table 2.5.

As can be seen in Figures 2.2 and 2.3, nearly the entire range of operating velocities for the REMUS vehicle is in the turbulent region. The REMUS vehicle transitions from the turbulent region at approximately 0.071863 m/s. Therefore, the 3DOF model assumes there

is slight to moderate Reynolds number dependence when calculating C_d for the entire range of velocities.

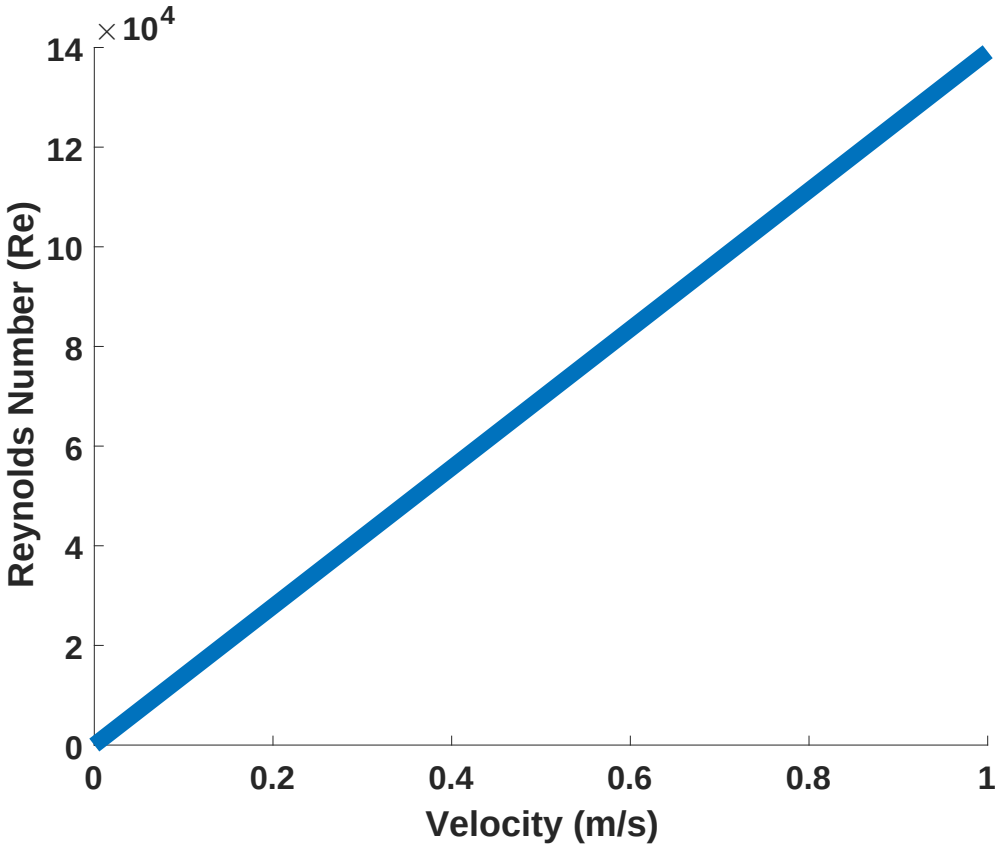

Figure 2.2. Reynolds Number vs. REMUS velocity

Table 2.5. Reynolds Number Regimes. Adapted from [2], [13].

Re Range	Behavior
$0 < Re < 1$	Highly viscous laminar creeping motion
$1 < Re < 100$	Laminar, strong Reynolds number dependence
$100 < Re < 10^3$	Laminar, boundary layer theory useful
$10^3 < Re < 10^4$	Transition to turbulence
$10^4 < Re < 10^5$	Turbulent, moderate Reynolds number dependence
$10^5 < Re < \infty$	Turbulent, slight Reynolds number dependence

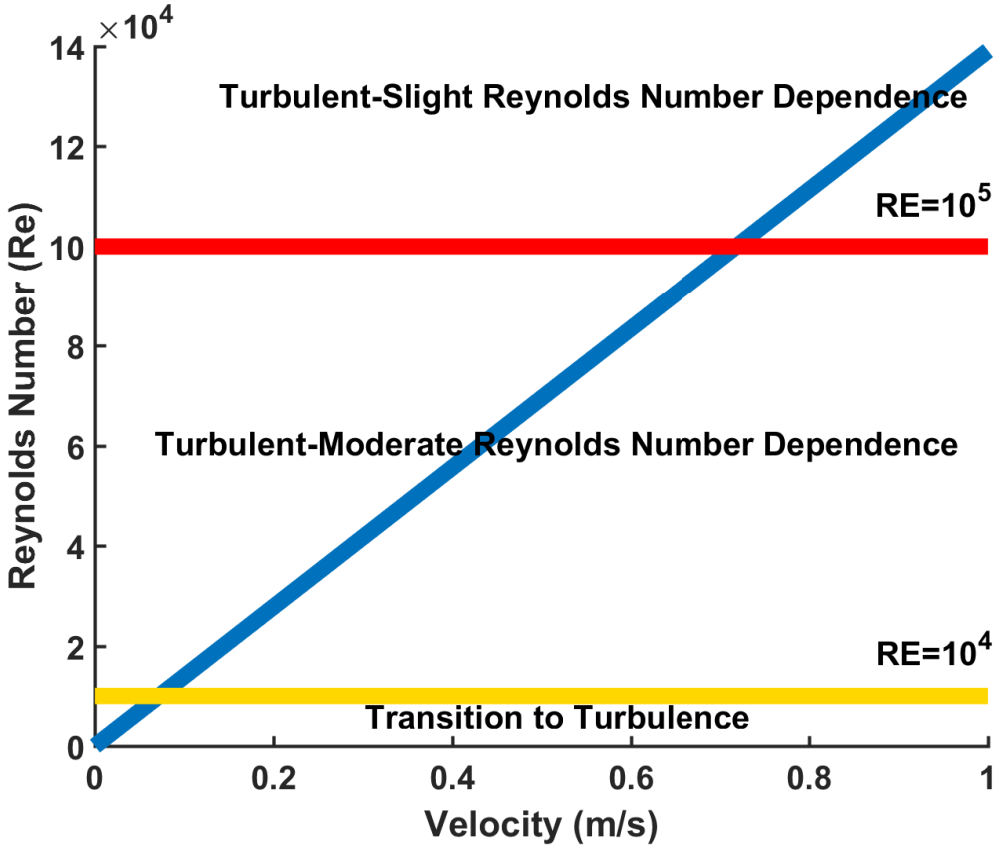

Figure 2.3. Transition Thresholds of the Reynolds Number for the REMUS

Due to the Reynolds number behavior for the REMUS vehicle, seen in Figures 2.2 and 2.3, C_d will remain constant at all speeds for the 3DOF model. C_d for this research was taken from previous research conducted by [13] and [15]. For a blunt spherical object such as the nose cone of a REMUS, with a $Re \geq 10^4$ and with $D/L \approx 10$ (REMUS $D/L = 11.59$), $C_d \approx 0.82$ according to [13] or $C_d \approx 0.85$ according to [15]. $C_d = 0.85$ was used in the model presented in this paper.

Using the C_d above, $X_{u|u|}$ can be calculated for the entire operating region of a REMUS vehicle which implements cross-tunnel thrusters.

$$X_{u|u|} = -\frac{1}{2} * 1030 \frac{kg}{m^3} * .85 * 2.85 * 10^{-2} m^2 \tag{2.20}$$

$$X_{u|u|} = -12.4759\frac{kg}{m} \tag{2.21}$$

The cross flow drag coefficient ($Z_{w|w|}$) can be broken up into two components, $Z_{w|w|,Body}$ and $Z_{w|w|,Fins}$, expressed in equation 2.22:

$$Z_{w|w|} = Z_{w|w|,Body} + Z_{w|w|,Fins} \tag{2.22}$$

The Reynolds Numbers in the Z-direction will be much higher than the Reynolds Numbers in the X-direction due to the larger associated area of fluid interaction. It was proven in the $X_{u|u|}$ section that the REMUS vehicle is always operating in a turbulent flow regime. Since the vehicle is always in a turbulent flow, the cross flow drag coefficient C_{dc} can be determined and the assumption that $Re \geq 10^4$ in the Z-direction is valid.

For a cylinder with a $Re \geq 10^4$ and with $D/L \approx 10$ (REMUS $D/L = 11.59$), the C_{dc} is approximately 0.82 according to [13] or C_{dc} is approximately 0.85 according to [15]. $C_{dc} = 0.82$ was used in the model presented in this paper. Giving us the following value for $Z_{w|w|,Body}$:

$$Z_{w|w|,Body} = -\frac{1}{2}\rho C_{dc} A_p = -181.8705\frac{kg}{m} \tag{2.23}$$

Using the cross flow drag coefficient (C_{df}) developed by Whicker and Fehlner [14] and the fin taper ratio (t) the following equations are derived:

$$C_{df} = 0.1 + 0.7t = 0.1 + 0.7 * 0.654 = 0.56 \tag{2.24}$$

$$Z_{w|w|,Fins} = 2 * \frac{1}{2}\rho C_{df} S_{fin} = -3.75\frac{kg}{m} \tag{2.25}$$

Therefore,

$$Z_{w|w|} = -185.621\frac{kg}{m} \tag{2.26}$$

The cross flow coefficient ($Z_{w|w|}$) above is valid for the entire range of REMUS operating velocities since the vehicle is always operating in the turbulent flow regime where there is slight to moderate Reynolds number dependence.

Cross flow drag ($M_{w|w|}$) is calculated in a similar way as the cross flow coefficient ($Z_{w|w|}$):

$$M_{w|w|} = M_{w|w|,Body} + M_{w|w|,Fins} \tag{2.27}$$

where, $M_{w|w|,Body} = 0$, due to the assumption that the center of buoyancy lies on the center of the vehicle, equidistant from the nose and tail. With this assumption, the following equation is valid:

$$M_{w|w|} = M_{w|w|,Fins} \tag{2.28}$$

where

$$M_{w|w|,Fins} = 2 * x_{finpost} * (-\frac{1}{2}\rho C_{df} S_{fin}) \tag{2.29}$$

therefore,

$$M_{w|w|} = 4.00357kg \tag{2.30}$$

The cross flow drag coefficient ($M_{w|w|}$) above is valid for the entire range of REMUS 100 operating velocities since the vehicle is always operating in the turbulent flow regime where there is slight Reynolds number dependence.

The fin lift force ($Z_{uu\delta s}$) is determined by the following equation:

$$Z_{uu\delta s} = 2 * (-\frac{1}{2}\rho c_{L\alpha} S_{fin}) = -21.37 kg/(m \cdot rad) \tag{2.31}$$

The fin lift moment ($M_{uu\delta s}$) is determined by the following equation:

$$M_{uu\delta s} = 2 * (-\frac{1}{2}\rho c_{L\alpha} S_{fin} x_{finpost}) = -22.3855 kg/rad \tag{2.32}$$

2.6 Other Coefficients

The following coefficients are the minor contributors to the equations of motion in a variable speed cross-tunnel thruster model. These coefficients were deemed minor due to the lower velocities and accelerations associated with the listed coefficients:

1. X_{udot}-Added Mass Coefficient,
2. Z_{wdot}-Added Mass Coefficient,
3. Z_{uw}-Body Lift and Fin Lift Coefficient,
4. M_{uw}-Body Lift and Fin Lift and Munk Moment Coefficient,
5. M_{uq}-Added Mass Cross Term and Fin Lift Coefficient.

The behavior of these minor contributors regarding variable velocity is not addressed in this research. However, the constants for these coefficients were derived in previous research for the REMUS vehicle and can be found in [1] and [7].

2.7 Direct Force and Torque Inputs

The following are the direct force and torque inputs applied to the equations of motion for the 3DOF model:

1. $F_{Propeller} = X_p$,
2. $F_{vert-CTT,Total} = Z_{CTT}$,
3. $T_{vert-CTT,Total} = M_{CTT}$.

$F_{Propeller}$ (X_p) for the REMUS 100 was derived through experimentation utilizing a FUTEK strain gauge. The following equation relates vehicle RPM (n) to $F_{Propeller}$ in Newtons:

$$F_{Propeller} = 2.93 \times 10^{-12} \times n^4 - 2.69 \times 10^{-9} \times n^3 + 7.23 \times 10^{-6} \times n^2 + 0.0105 \times n \quad (2.33)$$

The equation for $F_{Propeller}$ has the behavior seen in Figure 2.4.

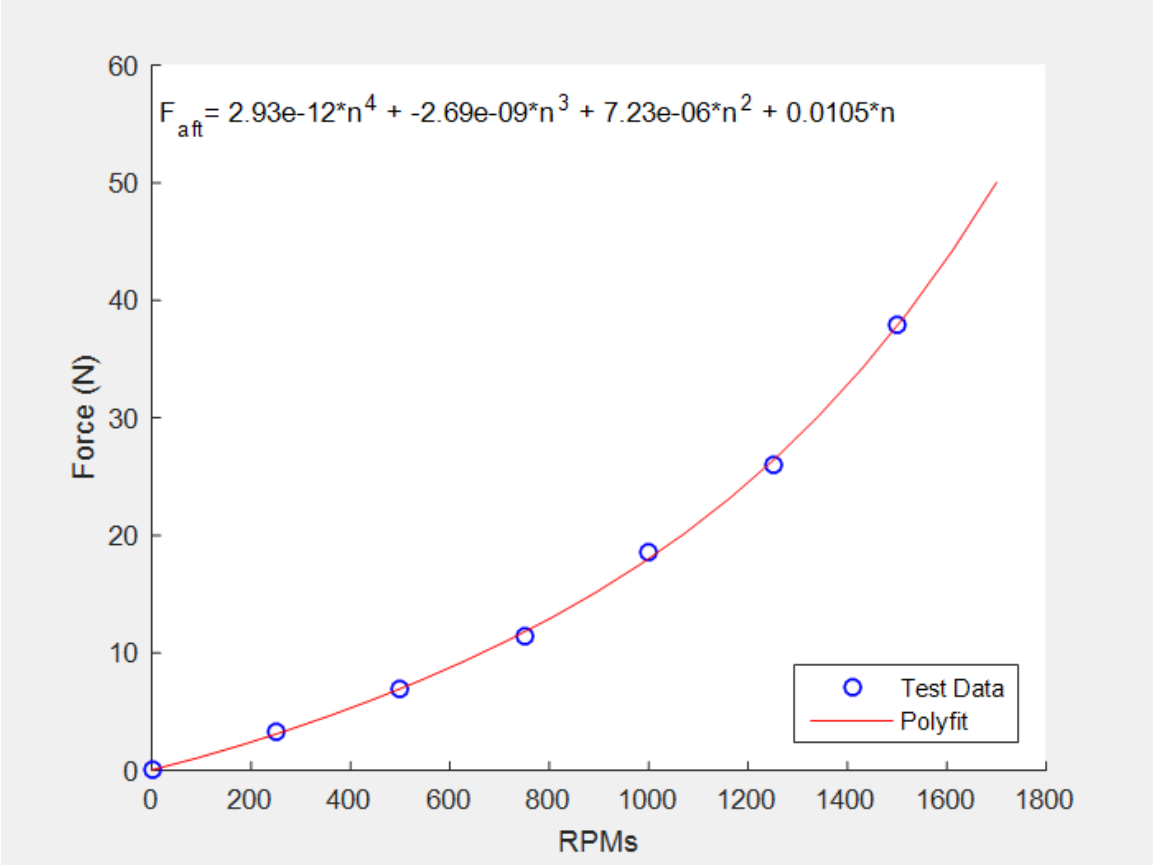

Figure 2.4. $F_{Propeller}$ vs. Propeller RPM. Source: [1].

$F_{vert-CTT,Total}$ (Z_{CTT}) for the REMUS 100 was derived through experimentation utilizing a FUTEK strain gauge. The strain gauge experiments were conducted to find the force generated by one cross-tunnel thruster at a certain RPM (n) in the downward direction (F_{down}). The experiments yielded a different force equation when the thrusters were operating at a certain RPM (-n) in the upward direction (F_{up}). With this research assumptions, the

following relation is true:

$$F_{vert-CTT,Total} = \begin{cases} 2 * F_{down}, & \text{when } n > 0 \\ -2 * F_{up}, & \text{when } n < 0 \end{cases}$$

The following equations relate vehicle RPM (n) to F_{down} and F_{up} in Newtons:

$$F_{down} = 3.89 \times 10^{-15} \times n^4 + 3.5 \times 10^{-11} \times n^3 + 1.81 \times 10^{-7} \times n^2 + 3.3 \times 10^{-4} \times n \quad (2.34)$$

$$F_{up} = -6.85 \times 10^{-15} \times n^4 + 7.3 \times 10^{-11} \times n^3 + 9.26 \times 10^{-8} \times n^2 + 4.97 \times 10^{-4} \times n \quad (2.35)$$

The equations F_{up} and F_{down} have the behavior seen in Figures 2.5 and 2.6.

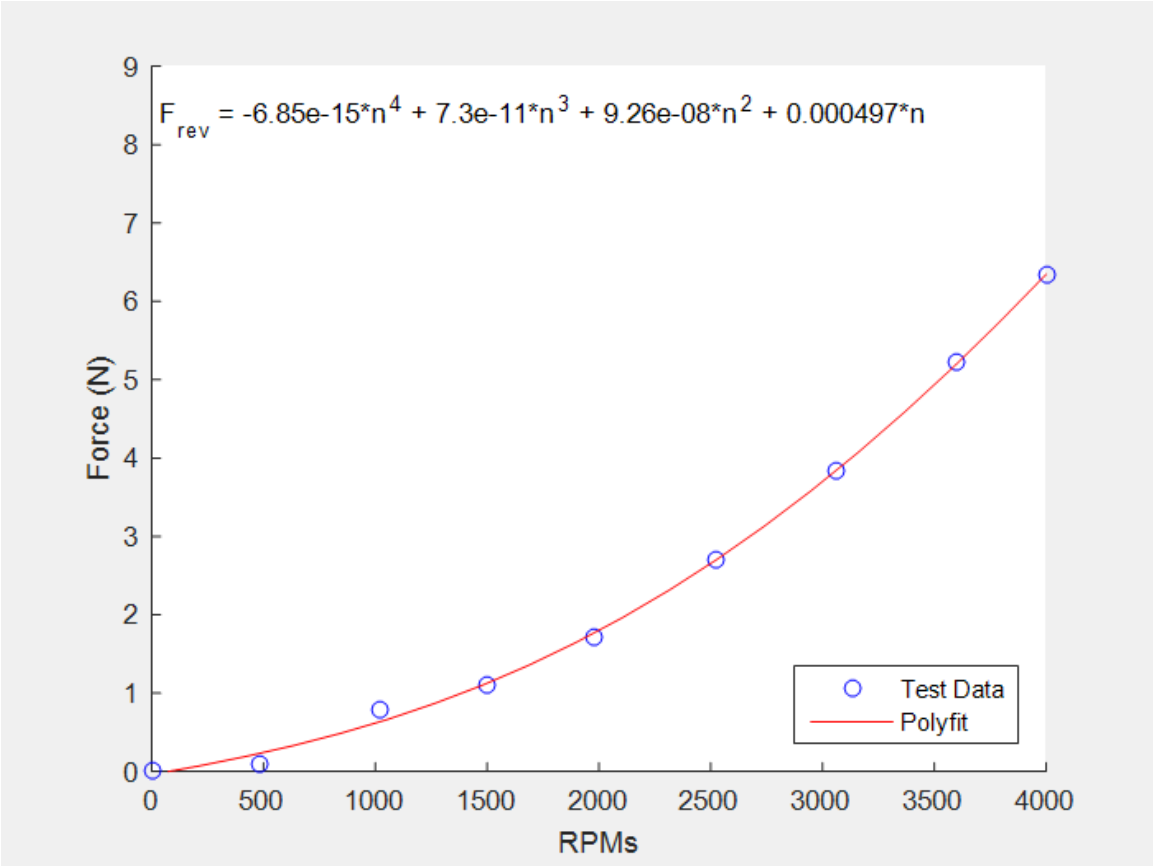

Figure 2.5. F_{up} vs. Cross-Tunnel Thruster RPM. Source: [1].

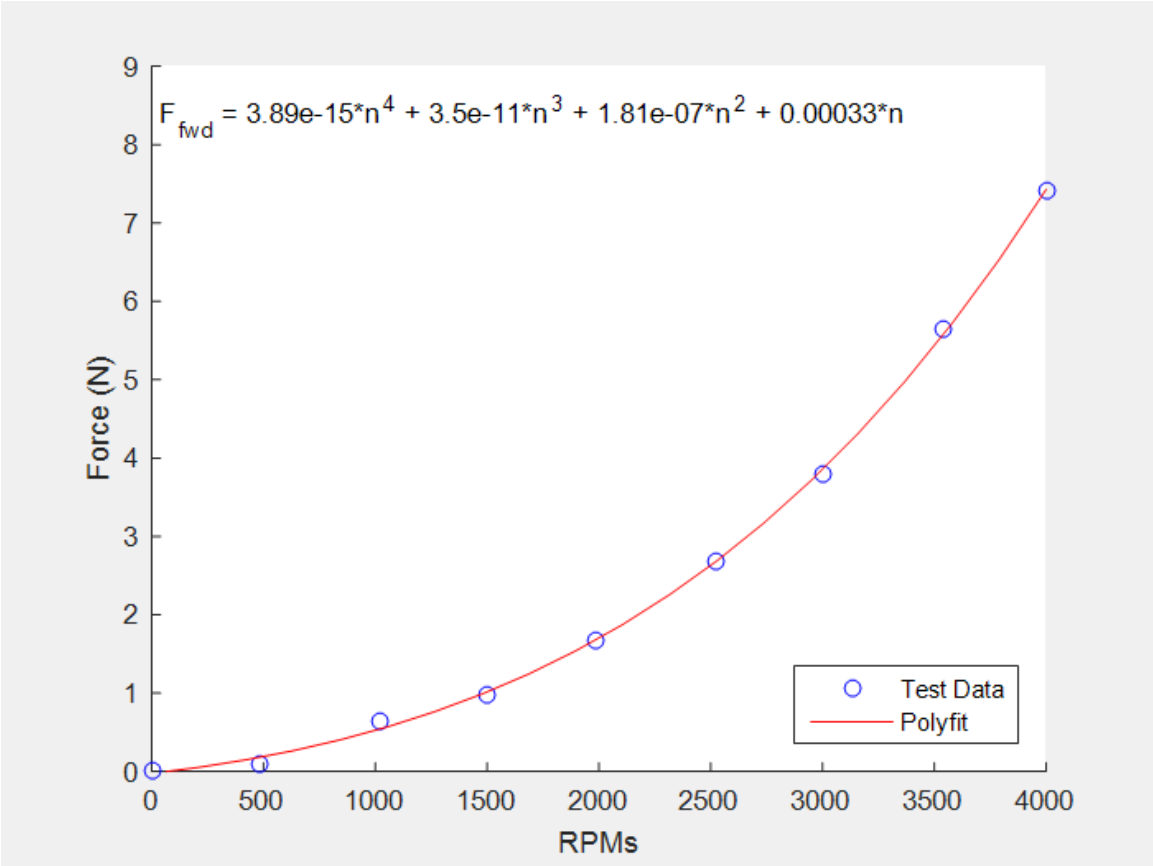

Figure 2.6. F_{down} vs. Cross-Tunnel Thruster RPM. Source: [1].

Torque ($T_{vert-CTT,Total}$ or M_{CTT}) due to output of the horizontal cross-tunnel thrusters in the model is assumed to have the following property:

$$|T_{vert-CTT,aft}| = |T_{vert-CTT,fwd}| \tag{2.36}$$

Therefore,

$$T_{vert-CTT,Total} = 0 \tag{2.37}$$

THIS PAGE INTENTIONALLY LEFT BLANK

CHAPTER 3:
Design of a 3DOF Computer Model

This chapter is an overview of the design of the computer model created in MATLAB Simulink for the REMUS 100. The 3DOF model presented in this chapter is partially verified through experiments in Monterey Bay, CA. This chapter is included in this thesis to provide a more in-depth understanding of the model for future researchers that continue the verification and validation process. It will also provide an overview of how an individual could create their own variable speed model of an AUV.

3.1 Equations of Motion

The first step in creating a variable speed model was implementing the equations of motion, found in Chapter 2, into a Simulink 3DOF model. The implementation for the surge, heave, and pitch equations are depicted in Figures 3.1, 3.2, and 3.3.

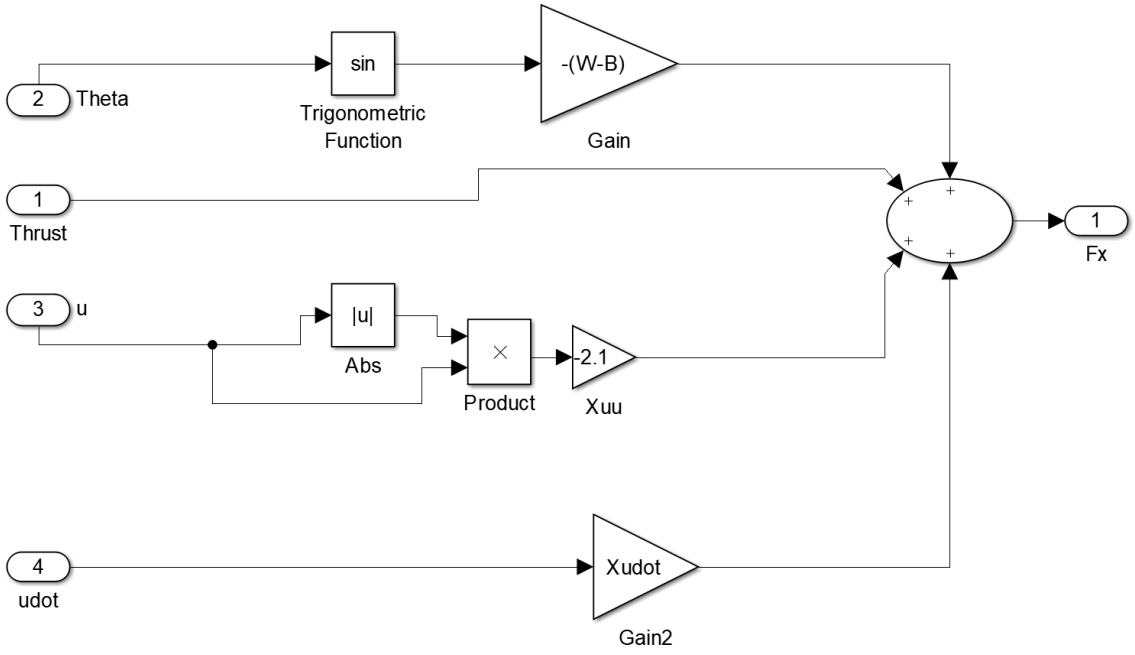

Figure 3.1. 3DOF Surge Equation

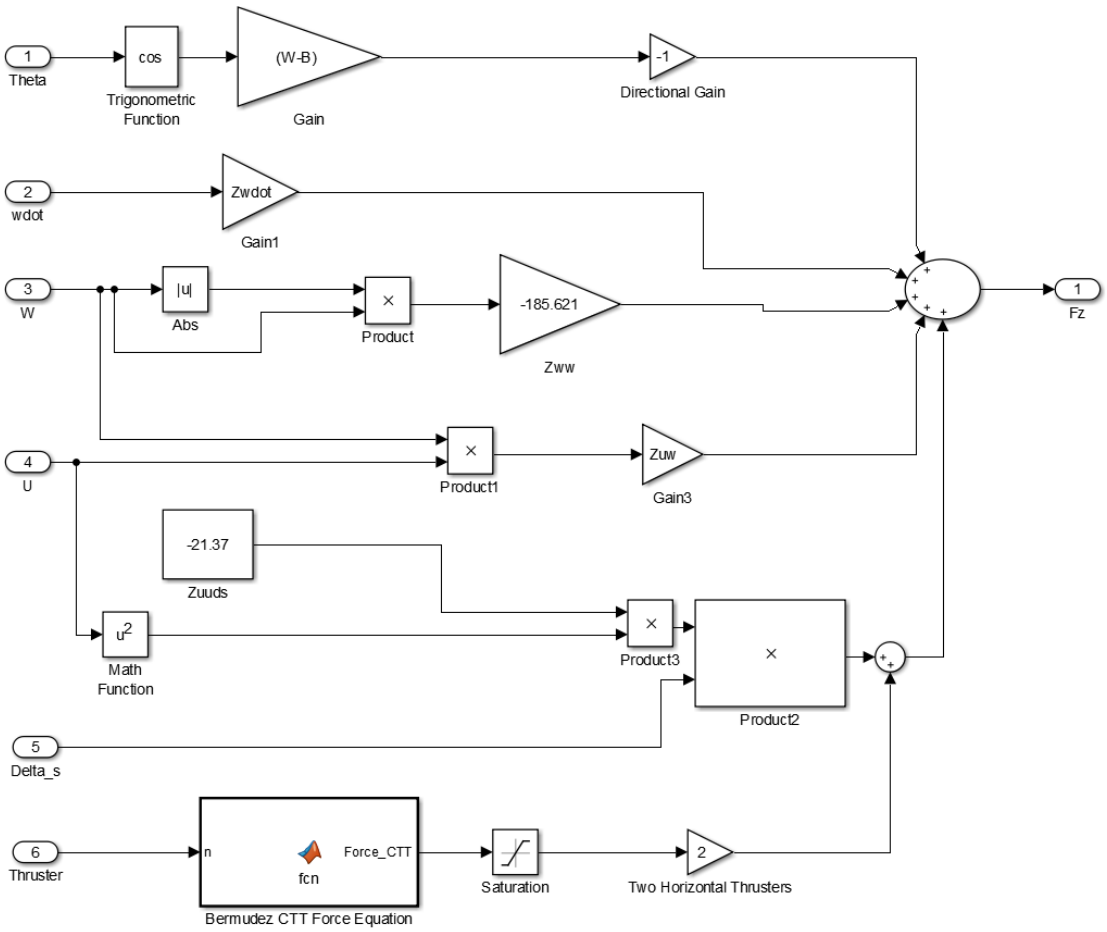

Figure 3.2. 3DOF Heave Equation

The Bermudez force equation block in Figure 3.2 contains the CTT RPM to Force equation derived by [1]. The input to this block is the RPM for both VCTTs and the output is the Force (N) that is generated by the simulated VCTTs.

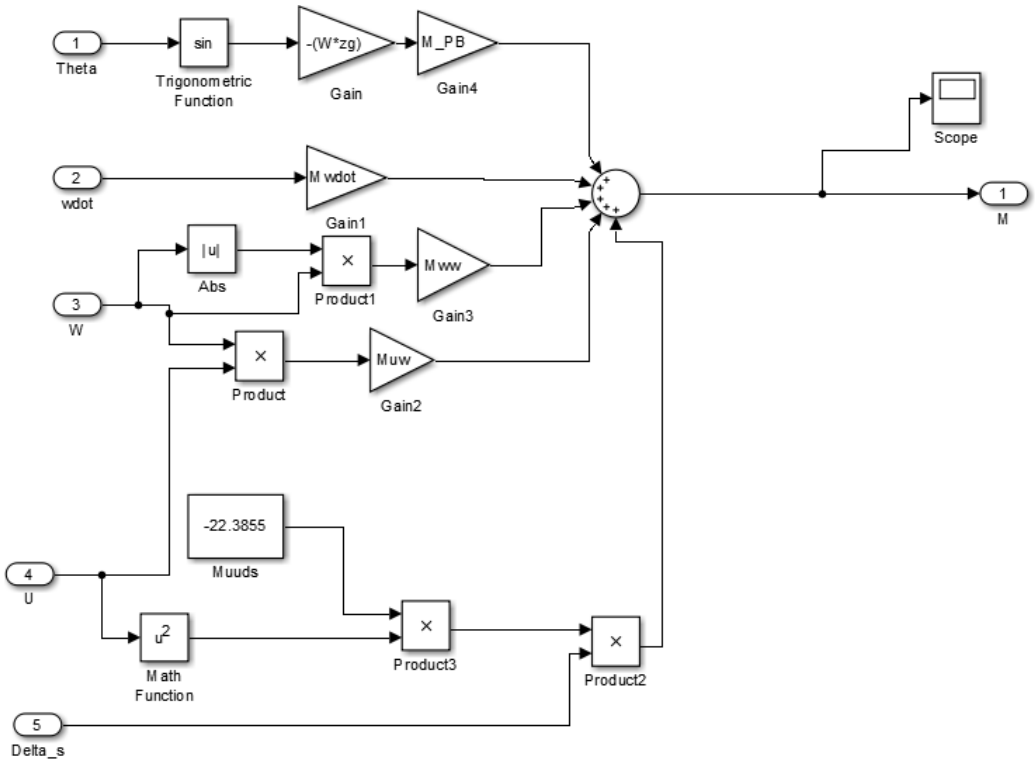

Figure 3.3. 3DOF Pitch Equation

3.2 Transformation From Body Fixed to Global Reference Frame

The next step was transforming the forces in a body fixed coordinate frame into motion in the flat earth global reference frame. This transformation was easily performed using a function block from the Aerospace Toolbox in Simulink which converted the forces generated by the equations of motion into motion in the global frame. The Aerospace function block is seen in Figure 3.4.

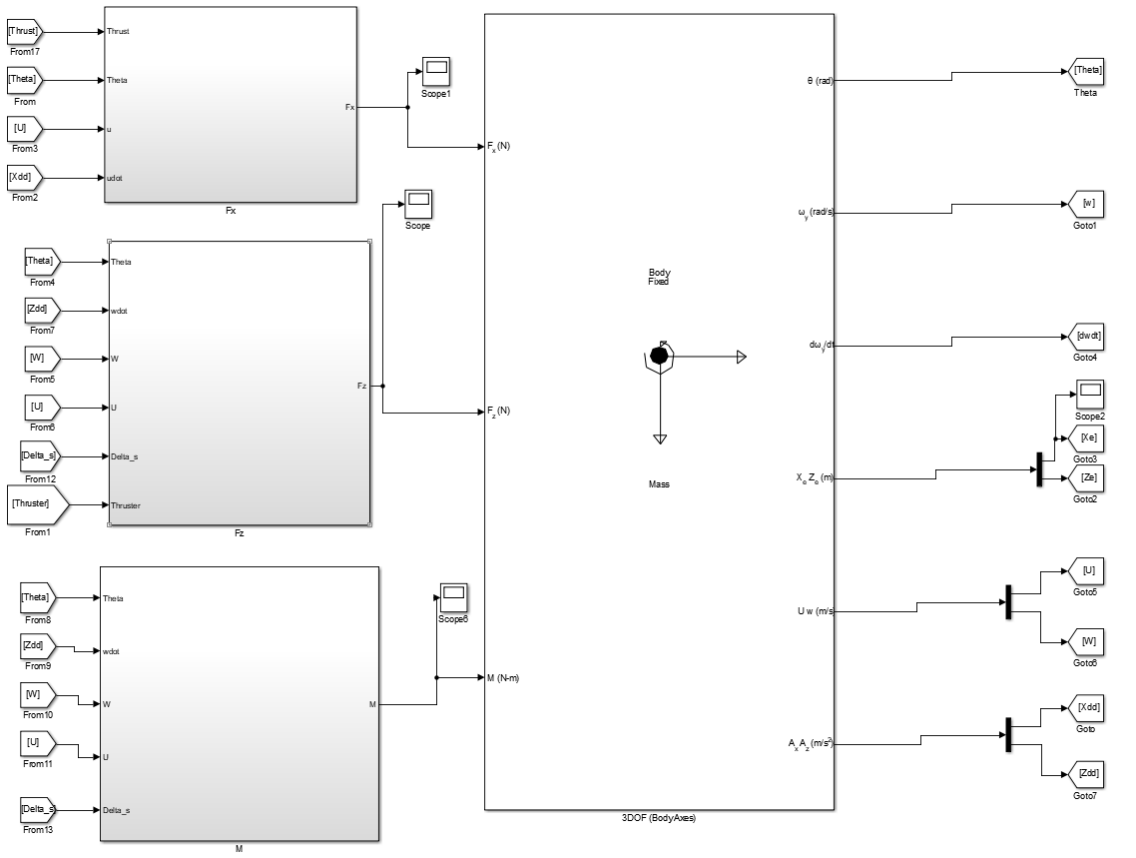

Figure 3.4. Equations of Motion Transformed from Body Fixed to Global Reference Frame

3.3 Implementation of the REMUS Controller

The third step in the design process required commands (i.e. depth and RPM commands) to compare, through the use of a feedback loop, the current position of the model to the commanded position. To verify that the model's behavior was similar to the actual vehicle's behavior, real world commands from previous missions were required. The model was then verified by issuing these recorded real world commands to the model and comparing the model's behavior to the recorded behavior of the REMUS vehicle operating in Monterey Bay. A detailed analysis of the model's performance can be seen in Chapter 4. The real world commands were imported into the Simulink model as an array and were issued to the model at the rate seen by the actual REMUS vehicle. The commands issued to the model's

controller were depth and propeller RPM commands. The implementation of the real world commands is shown in Figure 3.5.

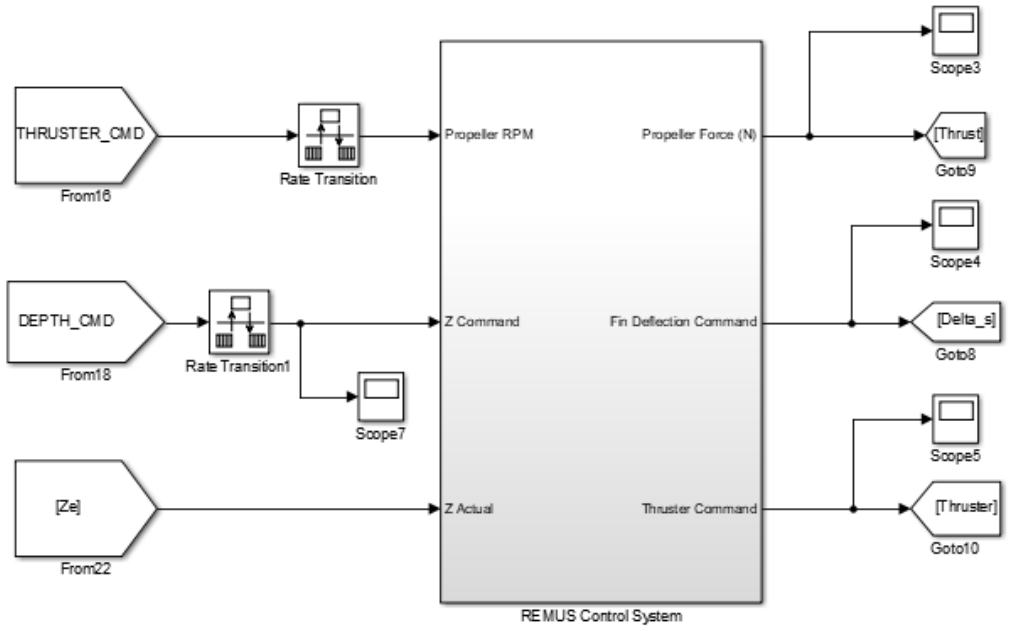

Figure 3.5. Controller Importing Real World Commands.

The real world commands were accepted by the model's controller, seen in Figure 3.5. The controller in the model is actually a group of PID controllers, controlling Propeller RPM, Depth, and Cross-Tunnel Thruster RPM of the model. The modeled controller mimics the PID controllers implemented by the REMUS vehicle, however it is not an exact copy of the REMUS vehicle's controller due to the actual REMUS controllers' design and parameters being proprietary information. However, even with a slightly different controller implemented in the model, the actuation of the control surfaces, thrusters, and propeller occur so rapidly that the model's behavior was not affected significantly (refer to model performance in Chapter 4).

3.4 Complete Model

The equations of motion, body-fixed to global reference frame transformation, real-world command inputs, and PID controllers comprise a full 3DOF model to simulate the AUV vertical plane motion at various speeds, depicted in Figure 3.6.

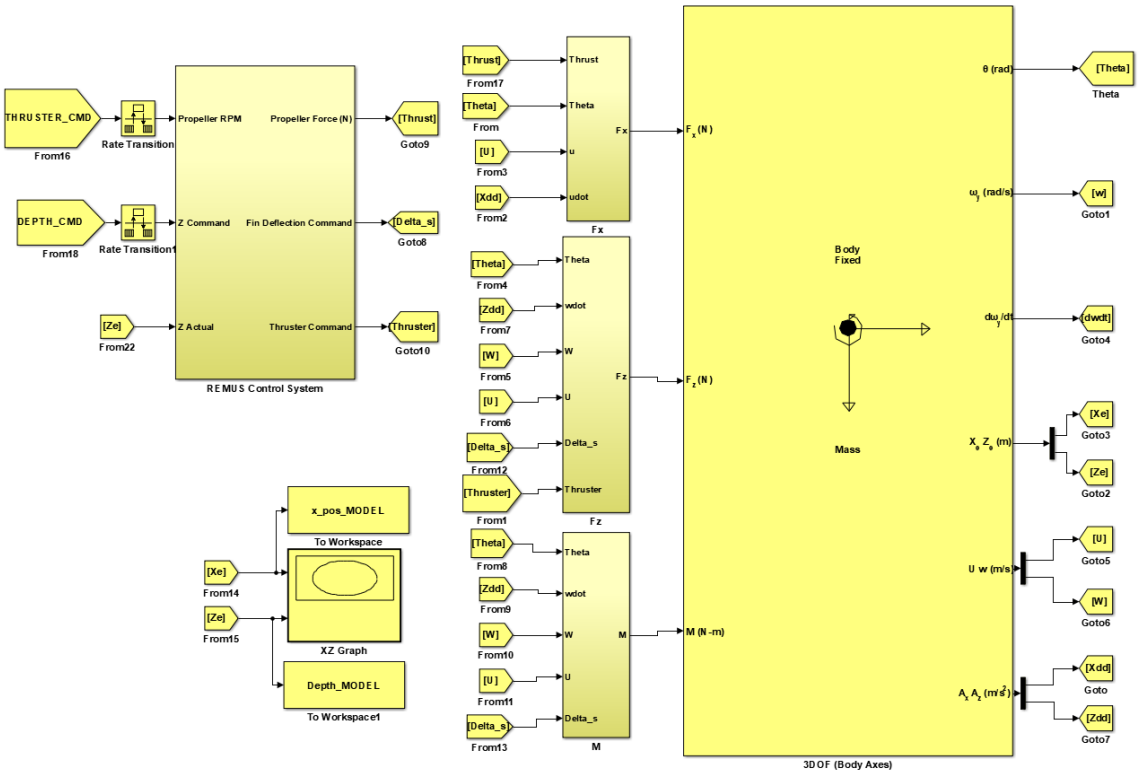

Figure 3.6. Complete Variable Speed REMUS Model Utilizing Cross-Tunnel Thrusters.

The reason the program seen in Figure 3.6 works at various vehicle velocities is that the equations of motion are recomputed at each iterative time step, whose duration is set in the model's parameters. This iterative calculation process is a stark change from previously presented models of the REMUS vehicle and allows for a more detailed and representative analysis of the vehicle's behavior. The time step used for this model was 0.002 seconds. At this time step interval the modeled vehicle can accept all commands from real world missions and compute the vehicle's behavior in real-time or faster than real-time. The model's fixed time step is limited by the data rate of the vehicle's sensors and commands. The 0.002 second time step was selected because at this time interval the model is able to

accept these real world data and commands while calculating the vehicle's behavior to a high accuracy.

THIS PAGE INTENTIONALLY LEFT BLANK

CHAPTER 4:
REMUS 3DOF Model Verification

Presented in this chapter are the verification experiments of the 3DOF model's depth behavior. Depth control at the early stages of this research was considered to be the parameter of greatest concern when modeling a REMUS vehicle. Depth control is a difficult element to model due to the constant positive buoyancy force acting on the vehicle and the changing efficiency of the dive fins at various speeds. To maintain depth without CTTs, the REMUS must maintain a certain speed to ensure adequate flow over the dive fins. At slow speeds, CTTs are the only way to maintain depth control. Slow speed maneuvering is paramount when modeling an AUV attempting to dock.

4.1 Variable Speed Verification

The 3DOF model verification was conducted in two parts. The first part of the verification process was conducted by obtaining REMUS commands and data from experiments in the field. A thousand seconds of depth and RPM commands from a REMUS vehicle operating in Monterey Bay were imported into the 3DOF model. In the first part of the verification, cross-tunnel thrusters were not enabled on the vehicle. However, depth and RPM commands did vary during the analyzed thousand second window. The 3DOF model's behavior in the Z-direction was then plotted against the actual vehicle behavior and a sensitivity analysis was conducted. The results are represented in Figures 4.1, 4.2, and 4.3.

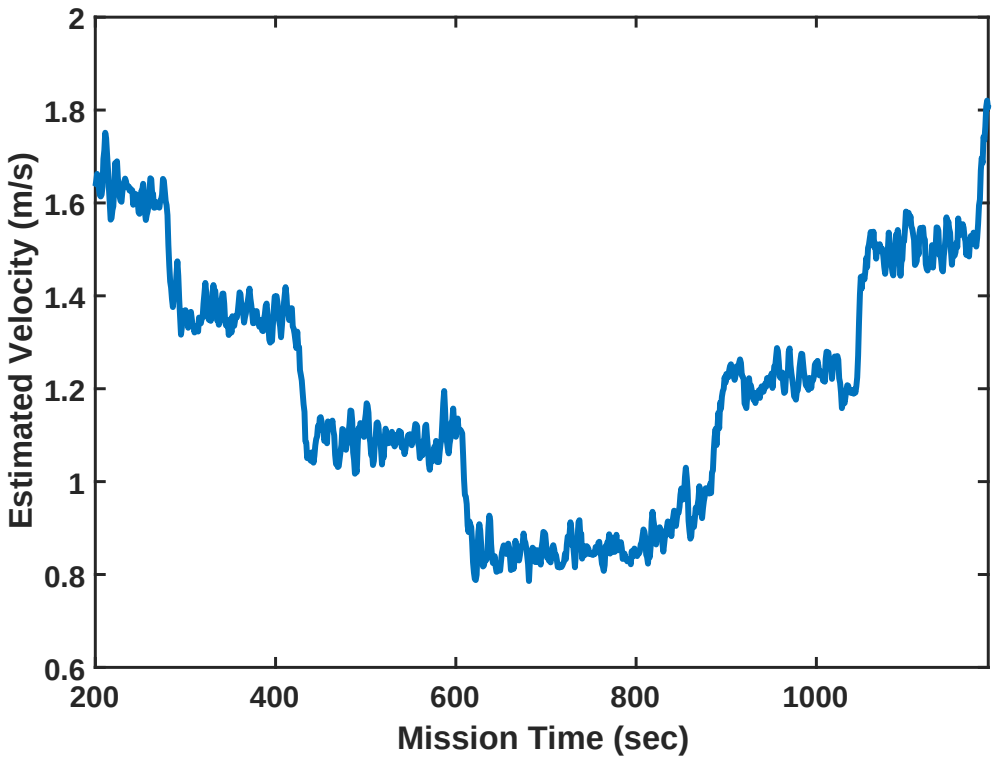

Figure 4.1. REMUS Estimated Forward Velocity

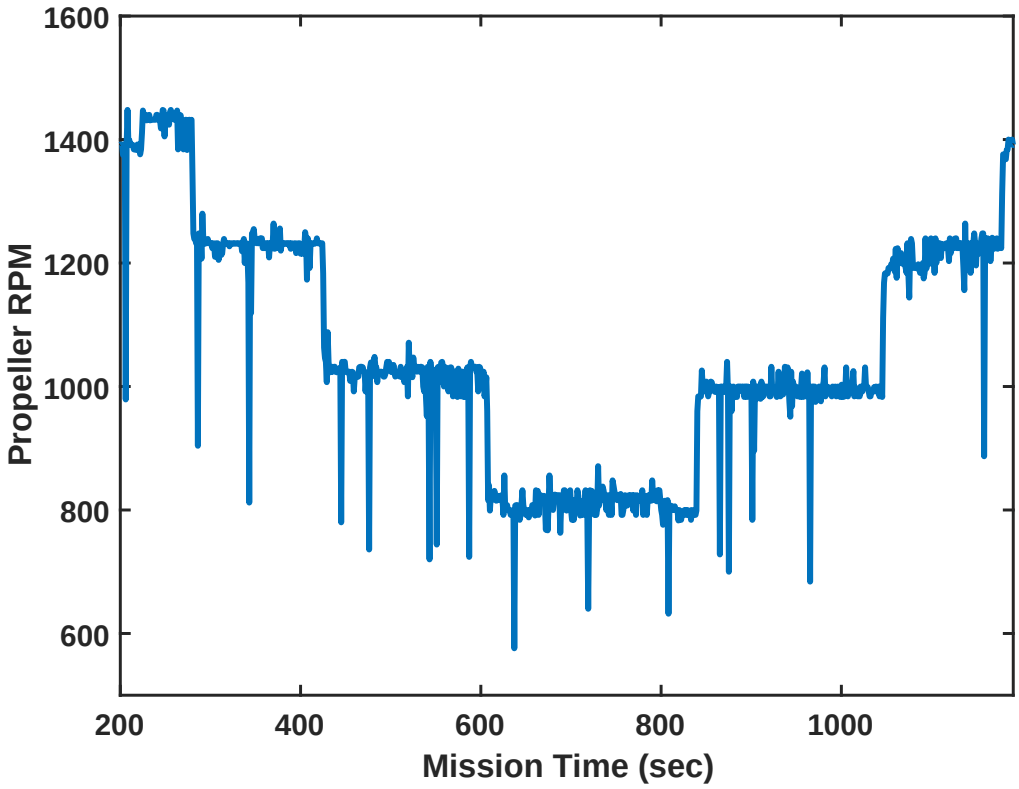

Figure 4.2. Real World RPM Commands

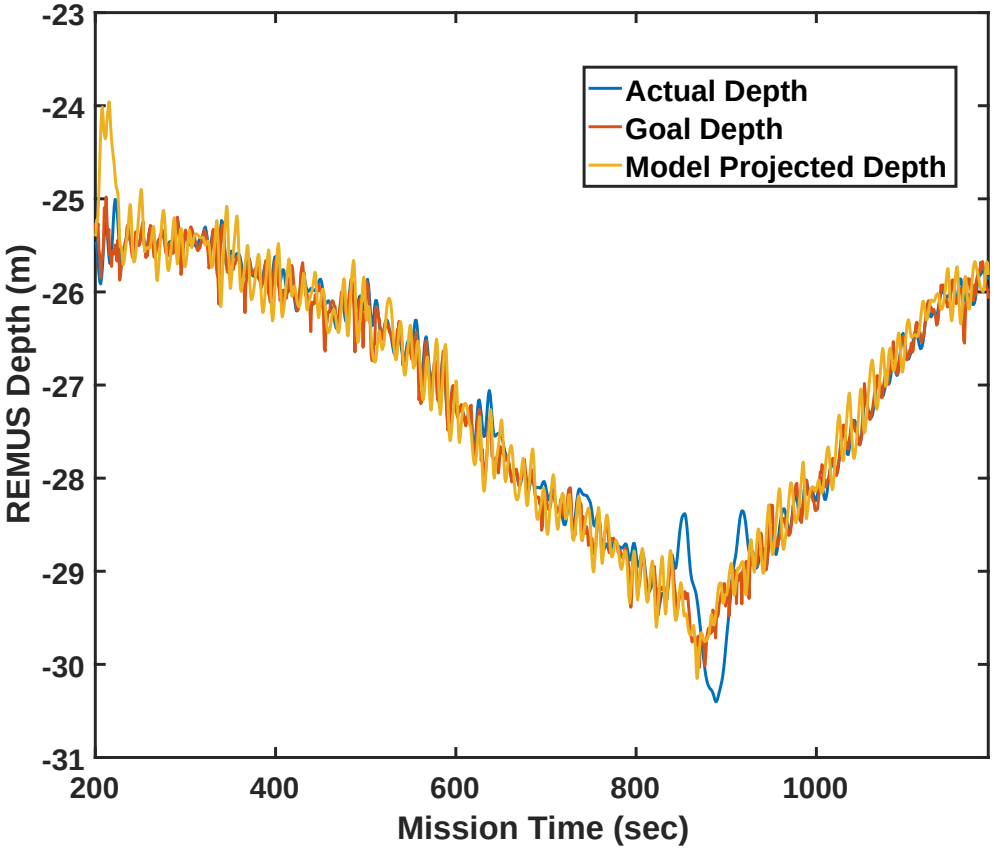

Figure 4.3. REMUS Real World vs. Modeled Behavior

In Figure 4.3, at the beginning of the plot, there is a noticeable difference between the REMUS vehicle's actual depth and the model's depth. This difference is due to the initialization of the model at a depth and speed slightly different than the actual vehicle. As the model's depth controller reacts to the depth commands imported from the actual mission and the buoyancy force, the model's dive fin angle changes and its behavior stabilizes to the depth of the actual vehicle. Also, as the model's velocity more closely follows the actually vehicle's velocity, it is able to decrease the error in its depth control behavior.

At approximately 840 seconds, the actual vehicle loses some of its depth control capability. This behavior is caused by a reduction of flow over the dive fin surface. The reduction of flow across the dive fins may have been caused by a difference in current at this depth and a decrease in vehicle velocity. The vehicle's propeller RPM at this time was 799 RPM which

is low in its normal operating range without CTTs enabled.

The mission profile for Figures 4.1, 4.2, and 4.3 was selected because the actual REMUS vehicle operated at various depths between 25 and 30 meters while also reducing RPM from 1640 RPM to 790 RPM and then increasing RPM back to 1640 RPM. This provided the model a variable range of depths and velocities against which it could be analyzed.

Through performing a sensitivity analysis, it was determined that the mean of the error between the real world REMUS behavior and the model behavior was -12.8 cm with a standard deviation of 34.4 cm. This error calculation was for the entire thousand second mission.

4.2 Cross-Tunnel Thruster Verification

The second part of the 3DOF model verification process tested the cross-tunnel thruster portion of the model. Another 1000 second window was selected from field experimentation conducted in Monterey Bay. The REMUS vehicle was operating at various speeds with varying cross-tunnel thruster inputs. Again, depth and RPM commands were fed to the 3DOF model and the model's behavior in the Z-direction was plotted against the actual vehicle's behavior and a sensitivity analysis was conducted. The results are seen in Figures 4.4, 4.5, 4.6, and 4.7.

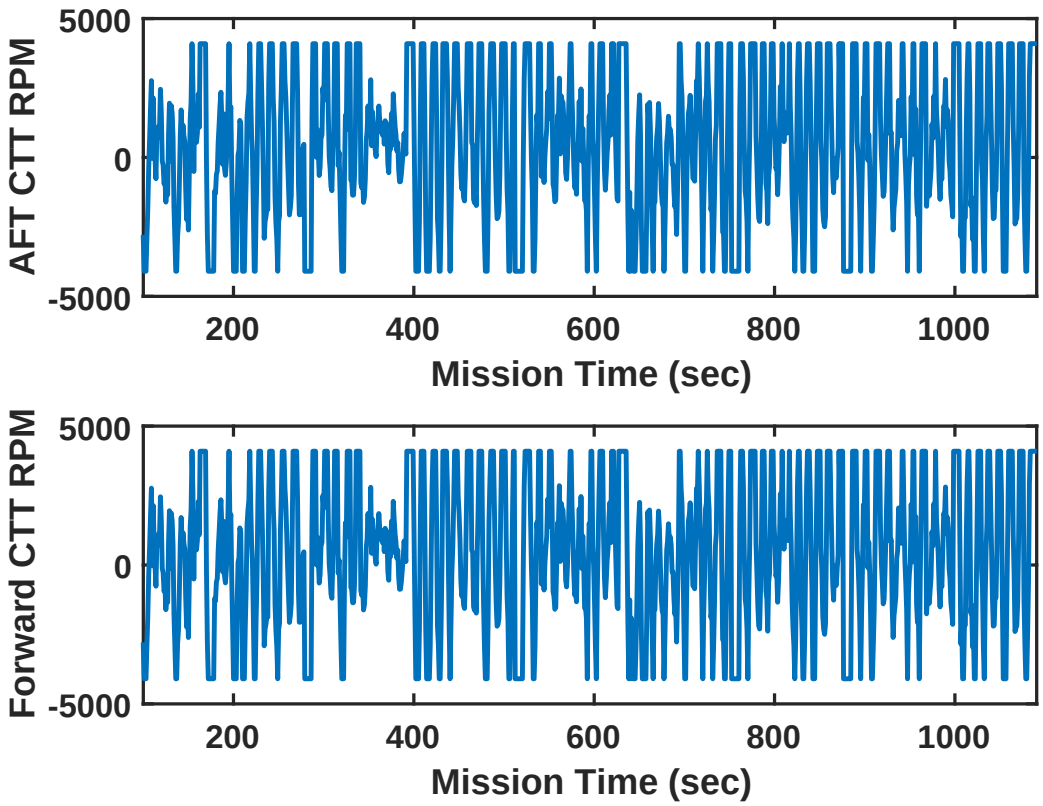

Figure 4.4. REMUS Real World Cross-Tunnel Thruster Commands

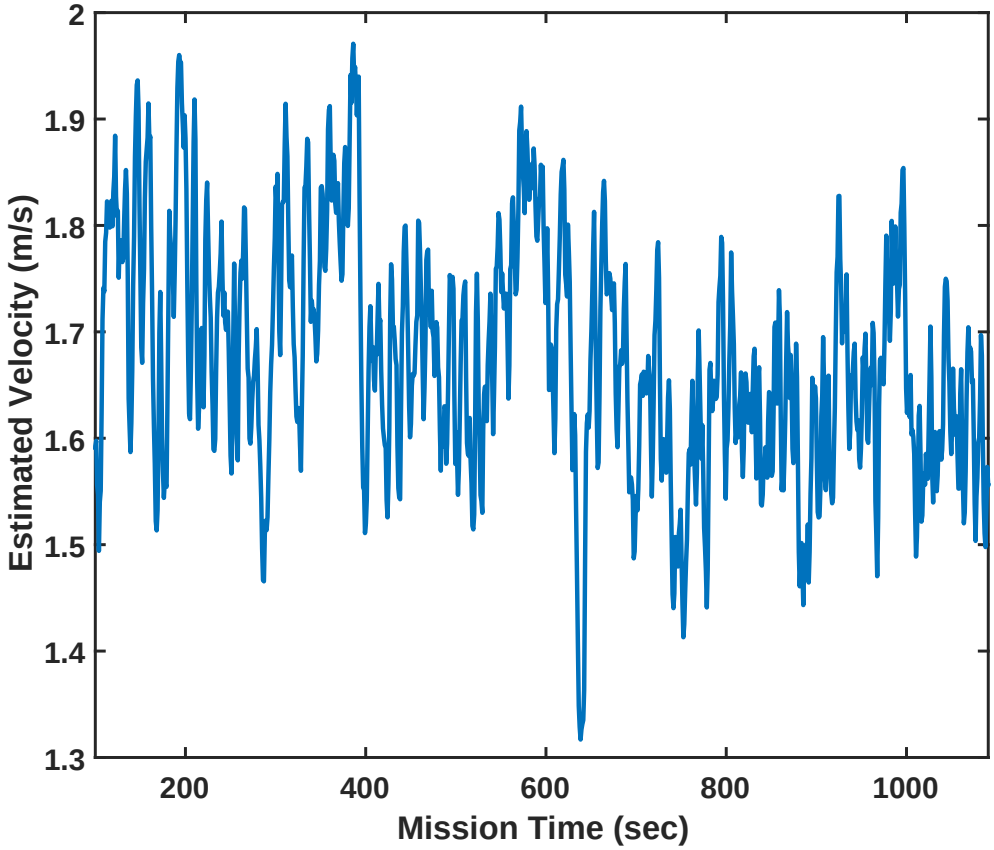

Figure 4.5. REMUS Estimated Forward Velocity

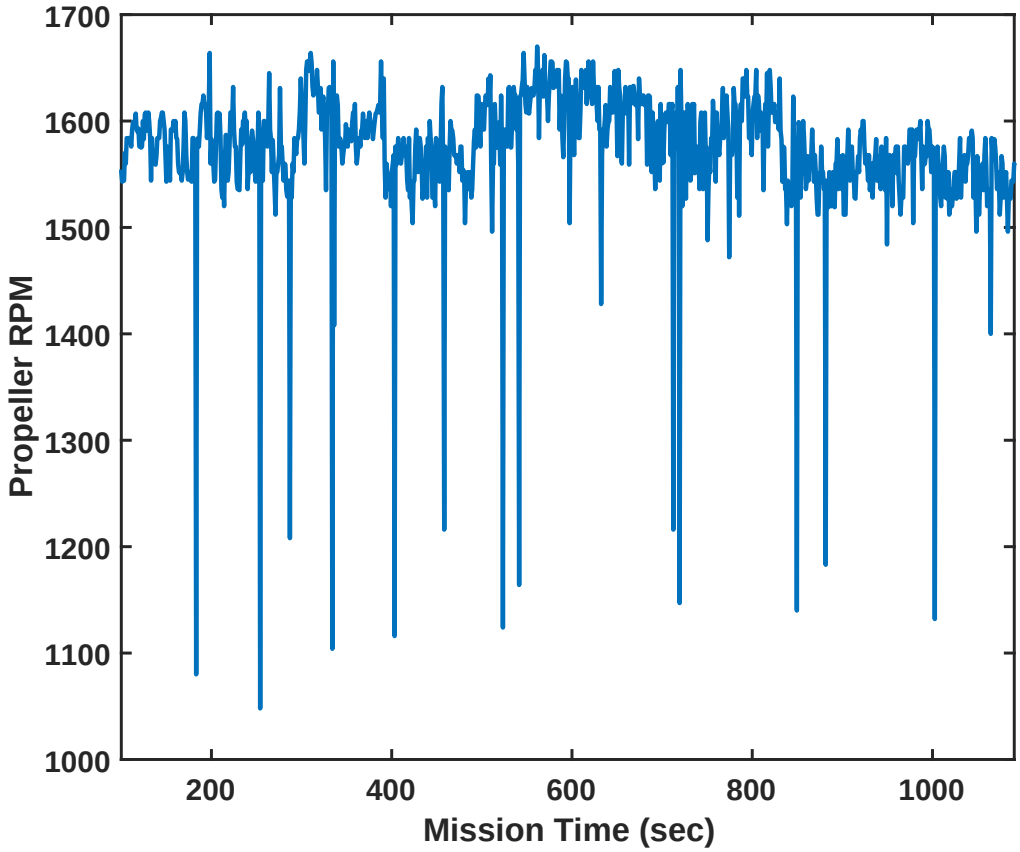

Figure 4.6. REMUS Real World RPM Commands

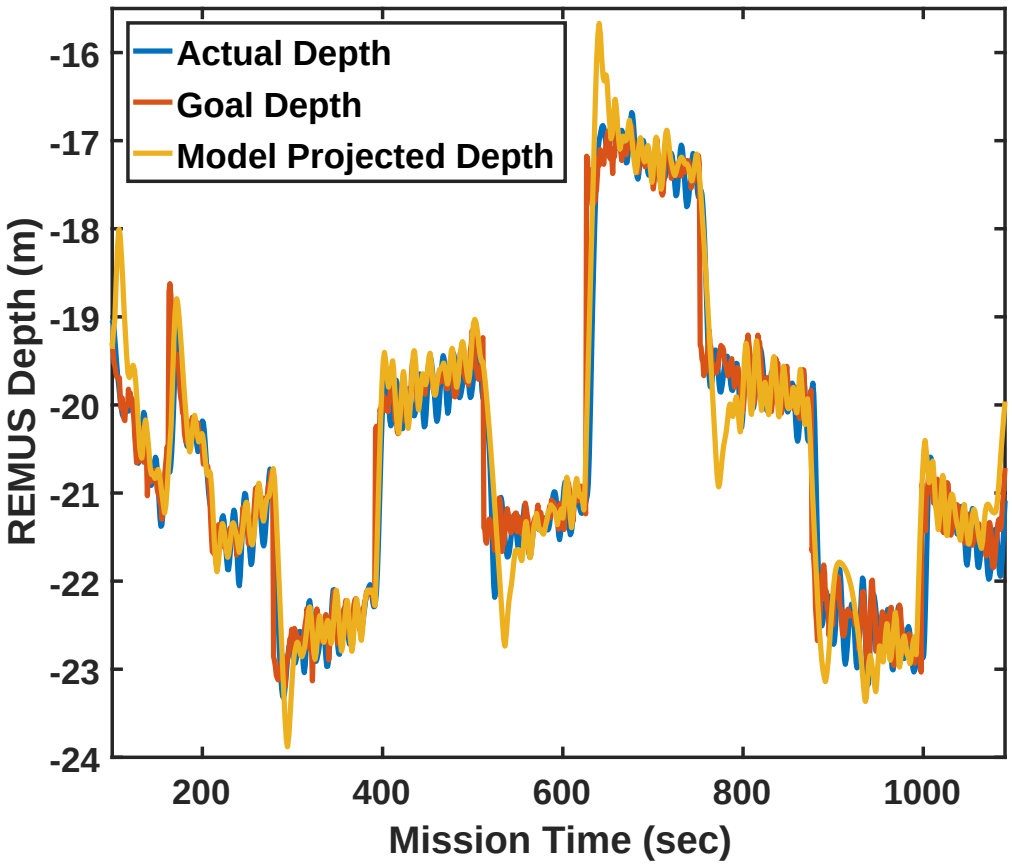

Figure 4.7. REMUS Real World vs. Modeled Behavior

In Figure 4.7, at the beginning of the plot, there is a noticeable difference between the REMUS vehicle's actual depth and the model's depth. Many of the initialization considerations that applied to the CTT disabled mission also apply to this CTT enabled mission. The vehicle velocity and flow over the dive fins do not heavily impact the actual and modeled vehicles' depth behavior in a CTT enabled mission. The actual and modeled vehicles are able to achieve the commanded depth faster than CTT disabled vehicles. There is a slight overshoot of the commanded depth by the modeled REMUS vehicle due to the implementation of a less efficient depth controller. This overshoot may be corrected by a closer tuning of the depth controller in the model. The model implemented bang/bang control of the VCTTs which is an energy inefficient implementation of a controller but closely represented the VCTT behavior of the actual REMUS vehicle.

Through performing a sensitivity analysis, it was determined that the mean of the error between the real world REMUS behavior and the model behavior was 8.8 cm with a standard deviation of 43.4 cm. This error calculation was for the entire thousand second mission.

The verification experiments of the model's depth control proved that the equations and controllers utilized in the 3DOF model provided a high fidelity representation of the depth behavior of a REMUS vehicle. This model can be used to simulate the M, X, and Z-direction behaviors of a REMUS vehicle. It can be useful in determining a successful docking strategy and optimal docking trajectory. This model can also aid in the design of future docking stations by providing designers an accurate representation of the vehicle's depth control. Docking station capture cages can now be designed to ensure the maximum probability of the vehicle successfully docking based on the selected docking strategies and trajectories.

CHAPTER 5:
6DOF Model Development

Once a 3DOF model of an AUV was designed, the research was expanded to create a 6DOF model for a REMUS vehicle operating at various speeds with CTTs. The 6DOF model presented in this chapter includes the equations and coefficients calculated in Chapter 2, but also includes equations and coefficients presented by [7] and [8].

5.1 Equations of Motion

The assumptions found in Chapter 2 were also used for the 6DOF model. One added assumption for the 6DOF model is that roll of the REMUS vehicle is negligible. This assumption reduces the computational burden of one degree of freedom. This assumption is valid because the roll of a REMUS vehicle varies between -3 to 3 degrees in a normal mission. This is a slight difference in roll angle and the variation does not appreciably effect the vehicle's overall behavior. The reference frames presented in Chapter 2 are also used in the development of the 6DOF model. A detailed derivation of the 6DOF model equations is provided in [2] and [12].

Surge Equation

Table 5.1. 6DOF Surge Equation Hydrodynamic Coefficients

Coefficients	Description	Value	Units
$X_{u\|u\|}$	Axial-Flow Drag Coefficient	-12.4759	$\frac{kg}{m}$
$X_{\dot{u}}$	Added Mass Coefficient	-0.930	kg
X_{wq}	Added Mass Cross-Term Coefficient	-77.8	$\frac{kg}{rad}$
X_{qq}	Added Mass Cross-Term Coefficient	-1.93	$\frac{kg \cdot m}{rad}$
X_{vr}	Added Mass Cross-Term Coefficient	35.5	$\frac{kg}{rad}$
X_{rr}	Added Mass Cross-Term Coefficient	-1.93	$\frac{kg \cdot m}{rad}$

The following equations derive the summation of forces acting in the X-direction on the vehicle. These forces are a summation of hydrostatic, added mass, hydrodynamic, and propeller forces.

$$\sum X = X_{HS} + X_A + X_{HD} + X_P \tag{5.1}$$

$$\sum X = -(W - B)\sin(\theta) + X_{u|u|}u|u| + X_{\dot{u}}\dot{u} + X_{wq}wq + X_{qq}q^2 + X_{vr}vr + X_{rr}r^2 + (1 - \tau_p)T_{n|n|}n|n| \tag{5.2}$$

The propeller force is simplified to a single variable, $F_{Propeller}$, which is a function of propeller RPM.

$$(1 - \tau_p)T_{n|n|}n|n| = F_{Propeller} \tag{5.3}$$

The alternate force equation is now:

$$\sum X = -(W - B)sin(\theta) + X_{u|u|}u|u| + X_{\dot{u}}\dot{u} + X_{wq}wq + X_{qq}q^2 + X_{vr}vr + X_{rr}r^2 + F_{Propeller} \tag{5.4}$$

Sway Equation

Table 5.2. 6DOF Sway Equation Hydrodynamic Coefficients

Coefficients	Description	Value	Units
Y_{uv}	Body Lift Force and Fin Lift Coefficient	-28.6	$\frac{kg}{m}$
$Y_{v\|v\|}$	Cross-Flow Drag Coefficient	-2850	$\frac{kg}{m}$
$Y_{r\|r\|}$	Cross-Flow Drag Coefficient	0.632	$\frac{kg \cdot m}{rad^2}$
$Y_{\dot{v}}$	Added Mass Coefficient	-77.8	kg
$Y_{\dot{r}}$	Added Mass Coefficient	4.16	$\frac{kg \cdot m}{rad}$
Y_{ur}	Added Mass Cross-Term and Fin Lift Coefficient	5.22	$\frac{kg}{rad}$
$Y_{uu\delta_r}$	Fin Lift Force Coefficient	9.64	$\frac{kg}{m \cdot rad}$

The following equations derive the summation of forces acting in the Y-direction on the vehicle. These forces are a summation of hydrostatic, added mass, hydrodynamic, lift, and horizontal cross-tunnel thruster forces.

$$\sum Y = Y_{HS} + Y_A + Y_{HD} + Y_L + Y_{CTT} \tag{5.5}$$

$$\begin{aligned}\sum Y = {} & (W - B)\cos\theta \sin\phi + Y_{uv}uv + Y_{v|v|}v|v| + Y_{r|r|}r|r| + Y_{\dot{v}}\dot{v} + Y_{\dot{r}}\dot{r} \\ & + Y_{ur}ur + Y_{wp}wp + Y_{pq}pq + Y_{uu\delta_r}u^2\delta_r + F_{horizontal-CTT,fwd} + F_{horizontal-CTT,aft}\end{aligned} \tag{5.6}$$

Since vehicle roll is assumed to be 0, the sway equation can be simplified to the following:

$$\begin{aligned}\sum Y = {} & Y_{uv}uv + Y_{v|v|}v|v| + Y_{r|r|}r|r| + Y_{\dot{v}}\dot{v} + Y_{\dot{r}}\dot{r} + Y_{ur}ur \\ & + Y_{uu\delta_r}u^2\delta_r + F_{horizontal-CTT,fwd} + F_{horizontal-CTT,aft}\end{aligned} \tag{5.7}$$

Heave Equation

Table 5.3. 6DOF Heave Equation Hydrodynamic Coefficients

Coefficients	Description	Value	Units
$Z_{\dot{w}}$	Added Mass Coefficient	-77.8	kg
$Z_{\dot{q}}$	Added Mass Coefficient	-4.16	$\frac{kg \cdot m}{rad}$
Z_{uq}	Added Mass Cross-Term and Fin Lift Coefficient	-12.22	$\frac{kg}{rad}$
$Z_{q\|q\|}$	Cross Flow Drag Coefficient	-0.632	$\frac{kg \cdot m}{rad^2}$
Z_{uw}	Body Lift Force and Fin Lift Coefficient	-28.6	$\frac{kg}{m}$
$Z_{w\|w\|}$	Cross-Flow Drag Coefficient	-185.621	$\frac{kg}{m}$
$Z_{uu\delta_s}$	Fin Lift Force Coefficient	-21.37	$\frac{kg}{m \cdot rad}$

The following equations derive the summation of forces acting in the Z-direction on the vehicle. These forces are a summation of hydrostatic, added mass, hydrodynamic, lift, and vertical cross-tunnel thruster forces.

$$\sum Z = Z_{HS} + Z_A + Z_{HD} + Z_L + Z_{CTT} \tag{5.8}$$

$$\begin{aligned}\sum Z = {} & (W - B)\cos\theta\cos\phi + Z_{\dot{w}}\dot{w} + Z_{\dot{q}}\dot{q} + Z_{uq}uq + Z_{vp}vp + Z_{rp}rp \\ & + Z_{w|w|}w|w| + Z_{q|q|}q|q| + Z_{uw}uw + Z_{uu\delta_s}u^2\delta_s + F_{vert-CTT,fwd} + F_{vert-CTT,aft}\end{aligned} \tag{5.9}$$

It is assumed that the two vertical cross-tunnel thrusters can be treated as a single force acting in the Z-Direction:

$$F_{vert-CTT,fwd} + F_{vert-CTT,aft} = F_{vert-CTT,Total} \tag{5.10}$$

The modified heave equation is now:

$$\sum Z = (W - B)\cos\theta\cos\phi + Z_{\dot{w}}\dot{w} + Z_{\dot{q}}\dot{q} + Z_{uq}uq + Z_{vp}vp + Z_{rp}rp + Z_{w|w|}w|w| + Z_{q|q|}q|q| + Z_{uw}uw + Z_{uu\delta_s}u^2\delta_s + F_{vert-CTT,Total} \quad (5.11)$$

Since vehicle roll is assumed to be 0 in this model, the heave equation can be further simplified to the following:

$$\sum Z = (W - B)\cos\theta + Z_{\dot{w}}\dot{w} + Z_{\dot{q}}\dot{q} + Z_{uq}uq + Z_{w|w|}w|w| + Z_{q|q|}q|q| + Z_{uw}uw + Z_{uu\delta_s}u^2\delta_s + F_{vert-CTT,Total} \quad (5.12)$$

Roll Equation

The following equations derive the summation of moments contributing to the roll of the vehicle. These moments are a summation of hydrostatic, added mass, hydrodynamic, and propeller moments.

$$\sum K = K_{HS} + K_A + K_{HD} + K_P \quad (5.13)$$

For a full 6DOF model, the sum of the moments for roll would be defined by the following equation:

$$\sum K = -z_G W\cos\theta\sin\phi + K_{\dot{p}}\dot{p} + K_{p|p|}p|p| + Q_{n|n|}n|n| \quad (5.14)$$

However, for a torpedo shaped vehicle such as the REMUS, roll can be assumed to be negligible in most circumstances. Therefore, the sum of roll moments for the model presented in this research is represented by the following equation:

$$\sum K = O \quad (5.15)$$

Pitch Equation

Table 5.4. 6DOF Pitch Equation Hydrodynamic Coefficients

Coefficients	Description	Value	Units
$M_{\dot{q}}$	Added Mass Coefficient	-30	$\frac{kg \cdot m^2}{rad}$
$M_{q\|q\|}$	Cross-Flow Drag Coefficient	-188	$\frac{kg \cdot m^2}{rad^2}$
$M_{\dot{w}}$	Added Mass Coefficient	-4.16	$kg \cdot m$
M_{uw}	Body and Fin Lift and Munk Moment Coefficient	24.0	kg
M_{uq}	Add Mass Cross Term and Fin Lift Coefficient	-10.00	$\frac{kg \cdot m}{rad}$
$M_{w\|w\|}$	Cross-Flow Drag Coefficient	4.00357	kg
$M_{uu\delta_s}$	Fin Lift Moment Coefficient	-22.3855	$\frac{kg}{rad}$

The following equations derive the summation of moments contributing to the pitch of the vehicle. These moments are a summation of hydrostatic, added mass, hydrodynamic, lift, and cross-tunnel thruster moments.

$$\sum M = M_{HS} + M_A + M_{HD} + M_L + M_{CTT} \tag{5.16}$$

$$\begin{aligned}\sum M = &-z_G W \sin\theta + M_{\dot{w}}\dot{w} + M_{\dot{q}}\dot{q} + M_{uw}uw + M_{vp}vp + M_{rp}rp \\ &+ M_{uq}uq + M_{w|w|}w|w| + M_{q|q|}q|q| + M_{uu\delta_s}u^2\delta_s + T_{vert-CTT,aft} + T_{vert-CTT,fwd}\end{aligned} \tag{5.17}$$

The vertical thrusters are assumed to be equidistant from the center of buoyancy and are also assumed to be receiving the same RPM command. The reasoning for this assumption is found in Chapter 2 in the Pitch Equation subsection. Therefore,

$$T_{vert-CTT,aft} = -T_{vert-CTT,fwd} \tag{5.18}$$

The total vertical thruster torque is equal to a linear combination of the forward and aft

vertical thruster torques.

$$T_{vert-CTT,Total} = T_{vert-CTT,aft} + T_{vert-CTT,fwd} = 0 \tag{5.19}$$

This results in the following moment equation:

$$\sum M = -z_G W \sin\theta + M_{\dot{w}}\dot{w} + M_{\dot{q}}\dot{q} + M_{uw}uw + M_{vp}vp + M_{rp}rp + M_{uq}uq + M_{w|w|}w|w| + M_{q|q|}q|q| + M_{uu\delta_s}u^2\delta_s \tag{5.20}$$

Considering that roll is negligible for the REMUS vehicle, the pitch equation can be further simplified to the following:

$$\sum M = -z_G W \sin\theta + M_{\dot{w}}\dot{w} + M_{\dot{q}}\dot{q} + M_{uw}uw + M_{uq}uq + M_{w|w|}w|w| + M_{q|q|}q|q| + M_{uu\delta_s}u^2\delta_s \tag{5.21}$$

Pitch Behavior Parameter

It was found during the creation and verification of the 6DOF model that the righting force that stabilizes pitch of the REMUS 100 was too weak to counteract the impact of the cross-term coefficients in the equations of motion. To correct this error, a new coefficient was introduced called the pitch behavior parameter, M_{PB}. This parameter represents the vehicle's inherent tendency to return its pitch to a trim position. This inherent behavior is a result of the center of gravity being positioned below the vehicle's center of buoyancy. Whenever the vehicle's center of gravity is disturbed to a position other than directly under the center of buoyancy, the vehicle witnesses a large correcting moment that returns it to a trim position. Previous models didn't adequately simulate this rapid increase in pitching moment that forcefully and abruptly positions the vehicle to a trim position.

One explanation for the use M_{PB} is that 6DOF equations for pitching may have an error

in the $-z_G W \sin\theta$ term. This term only takes into account the force caused by the weight of the vehicle (W) and the righting moment arm. However, other studies on underwater vehicles show that the buoyancy force (B) has a substantial impact on the righting moment of an underwater vehicle, illustrated in Figures 5.1 and 5.2.

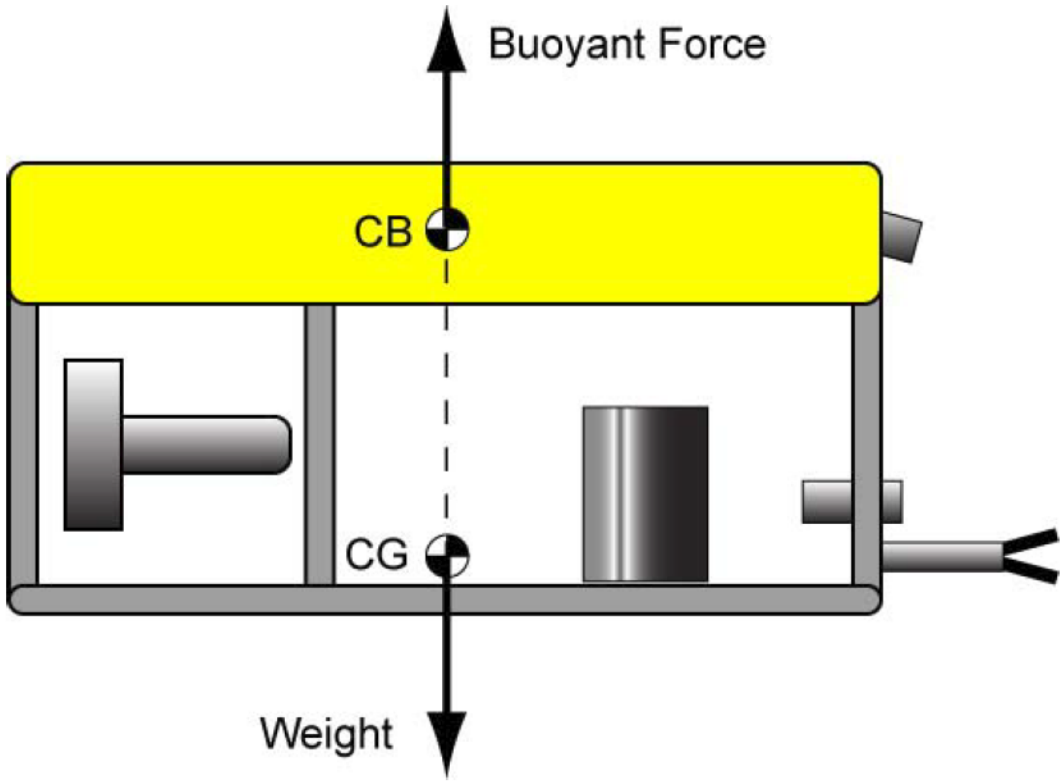

Figure 5.1. Center of Gravity (CG) and Center of Buoyancy (CB) in Equilibrium (Vehicle at Trim). Source: [16].

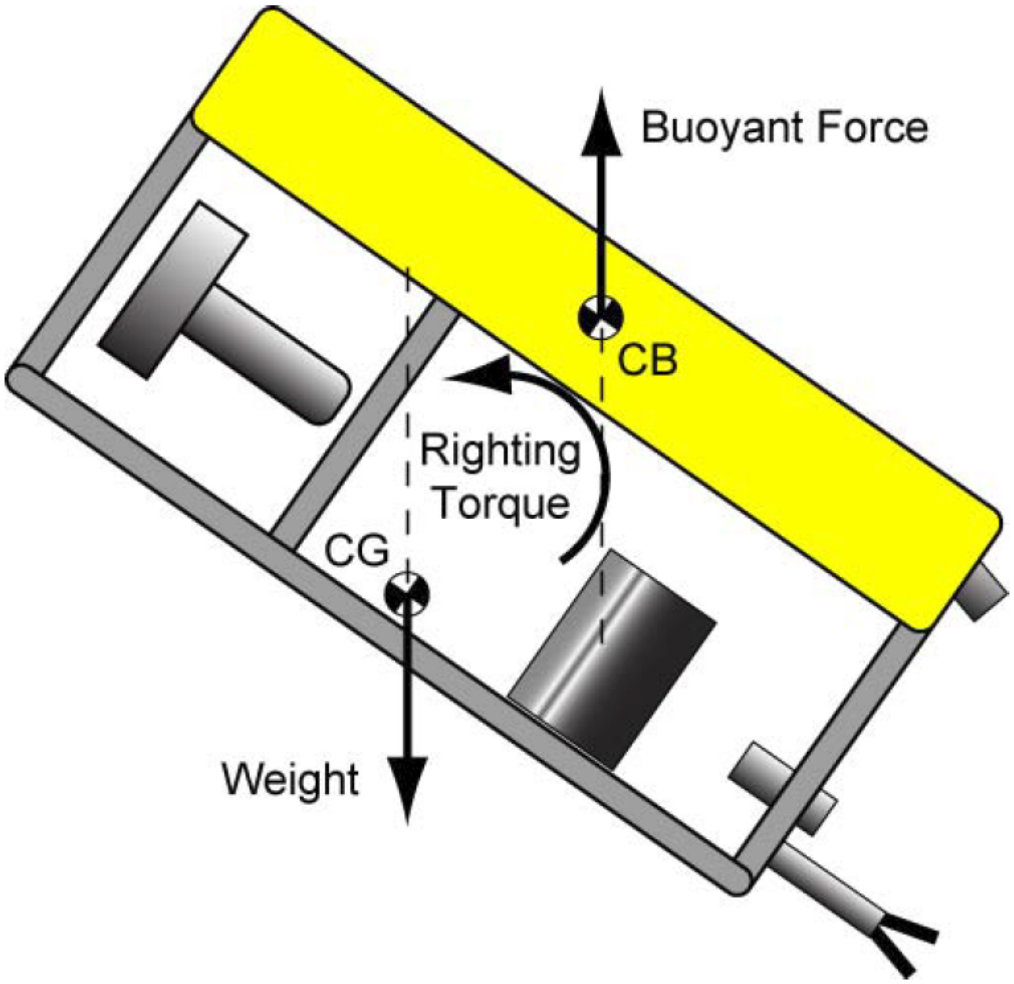

Figure 5.2. Weight and Buoyancy Working Together to Return the Vehicle to Trim. Source: [16].

If buoyancy force (B) does have the effect that is expressed in Figure 5.2, the $-z_G W \sin\theta$ term should be changed to $-z_G(W + B)\sin\theta$. This will more than double the righting moment caused by pitch of vehicle (θ). Also, there is speculation that the distance between center of gravity and center of buoyancy (z_G) is four to five times larger than the 1.96 cm defined by previous models. The largest z_G possible is the REMUS vehicle's diameter, 19.05 cm. When considering a maximum z_G and an influence of buoyancy force, there is the potential of increasing the magnitude of righting moment up to 18 times the original value. However, even with maximum z_G and the addition of buoyancy force to the model,

the model still does not have the righting moment behavior that is witnessed in the real world. There is possible influence from the long length and construction of the REMUS vehicle, as well as its distribution of ballast along this entire length, that creates an even stronger righting moment. The proposed moment equation with the buoyancy force taking part in the righting moment is:

$$\sum M = -z_G(W+B)\sin\theta + M_{\dot{w}}\dot{w} + M_{\dot{q}}\dot{q} + M_{uw}uw + M_{uq}uq + M_{w|w|}w|w| + M_{q|q|}q|q| + M_{uu\delta_s}u^2\delta_s \quad (5.22)$$

A simple experiment only needs to be performed to comprehend and grasp the importance of this trim correcting moment. If the REMUS were placed submerged in a pool and shoved in any direction or to any angle of pitch, the vehicle will inherently and quickly return to its stable trim position. The REMUS was specifically designed so that it would return to trim without external forces during a disturbance. M_{PB} was developed and implemented to model this inherent and rapid righting moment. This research intended to utilize the equations of motion developed and adhered to by previous researchers, thus a gain of M_{PB} was introduced to the pitch equation. The influence of M_{PB} will greatly vary depending on the payload and the ballast of the vehicle. Based on behavior witnessed in experimental tests and through verification with the 6DOF model, the NPS REMUS vehicles have a $M_{PB} \approx 50$. $M_{PB} = 50$ was utilized in the 3DOF and 6DOF models and the parameter can be seen in the corrected pitch equation, Equation 5.23. Further study and analysis of the pitch equation and pitch behavior is required to fully correct the 6DOF model.

$$\sum M = -M_{PB}z_G W\sin\theta + M_{\dot{w}}\dot{w} + M_{\dot{q}}\dot{q} + M_{uw}uw + M_{uq}uq + M_{w|w|}w|w| + M_{q|q|}q|q| + M_{uu\delta_s}u^2\delta_s \quad (5.23)$$

Yaw Equation

Table 5.5. 6DOF Yaw Equation Hydrodynamic Coefficients

Coefficients	Description	Value	Units
$N_{\dot{v}}$	Added Mass Coefficient	4.16	$kg \cdot m$
$N_{\dot{r}}$	Added Mass Coefficient	4.88	$\frac{kg \cdot m^2}{rad}$
N_{uv}	Body and Fin Lift and Munk Moment Coefficient	-24	kg
N_{ur}	Added Mass Cross-Term and Fin Lift Coefficient	-2	$\frac{kg \cdot m}{rad}$
$N_{v\|v\|}$	Cross-Flow Drag Coefficient	-3.18	kg
$N_{r\|r\|}$	Cross-Flow Drag Coefficient	-245	$\frac{kg \cdot m^2}{rad^2}$
$N_{uu\delta_r}$	Fin Lift Moment Coefficient	-22.3855	$\frac{kg}{rad}$

The following equations derive the summation of moments contributing to the yaw of the vehicle. These moments are a summation of hydrostatic, added mass, hydrodynamic, lift, and cross-tunnel thruster moments.

$$\sum N = N_{HS} + N_A + N_{HD} + N_L + N_{CTT} \tag{5.24}$$

$$\begin{aligned}\sum N = {} & N_{\dot{v}}\dot{v} + N_{\dot{r}}\dot{r} + N_{uv}uv + N_{wp}wp + N_{pq}pq + N_{ur}ur \\ & + N_{v|v|}v|v| + N_{r|r|}r|r| + N_{uu\delta_r}u^2\delta_r + T_{horizontal-CTT,aft} + T_{horizontal-CTT,fwd}\end{aligned} \tag{5.25}$$

Finally, since roll is negligible for the REMUS vehicle, the yaw equation can be further simplified to the following:

$$\begin{aligned}\sum N = {} & N_{\dot{v}}\dot{v} + N_{\dot{r}}\dot{r} + N_{uv}uv + N_{ur}ur \\ & + N_{v|v|}v|v| + N_{r|r|}r|r| + N_{uu\delta_r}u^2\delta_r + T_{horizontal-CTT,aft} + T_{horizontal-CTT,fwd}\end{aligned} \tag{5.26}$$

Vehicle Hydrodynamics, Added Mass, and Thrust Coefficients

Chapter 2 provides a derivation of the specific coefficients needed to model the REMUS vehicles owned by the CAVR. These are the vehicles that are used for the verification of the 6DOF model. For a more detailed derivation of the coefficients used in the 6DOF model, please refer to [1], [7], and [8]. A list of all coefficients used in both the 3DOF and 6DOF models are provided in the appendix.

5.2 Conclusion

The 6DOF model is inherently more complex than the 3DOF model due to the cross-coupling terms in the equations of motion. This research started with the development of a 3DOF model to ensure that each term in these equations were understood and correct values for the coefficients were used. Once the equations were analyzed and the correct values were selected, a 6DOF model that accurately represented the vehicles used by the CAVR was created. The six equations represented in this model are highly impacted by each other. Changing a cross-coupling coefficient in one equation may have large residual effects in others. Each manipulation of an equation or coefficient must be critiqued in a manner that takes into account the changes that will occur to the model as a whole.

CHAPTER 6:
6DOF Computer Model

The 6DOF model presented in this chapter is an extension of the 3DOF model in Chapter 3. However, there are some key differences and increased sophistication in the 6DOF model. The graphics and discussion are included in this thesis to provide a more in-depth understanding of the 6DOF model for future researchers and will be of assistance to any verification process that is to be conducted on the 6DOF model.

6.1 Equations of Motion

As with the 3DOF model, the equations of motion are the backbone of the programming process. Understanding the cross-term hydrodynamic coefficients becomes increasingly important when scaling the model from a 3DOF to a 6DOF model. The implementation of the surge, sway, heave, roll, pitch, and yaw equations are seen in Figures 6.1, 6.2, 6.3, 6.4, 6.5, and 6.6.

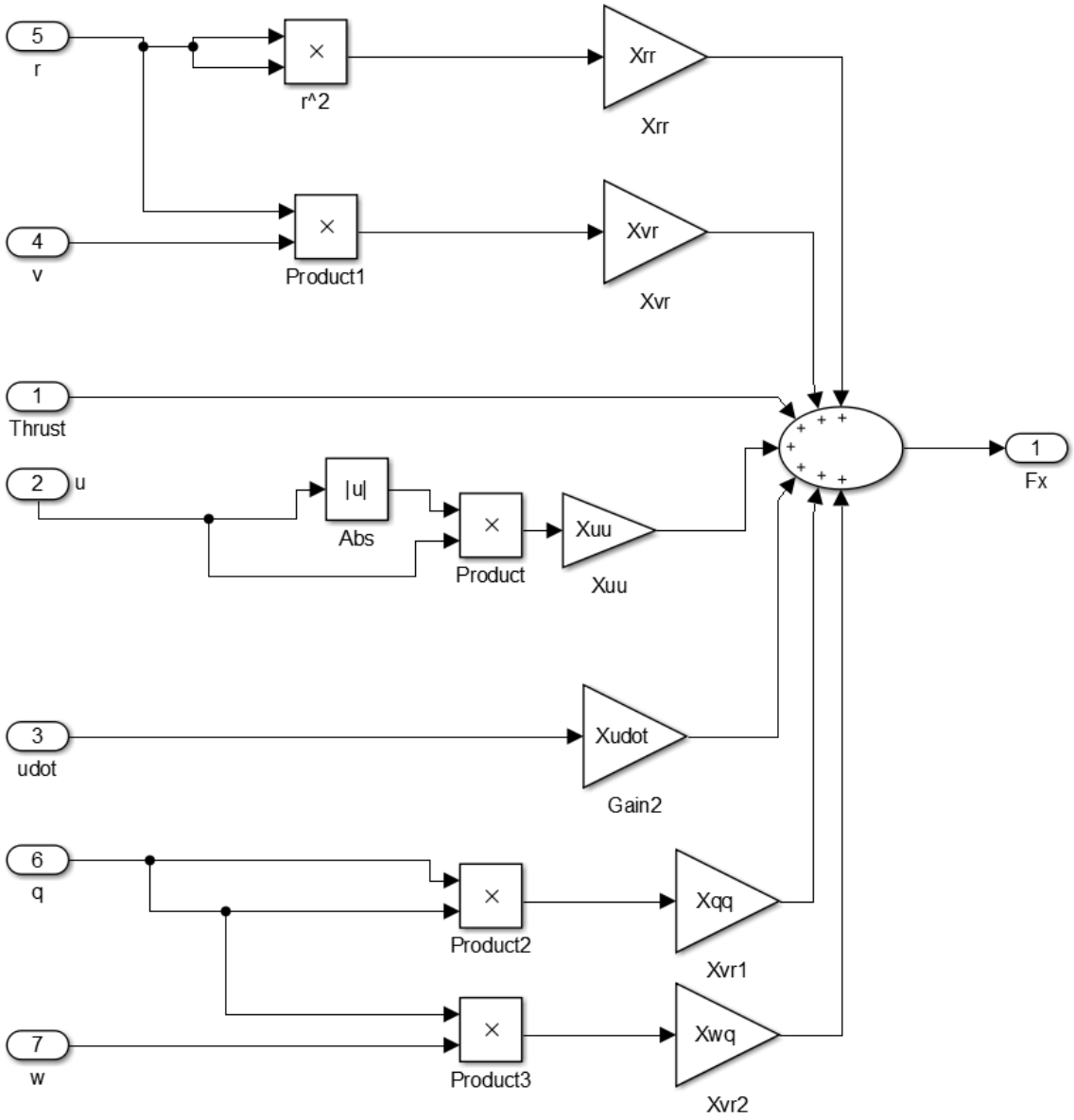

Figure 6.1. 6DOF Surge Equation

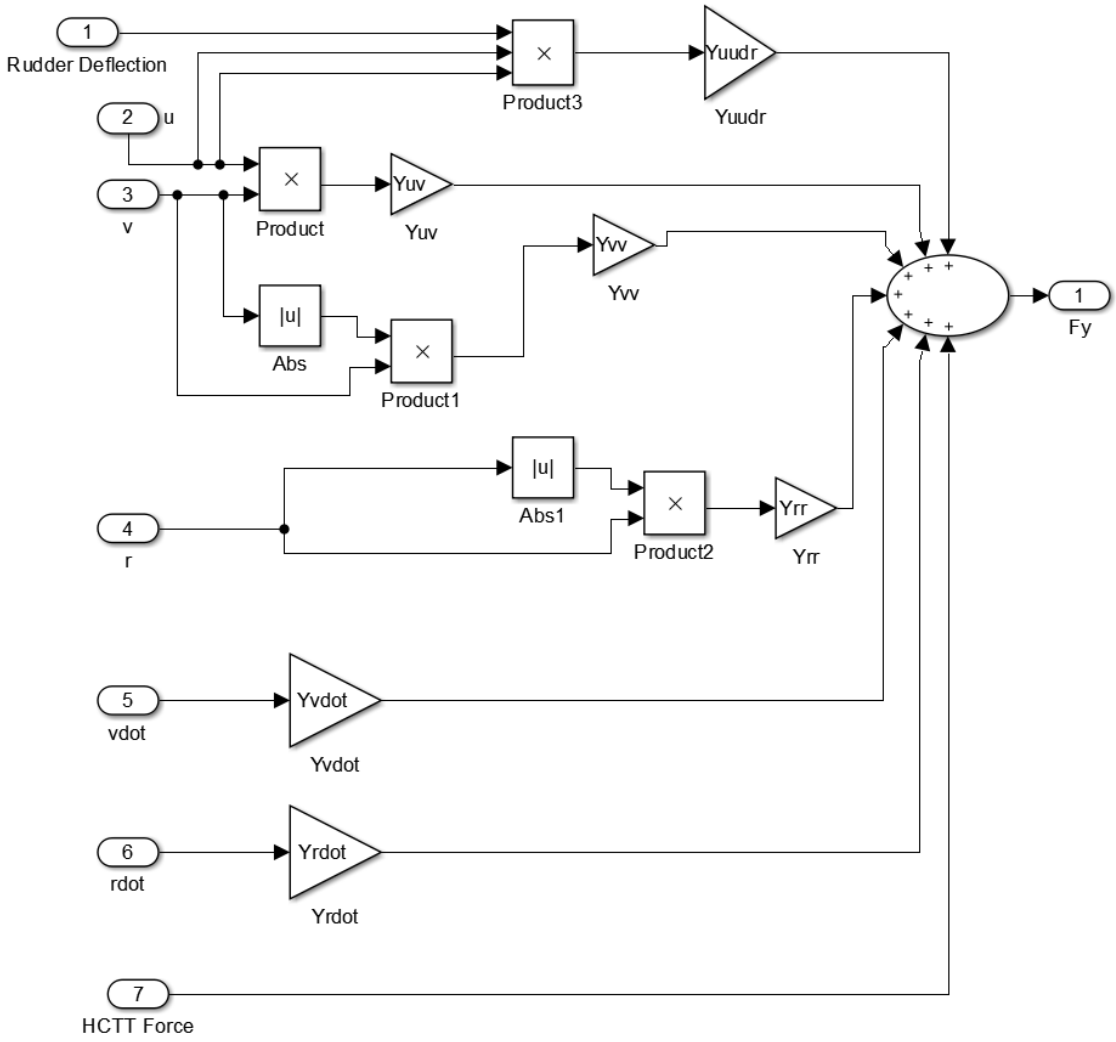

Figure 6.2. 6DOF Sway Equation

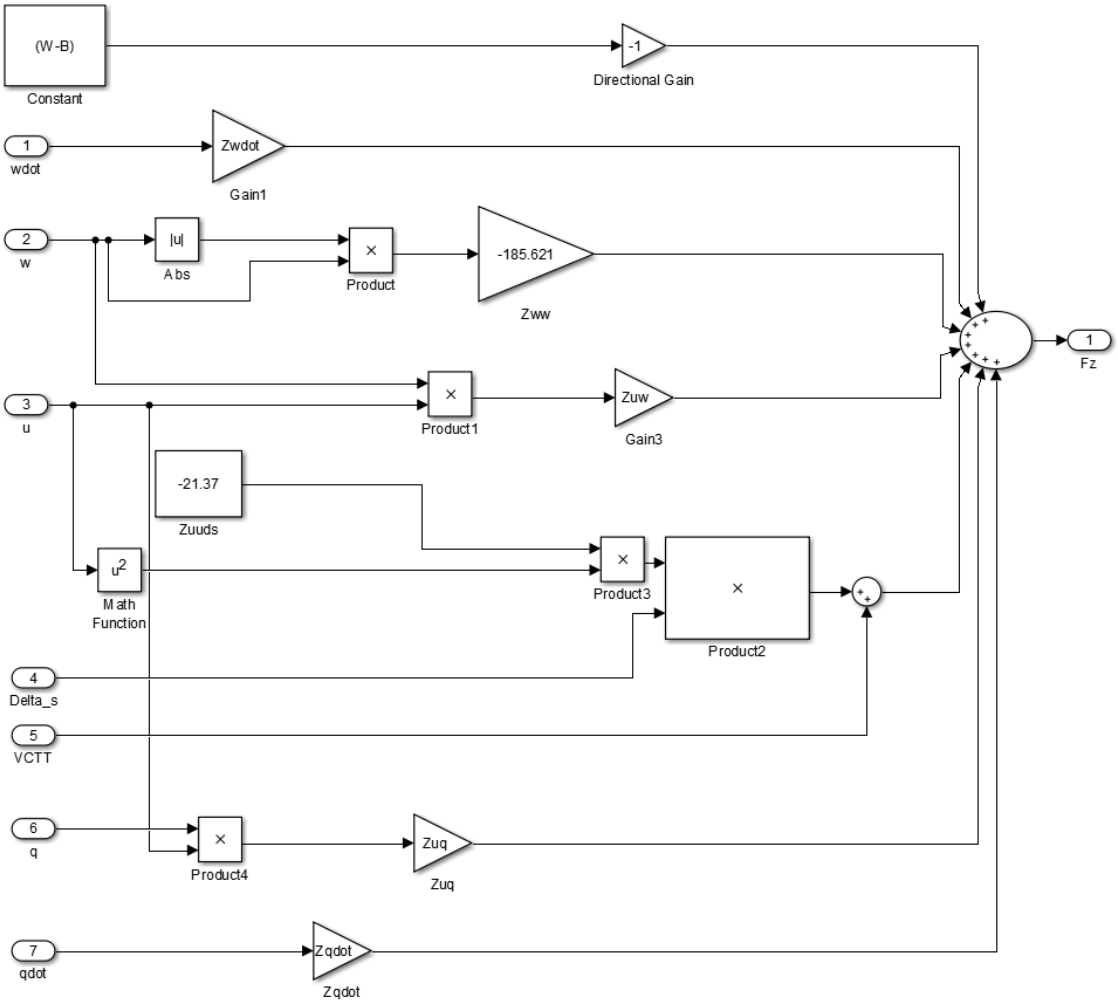

Figure 6.3. 6DOF Heave Equation

Figure 6.4. 6DOF Roll Equation

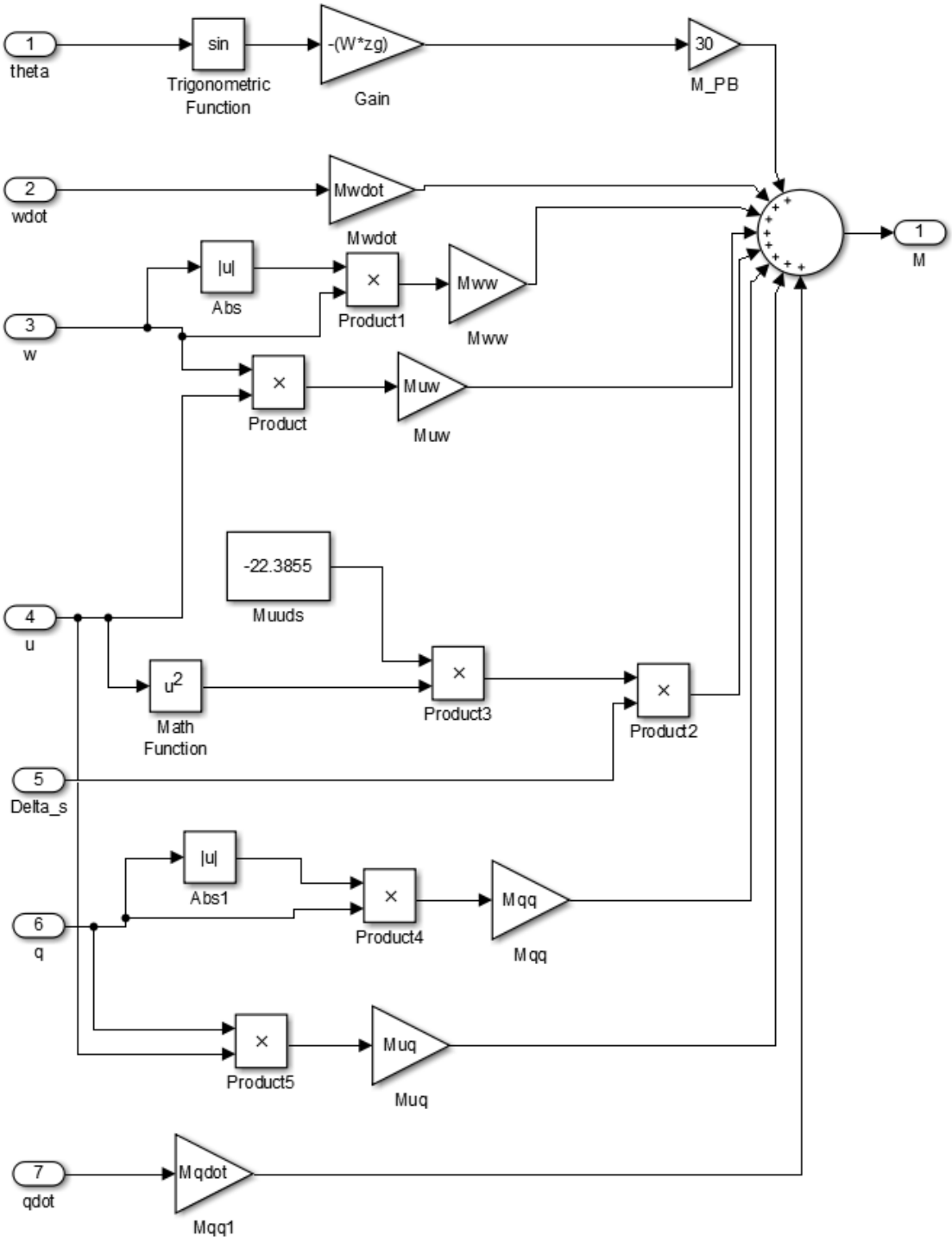

Figure 6.5. 6DOF Pitch Equation

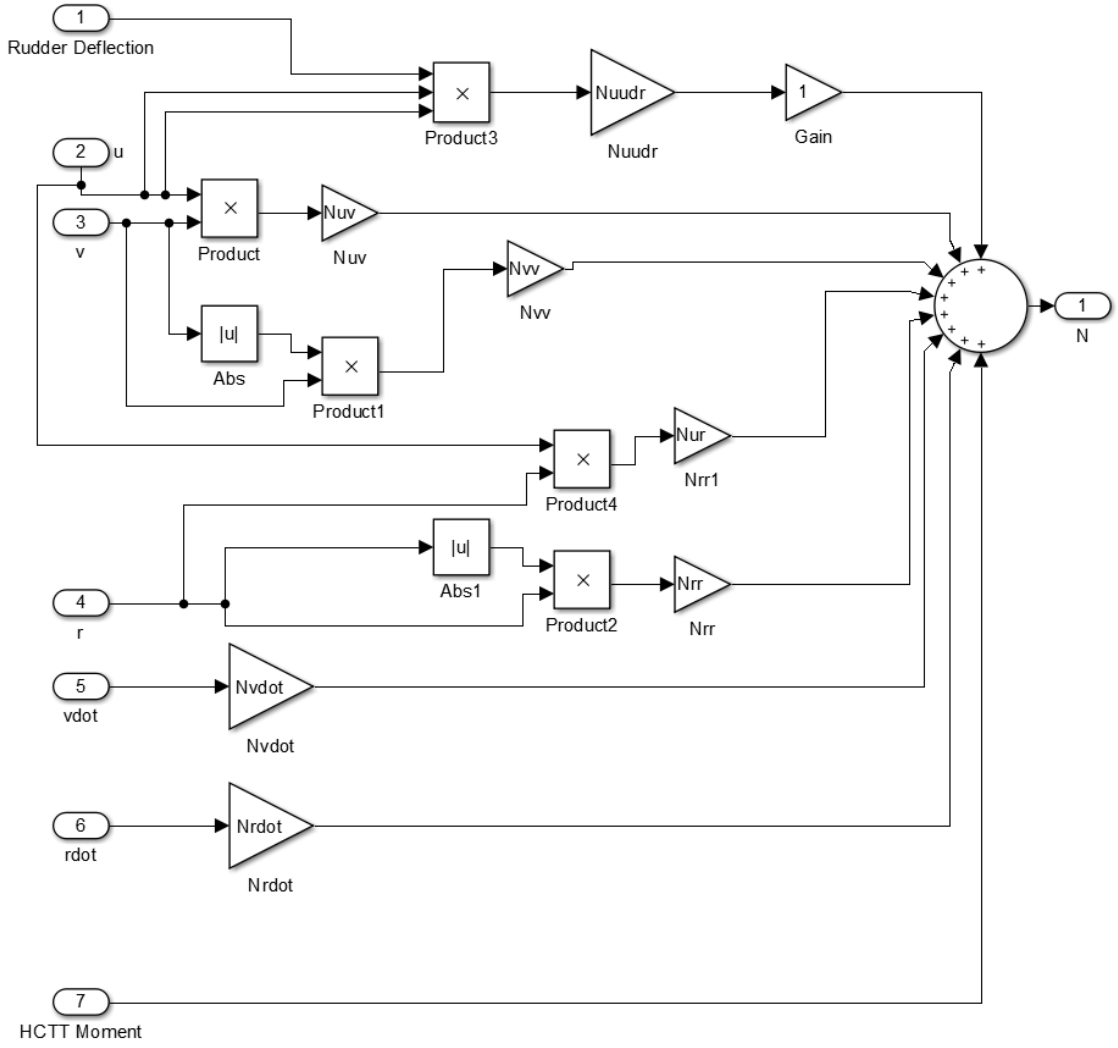

Figure 6.6. 6DOF Yaw Equation

6.2 Model Transformations

Similar to the 3DOF model, the forces acting on the body had to be converted to positions, velocities, and accelerations in the flat earth global reference frame. There is a 6DOF function block in the MATLAB Simulink Aerospace Toolbox that transforms the outputs of the equations of motion to positions, velocities, and accelerations in the flat earth global reference frame. The inputs and outputs associated with the 6DOF function block are seen in Figure 6.7.

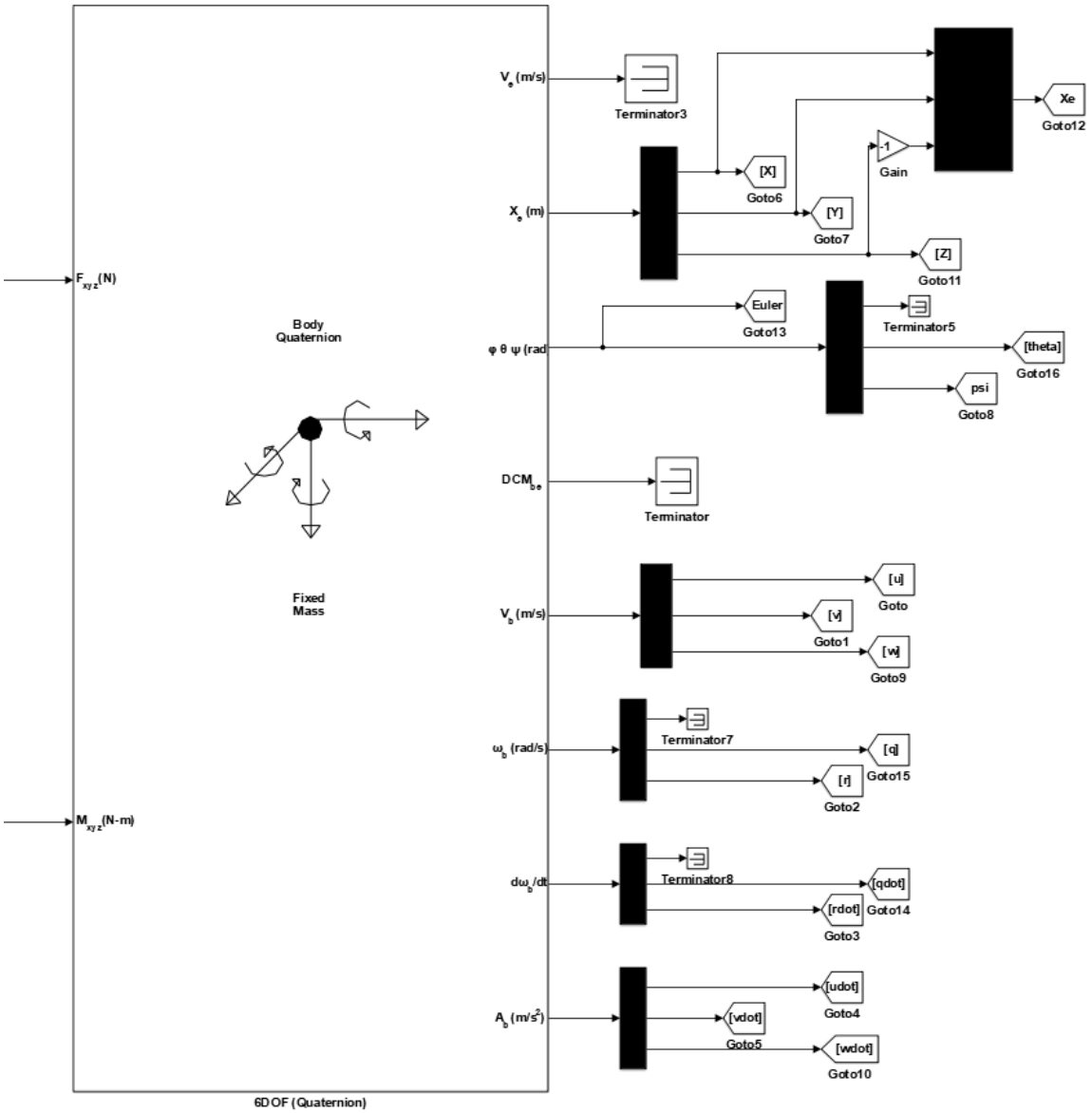

Figure 6.7. 6DOF Equations of Motion Transformed from Body Fixed to Flat Earth Global Reference Frame

6.3 Model Controllers and Issued Commands

The commands in Table 6.1 can be issued to the 6DOF vehicle model.

The command interface can be seen in Figure 6.8.

Table 6.1. 6DOF Model Commands

Command	**Range**	**Units**
Propeller Speed	0 to 2000	RPM
Depth	-50 to 0	Meters
Rudder Angle	-13.6 to 13.6	Degrees
Forward HCTT Speed	-5000 to 5000	RPM
Aft HCTT Speed	-5000 to 5000	RPM

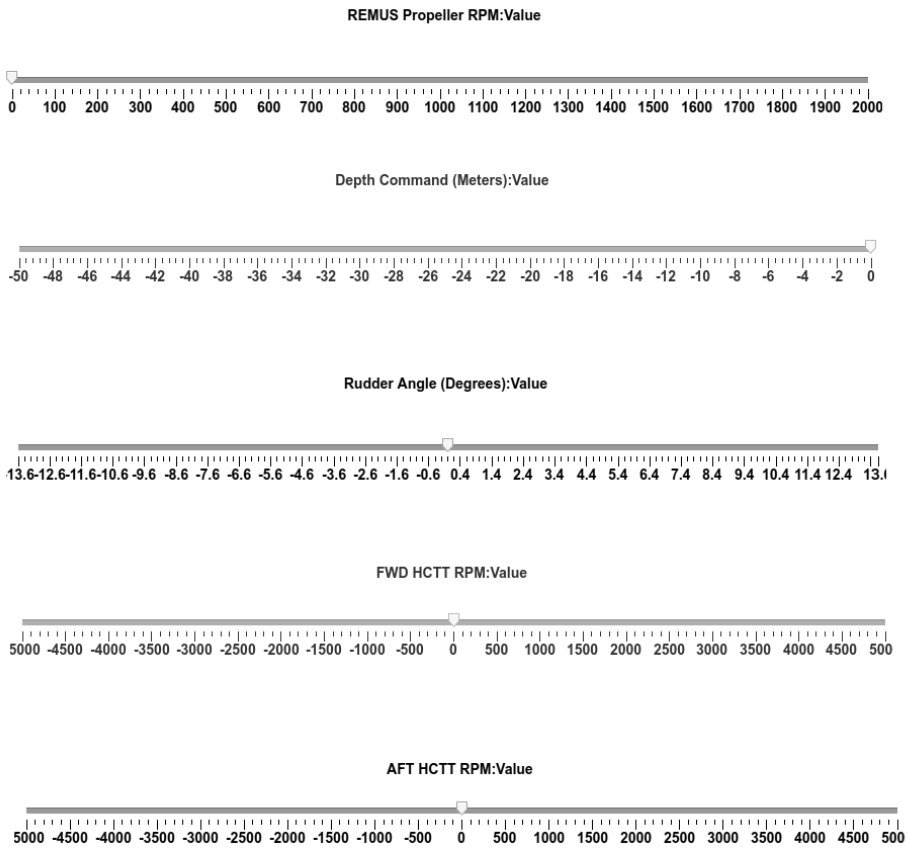

Figure 6.8. Command Interface for the 6DOF Hydrodynamic Model With Real Time User Specified Inputs (Set Here at 0 for All Parameters).

These commands were selected because direct control of these parameters aids in the verification process. The only command in the 6DOF model that utilizes controllers that simulate physical controllers on the REMUS vehicle is the depth command. Since the depth

controller was verified with high confidence in the 3DOF model, the same controller was utilized in the 6DOF model.

In an actual REMUS vehicle, the rudder angle and HCTT commands would be governed by a navigation/waypoint controller that would reduce the heading error of the vehicle attempting to achieve its next waypoint. This waypoint controller will need to be created and verified in further research. The RPM command in the physical REMUS vehicle is controlled by a speed controller. The scope of this research only includes the verification of the hydrodynamic model, but not the creation and verification of simulated controllers. To perform model verification, commands from a real world mission are sent to the 6DOF model, and the simulated vehicle's behavior is compared to the actual vehicle's behavior. The following experiments were used to verify the model's behavior in response to these issued commands:

1. Setting the rudder angle on the actual REMUS vehicle at various positions at a constant propeller RPM. The turn radius of the actual vehicle at various rudder angles and speeds is compared to the model's turn radius.
2. Importing real world REMUS propeller RPM and rudder angle data into the 6DOF model and comparing the vehicle's and model's speed.
3. Setting various amounts of differential thrust on the forward and aft HCTTs on the actual REMUS vehicle while in a hover. The rotation/yaw rate is then recorded for the actual vehicle. This differential HCTT thrust will then be applied to the model and the rotation/yaw rate will be compared to the real world data.
4. Real world vehicle propeller RPM, rudder angle, and depth commands are issued to the 6DOF model. The model's pitch is then compared to the REMUS vehicle's recorded pitch during the real wold mission.

The results for these verification experiments are presented in Chapter 7.

6.4 Complete 6DOF Model

The complete 6DOF hydrodynamic model presented in Figures 6.9, 6.10, 6.11, 6.12, and 6.13 represents a 6DOF variable speed hydrodynamic model of an AUV utilizing CTTs. This accurate model can be used to improve understanding of vehicle control for a wide variety of AUV operations in constrained environments, including terminal approach to a

docking station. Accurate 3DOF and 6DOF hydrodynamic models utilizing CTTs are an important capability for developing greater autonomy and enabling prolonged missions at sea.

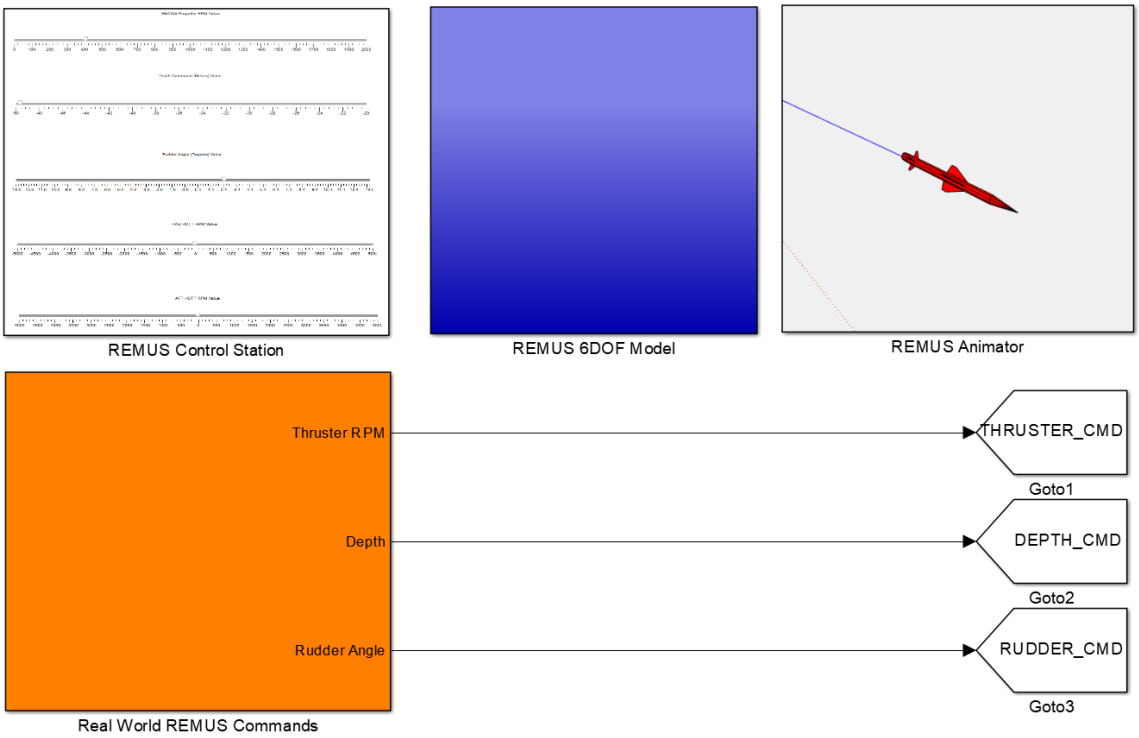

Figure 6.9. Complete 6DOF Variable Speed REMUS Model Utilizing Cross-Tunnel Thrusters with Animation Subsystem, Real World Command Import Subsystem, REMUS Model's Real Time Control Subsystem.

Figure 6.9 contains the REMUS Control Station (Figure 6.8), REMUS 6DOF Model(Figure 6.7), and the REMUS Animator. The REMUS Animator takes the outputs from the REMUS 6DOF Model and creates a 3D representation of a REMUS vehicle, with a fly along camera angle, so that vehicle behavior can be critiqued and analyzed. The Real World REMUS Command block imports commands recorded during a real world REMUS mission and sends those commands to the model at the same rate the actual vehicle received the commands.

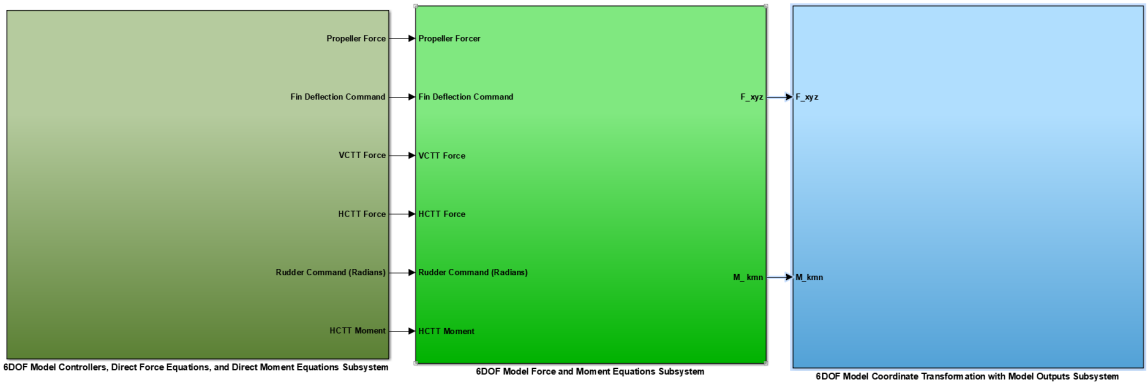

Figure 6.10. 6DOF Variable Speed REMUS Model Subsystems

Figure 6.10 shows the subsystems contained in the REMUS 6DOF Model block, previously seen in Figure 6.9. The left block in Figure 6.10 takes the imported Real World Commands, or the user defined REMUS Control Station commands, and translates them into inputs that the 6DOF equations of motion can utilize. The 6DOF Model Force and Moment Equations Subsystem, represented in Figure 6.12, contains the equations of motion represented in Figures 6.1, 6.2, 6.3, 6.4, 6.5, and 6.6. The 6DOF Model Coordinate Transformation with Model Outputs Subsystem, shown in Figure 6.13, contains the model's components that convert the force in body reference plane to position and motion in the flat earth reference frame. This transformation was shown in Figure 6.7.

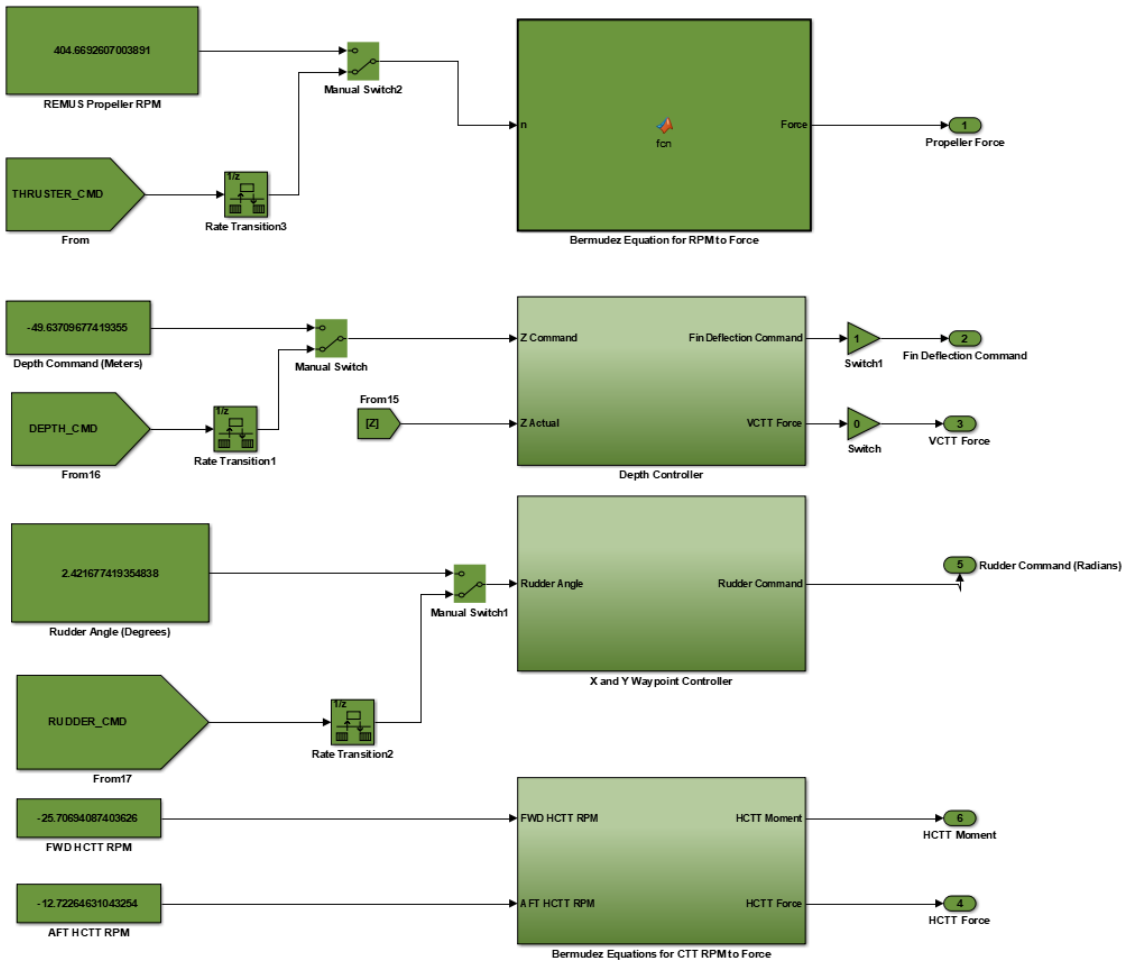

Figure 6.11. 6DOF Model Controllers, Direct Force Equations, and Direct Moment Equations Subsystem.

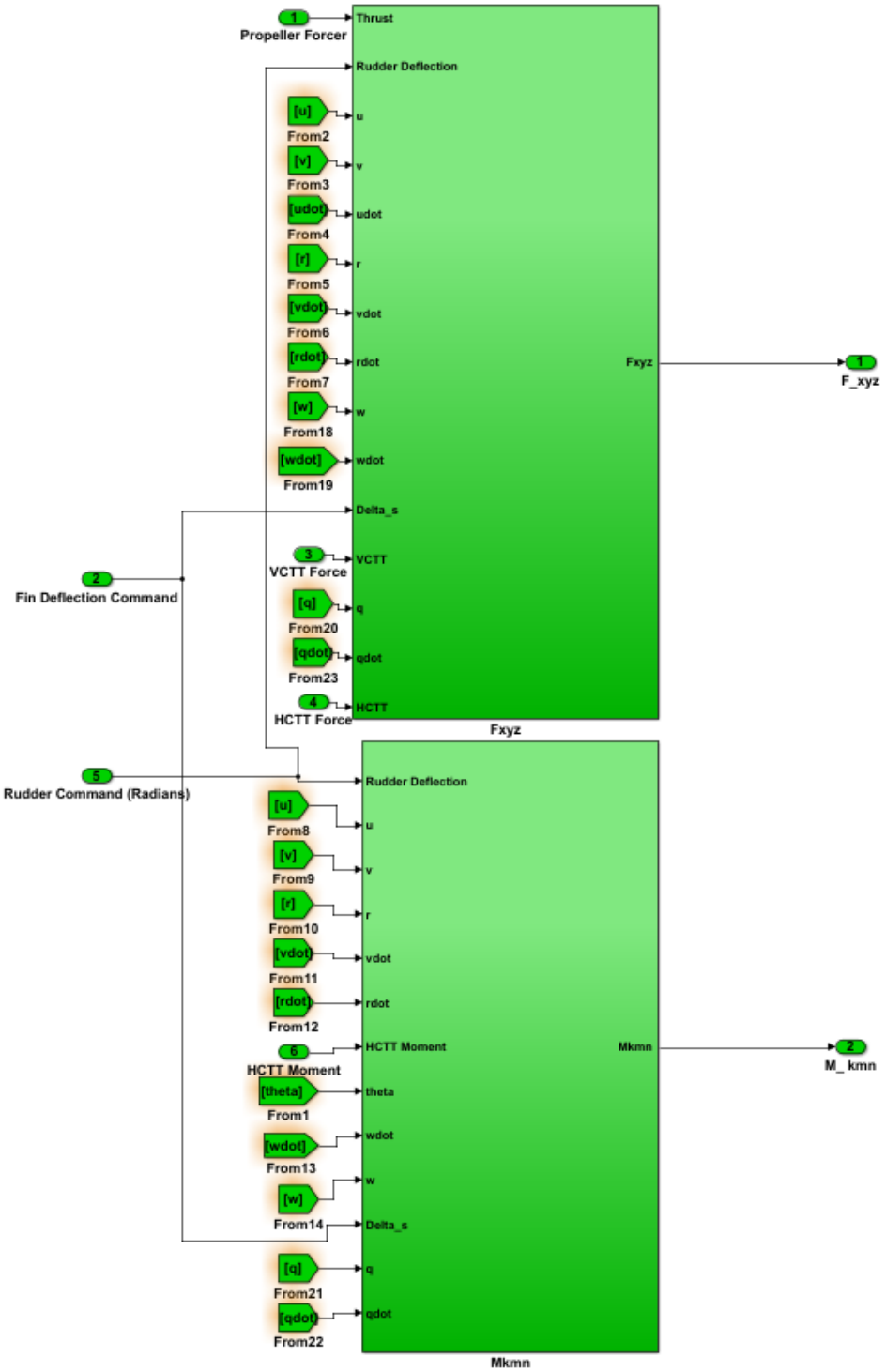

Figure 6.12. 6DOF Model Force and Moment Equations Subsystem.

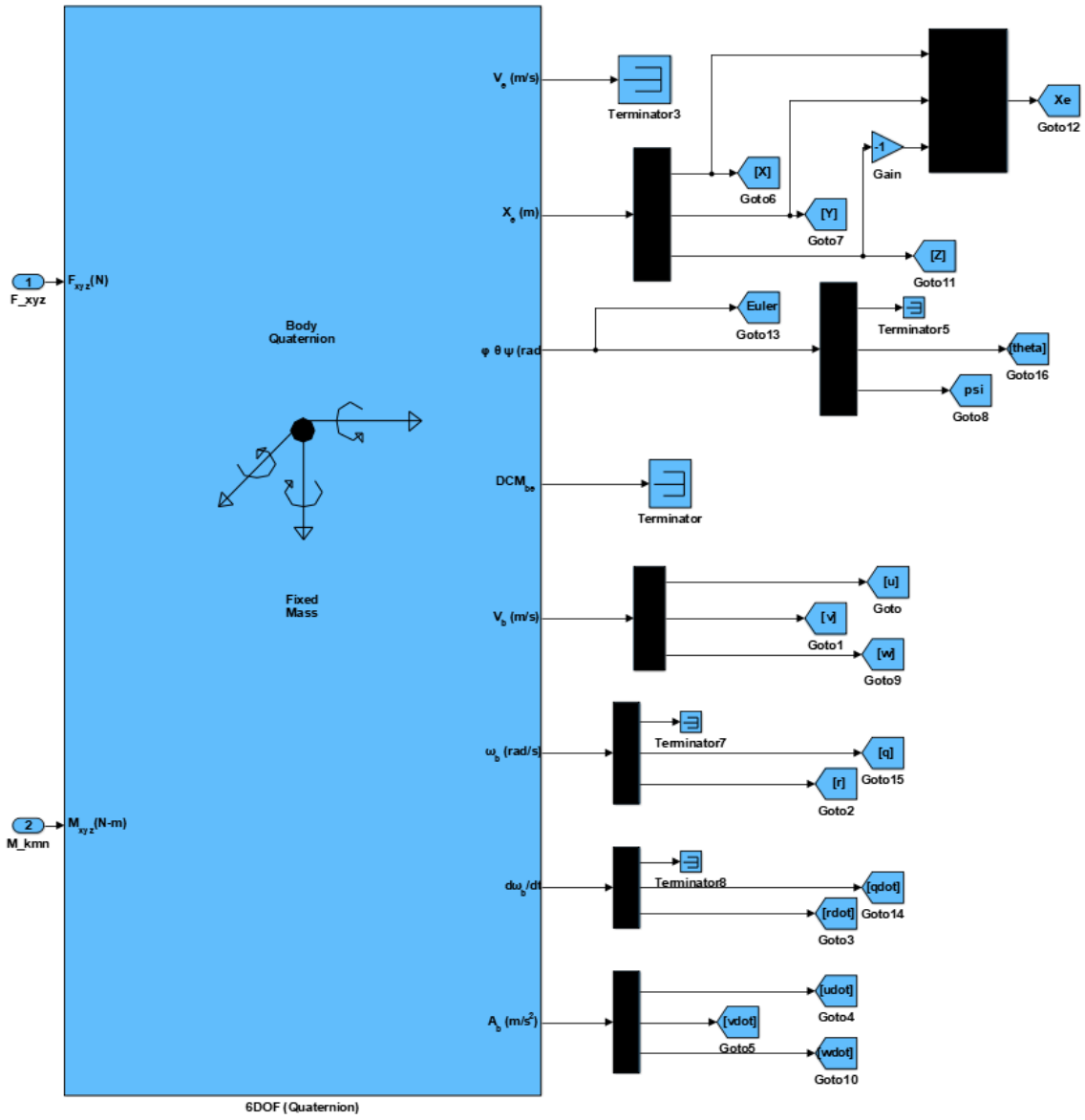

Figure 6.13. 6DOF Model Coordinate Transformation with Model Outputs Subsystem

CHAPTER 7:
6DOF Model Verification

The 6DOF hydrodynamic model verification was conducted through four separate experiments. These experiments where designed to provide a reference of the REMUS vehicle's behavior for comparison with the 6DOF model's behavior. The purpose of these experiments was to provide the same command inputs to the 6DOF model as was seen by the real world REMUS. By comparing the model's behavior with the REMUS vehicle's actual response, the model's fidelity was analyzed. These experiments are in no way a comprehensive verification of the 6DOF model, however the results do provide insight into the capabilities and limitations of the created model.

7.1 Surge Verification

The surge verification experiment was conducted by providing the propeller and rudder angle commands from two REMUS missions to the 6DOF model. The vehicle's speed, as recorded by the ADCP, was then compared to the model's speed. The results are seen in Figures 7.1 and 7.3 .

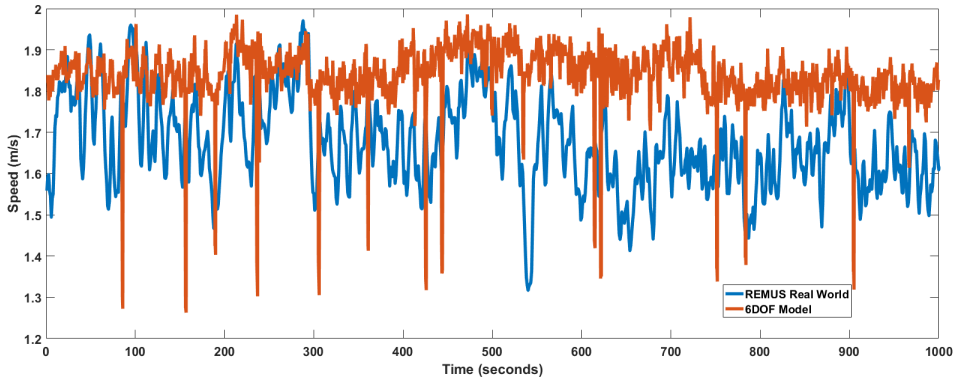

Figure 7.1. Speed of the 6DOF model vs. speed of the REMUS vehicle operating with CTTs and at various speeds

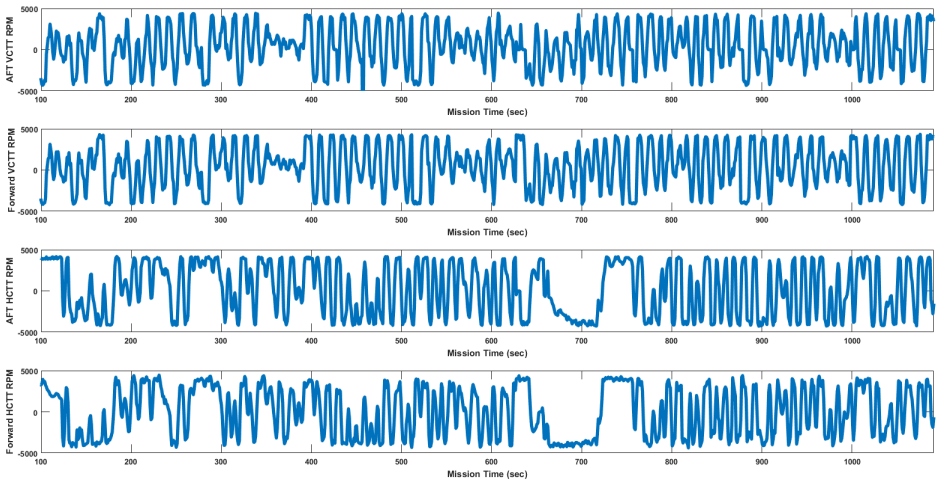

Figure 7.2. CTT RPMs During Surge Testing

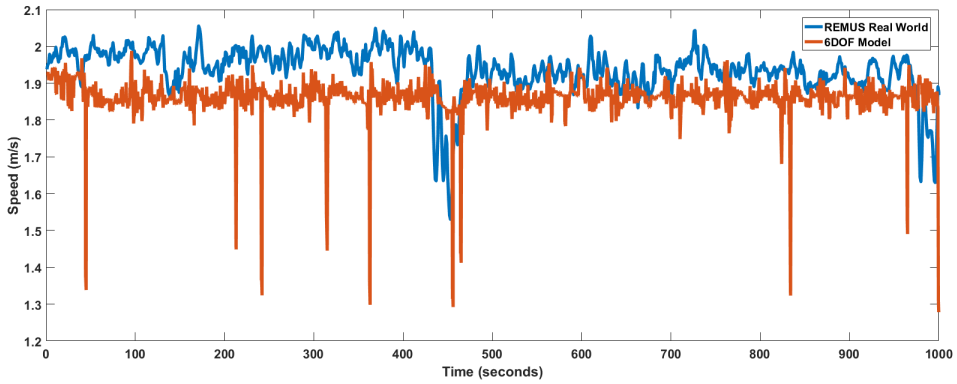

Figure 7.3. Speed of the 6DOF model vs. speed of the REMUS vehicle operating without CTTs and at various speeds

Figures 7.1 and 7.3 show that the mean speed of the model is approximately 4% to 9% higher or lower than the mean speed of the actual REMUS vehicle operating in Monterey Bay. One mission was conducted without CTTs activated and the other was conducted with CTTs activated. When considering that the currents seen by the REMUS vehicle were up to 4% of the vehicle's overall speed, the behavior of the model's speed is considerably accurate. A potential explanation for the speed discrepancy during the mission with CTTs enabled is that the CTTs created parasitic drag by increasing the turbulence around the REMUS vehicle,

possibly altering the coefficient of drag. The CTT RPMs during the CTT enabled mission is plotted in Figure 7.2. Both VCTTs and HCTTs were in operation at nearly maximum RPM, due to bang/bang control, for the entire mission. Constant CTT operation, along with altered fluid dynamic properties due to variations in the coefficient of drag, could explain why the REMUS vehicle's mean speed is slightly less (approximately 9 %) than the 6DOF model's speed for a CTT enabled mission. More testing and experimentation is needed to confirm this hypothesis.

7.2 Horizontal Cross-Tunnel Thruster/Yaw (Heading) Rate Verification

To verify the behavior of the CTTs in the horizontal plane the REMUS vehicle was ordered to maintain a certain depth with little to no movement. This maneuver is called a hover. While the vehicle maintained its hover at the specified depth, a differential thrust command was sent to the horizontal CTTs. This differential thrust induced a rotation in the horizontal plane. These same depth and differential thrust commands were also given to the 6DOF model. The heading of the actual vehicle and the model were compared and the results are illustrated in Figure 7.4.

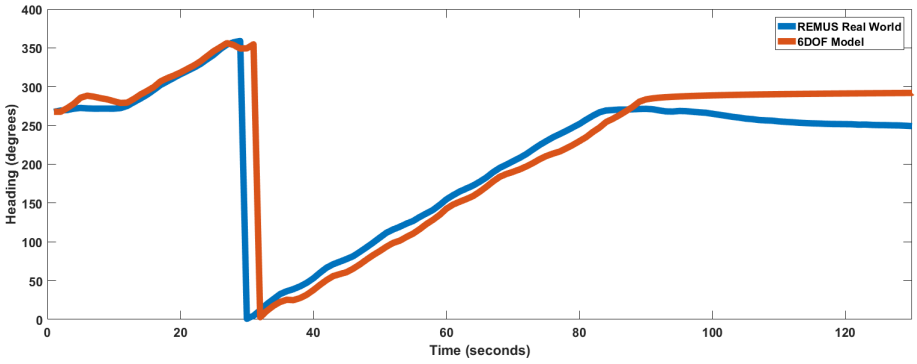

Figure 7.4. Heading of the 6DOF Model vs Heading of the REMUS Vehicle while performing a hover maneuver with differential commands being sent to the HCTTs

The model's yaw rate behavior is heavily influenced by the hydrodynamic coefficient $N_{r|r|}$. When $N_{r|r|}$ is properly estimated for the REMUS vehicle, an accurate yaw rate behavior is

witnessed, depicted in Figure 7.4.

7.3 Pitch Verification

The pitch of the vehicle during a mission is actively recorded. To verify the pitch behavior of the 6DOF model, the model was provided depth, propeller, and rudder commands from two REMUS missions in Monterey Bay. One mission was conducted without CTTs enabled and the other was conducted with CTTs enabled. Without CTTs, the REMUS vehicle's pitch has only one actuator input, its dive fin, for controlling pitch. With CTTs enabled, both REMUS and the 6DOF model have more control authority over the vehicle's pitch angle. When vertical CTTs are not activated, the vehicle has less control over its pitch. The pitch of the REMUS and the 6DOF model, over a 1000 second mission, can be seen in Figures 7.5 and 7.6.

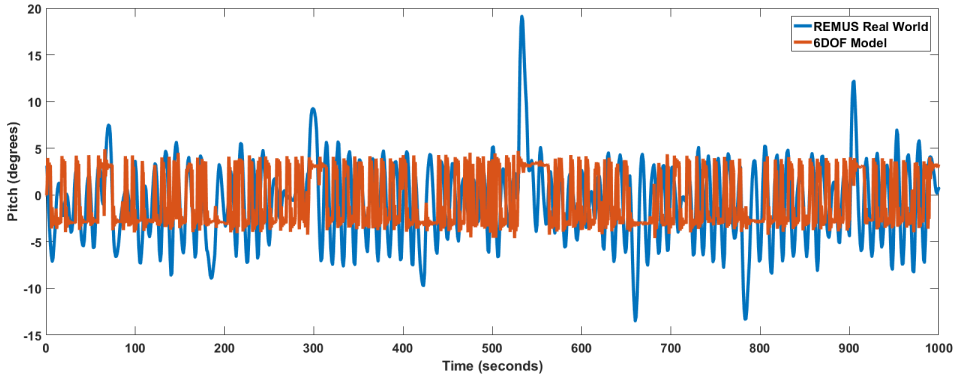

Figure 7.5. Pitch of the 6DOF Model vs. Pitch of the REMUS Vehicle Operating with CTTs and at Various Speeds

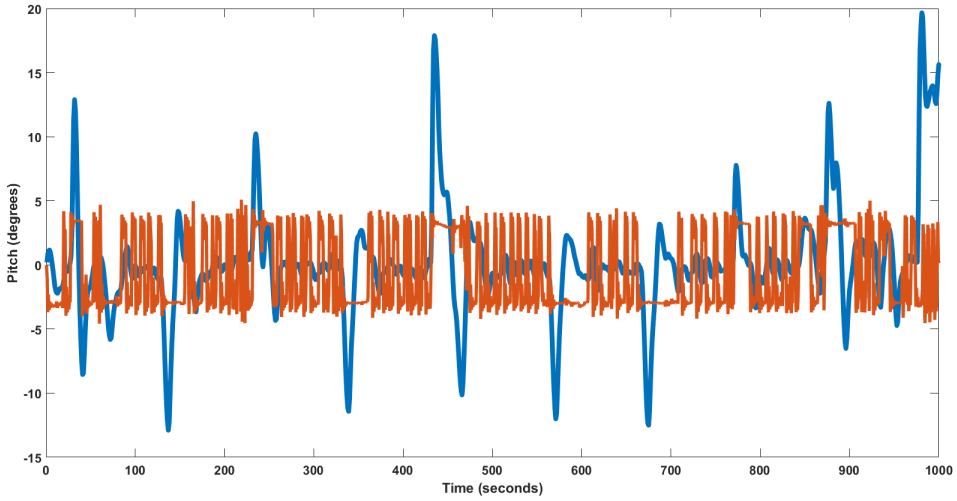

Figure 7.6. Pitch of the 6DOF Model vs. Pitch of the REMUS Vehicle Operating Without CTTs and at Various Speeds

The 6DOF model always had greater control authority over pitch than both real world REMUS missions. It is likely that this increased control authority over pitch is due to the assumption of benign environmental factors within the model and the assumptions made about vehicle configuration and trim. Nearly any environmental force acting in the Z-direction on the vehicle will induce a pitching moment increasing the pitch oscillation magnitude and frequency, especially if the force is variable. The model currently does not have the ability to model environmental factors, but environmental factors would have impacted the REMUS vehicle's pitch behavior while it was operating in Monterey Bay.

The assumptions about the modeled vehicle's weight distribution/payload, and the behavior of the actual REMUS vehicle's pitch controller (which is not modeled) are most likely the main causes of discrepancies in pitch behavior. The tuning of the real world REMUS's pitch controller will heavily influence the magnitude and frequency of pitch oscillations, as well as the pitch overshoot. Pitch overshoot is clearly seen in Figure 7.5. The overshoot magnitude in Figure 7.5 is almost three times the value of the normal magnitude of pitch oscillation. A possible explanation for this large overshoot is poor tuning of the pitch controller in the REMUS vehicle with CTTs disabled. The vehicles owned by the CAVR most likely had their pitch controllers tuned for CTT enable operations. The poor pitch

behavior witnessed in the CTT disabled mission may be a result of the REMUS vehicle's pitch controller not being tuned for a CTT disabled mission.

CHAPTER 8:
REMUS Controller Design

A 3DOF non-linear dynamical model was presented in Chapter 3 and a 6DOF non-linear dynamical model was presented in Chapter 5. With the development of these new models, the design of controllers for the simulated REMUS vehicle is now possible. The controllers presented in this thesis were designed to be robust and adaptable, while also simulating the behavior of the physical controllers in the actual REMUS vehicle.

8.1 Design Philosophy

The controllers for the 3DOF and 6DOF models where split into two separate depth control autopilots, the dive fin deflection controller and the VCTTs' controller (seen in Figures 8.1 and 8.2). The pair of controllers are combined to provide the global vehicle depth control system, illustrated in Figure 8.3. The actual REMUS vehicle utilizes relatively simple field-tuned Proportional Integral Derivative (PID) controllers [7]. PID controllers were therefore utilized in the simulated vehicle. PID tuning was performed on the model until the behavior of the modeled REMUS closely approximated the characteristic dive and thrust behaviors of the actual vehicle.

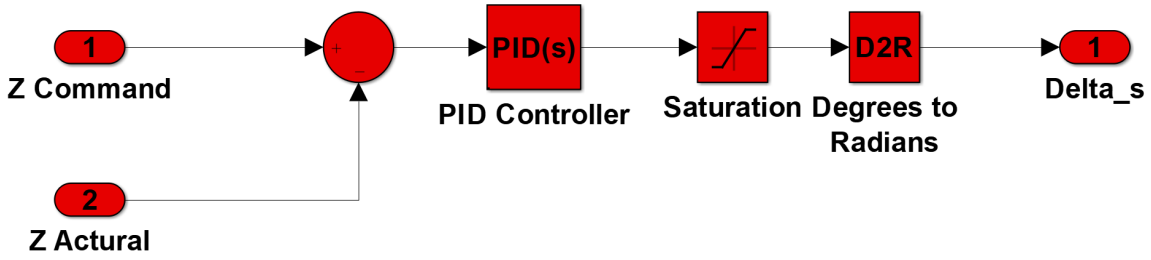

Figure 8.1. Dive Fin Deflection Controller in REMUS Models

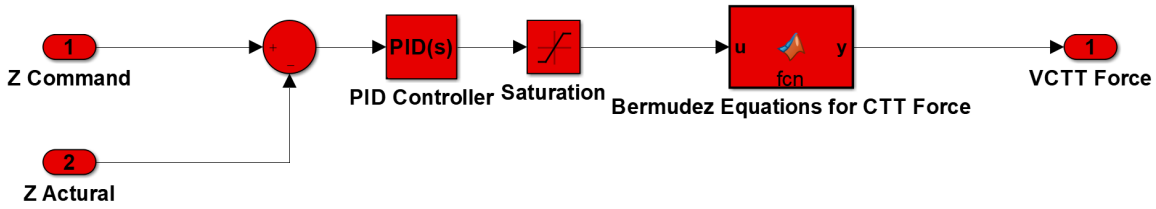

Figure 8.2. VCTTs' Controller in REMUS Models

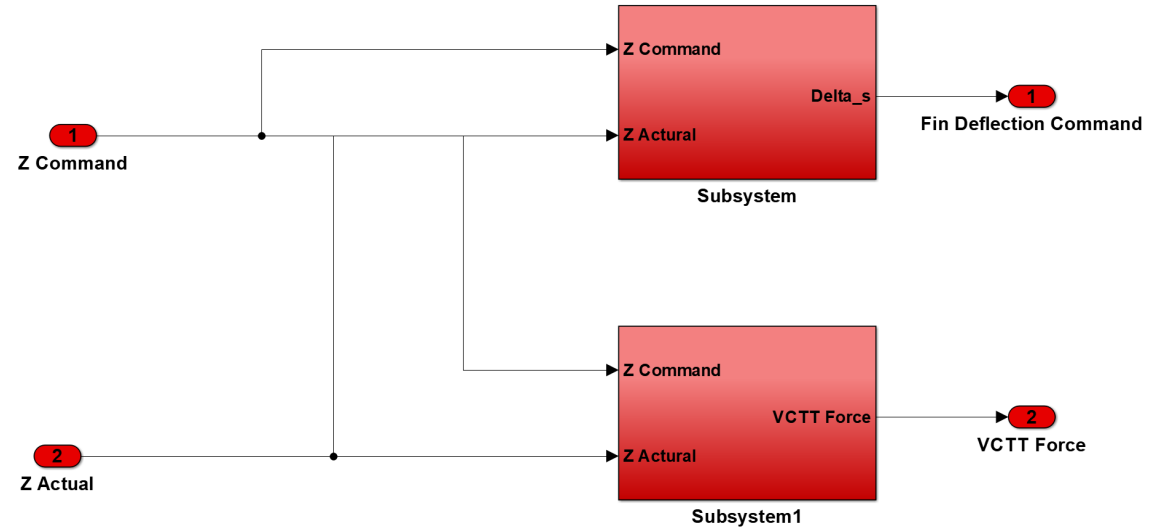

Figure 8.3. Combined Depth Controller in REMUS Models

8.2 PID Control

PID control is a classic control technique that provides a simple yet elegant method of controlling a dynamic system's behavior through feedback. A PID controller reacts to the error between the input/command signal and a desired output signal. PID controllers have three elements, the proportional element (P), the integral element (I), and the derivative element (D). A PID controller can be represented by the following equation:

$$K_P + K_I \int e dt + K_D \frac{de}{dt} \tag{8.1}$$

Where e is the tracking error for the system and K_P, K_I, and K_D are the proportional, integral, and derivative gains of the controller. According to [7], K_P handles immediate

error and its magnitude impacts rise time and steady state error. K_I impacts how well the controller can "learn" from past behavior. Increasing its magnitude can significantly reduce steady state error and lower rise time but can increase overshoot and introduce oscillations into the transient response of the system. K_D affects the system's "anticipation" of future errors. Increasing the magnitude of K_D typically increases the system's stability and dampens overshoot and oscillation during its transient response. K_P, K_I, and K_D are all highly interactive, and altering one gain can have a significant impact on the efficiency of the other gains. While automated procedures for tuning PID controllers do exist and were attempted while tuning the controllers in the 3DOF and 6DOF models, the best results for modeled vehicle behavior were found when models' controllers were field tuned to represent behaviors seen in actual REMUS missions.

8.3 Tuning of the Simulated PID Controllers

The model's PID depth controller was tuned to produce simulated vehicle behavior that was comparable to the actual REMUS depth control performance. The tuning procedure was similar to field-tuning the PID gains on the actual REMUS vehicle. First, the proportional gain, K_P, was tuned to provide a similar response time as seen in the real world. Next, the integral gain, K_I, was tuned to insure the proper offset between command depth and actual depth. Finally, the derivative gain, K_D, was tuned to remove any oscillations that the controller induced in the system's behavior.

Table 8.1. Depth Controller Gains Used in the 3DOF and 6DOF Models for Dive Fin Controller

Gain	Value
K_P	-800
K_I	1
K_D	2

Table 8.2. Depth Controller Gains Used in the 3DOF and 6DOF Models for VCTT Controller

Gain	Value
K_P	800
K_I	2.5
K_D	15.1

The values for the gains listed in Tables 8.1 and 8.2 were tuned and selected by constant experimentation and comparison between the models' behavior and the REMUS vehicle's behavior. Gains for the actual REMUS vehicle's depth controller are field tuned in much the same manner in an effort to provide the desired vehicle behavior during its programmed missions. The REMUS vehicles' controllers are field tuned by Kongsberg, the manufacturer.

CHAPTER 9:
Behavior and Significance of the Coefficient of Drag (Cd)

During the creation of the 3DOF model presented in this thesis, the Coefficient of Drag (Cd) significantly impacted the values of many other hydrodynamic coefficients. As the speed of a vehicle changes, Cd depends greatly on the size and speed of the vehicle in question. To create an accurate model of the REMUS vehicle, or any underwater vehicle, the value of Cd at various operating speeds must be known. Numerous calculations and verification through field testing in Monterey Bay, however, revealed that the Cd of the REMUS vehicle could be approximated as a constant value over almost the entire range of REMUS operating speeds. This realization significantly reduced the computational burden of a variable speed hydrodynamic model. This chapter provides a justification for this simplification, and suggests when this simplification is accurate (and appropriate) for use in the development of a variable speed model for an underwater vehicle.

9.1 Behavior of the Coefficient

It is known that the Coefficient of Drag, Cd, changes drastically with speed if the flow around the body is laminar. However, if the flow around the body of interest is turbulent, the coefficient of drag is relatively constant for nearly all speeds. This behavior can be seen in Figure 9.1.

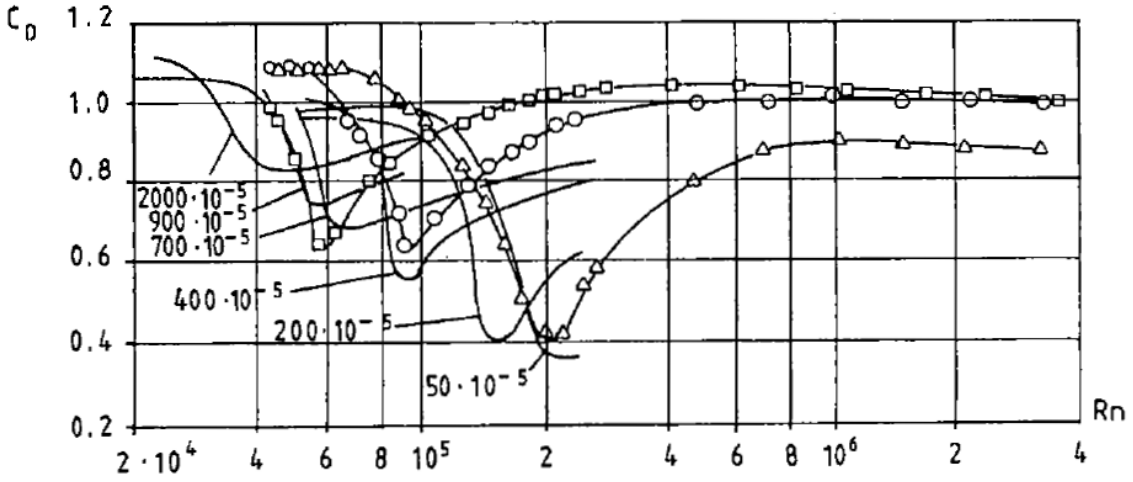

Figure 9.1. Drag Coefficient Cd of Rough Circular Cylinders in Steady Incident Flow for Different Surface Roughness Values k/D (k=Average Height of Surface Roughness, D=Cylinder Diameter, $Rn = U_\infty D/v$, U_∞=Incident Flow Velocity.) Triangle, $k/D = 110 * 10^{-5}$; Circle, $k/D = 450 * 10^{-5}$; Square, $k/D = 900 * 10^{-5}$; Line. Source: [17].

Previous research on the REMUS vehicle found the Cd at a nominal operating velocity of approximately 1.5 m/s. This Cd was used in many single speed models and proved to be accurate at simulating the hydrodynamic behavior of the REMUS at around 1.5 m/s. However, to build an accurate variable speed hydrodynamic model of the REMUS vehicle that can simulate low speed docking, the Cd over an entire spectrum of operating speeds must be known. The first step in understanding the behavior of the Cd for the REMUS vehicle was determining the speed at which flow over the vehicle transitions from laminar to turbulent. Reynolds number can be calculated using equation 9.1, as described in [13].

$$Re = \frac{\rho |U| D}{\mu} \tag{9.1}$$

After computing this parameter, Table 9.1 and Figure 9.1 can be used to determine the speed at which the flow on the REMUS vehicle is turbulent "enough" to assume Cd is constant. A Reynolds number of approximately 40,000 is the threshold where the REMUS vehicle is operating in the turbulent region.

Table 9.1. Behavior of Water in Certain Reynolds Number Regimes. Adapted from: [2], [13].

Re Range	Behavior
$0 < Re < 1$	Highly viscous laminar creeping motion
$1 < Re < 100$	Laminar, strong Reynolds number dependence
$100 < Re < 10^3$	Laminar, boundary layer theory useful
$10^3 < Re < 10^4$	Transition to turbulence
$10^4 < Re < 10^5$	Turbulent, moderate Reynolds number dependence
$10^5 < Re < \infty$	Turbulent, slight Reynolds number dependence

The fluid interaction area has a significant impact on the Reynolds number. For the Reynolds number calculations seen in Chapter 2, the fluid interaction area was conservatively chosen to be the smallest area exposed in any body plane, which is the REMUS nose surface area that has a characteristic diameter of 0.190492 m. Even when using the most conservative fluid interaction area for the Reynolds number calculations, it was found that the flow over the REMUS vehicle remained turbulent until the vehicle's speed dropped below 0.3 m/s.

9.2 Suggestions for Model Development

To find the critical velocity, $|T|(m/s)$, of an AUV with a certain diameter $D(meters)$ the following equation can be used,

$$|T|(m/s) = [0.054757(m^2/s)]/[D(meters)] \tag{9.2}$$

This equation was developed during this research by manipulating the coefficient of drag equation and assuming a Re of greater than 4000. The equation is provided for a quick reference for future researchers.

The critical velocity for the REMUS vehicle with D=0.190492 m is,

$$|T| = 0.288196m/s \tag{9.3}$$

It is reasonable to assume that even while operating with CTTs, the REMUS is almost exclusively operating in the turbulent region. The experiments conducted with the 3DOF and 6DOF models, which utilized a constant Cd, and the data collected from the REMUS vehicle operating in the field, validated this assumption. Most torpedo shaped AUV's will not be operating with CTTs. To maintain controllability of these AUVs, a minimum speed is required to ensure adequate fluid flow over their control surfaces. If a majority of torpedo shaped AUVs require at least a 0.5 m/s forward velocity to maintain controllability, the AUV diameter at which laminar flow is possible while operating at 0.5 m/s is about 11 centimeters. Therefore, there is a strong argument to be made that the Cd for nearly all torpedo-shaped AUVs can be assumed to be constant across their range of operational speeds. This realization is valuable for any person creating or designing a hydrodynamic model of an AUV operating at various speeds. Also, more research is required to fully understand the impact of operating at very low speeds, where flow over the vehicle may be laminar and Cd can no longer be assumed as constant.

CHAPTER 10:
Conclusion and Future Work

10.1 Conclusion

> All models are wrong, but some are useful.
>
> -George E. P. Box

This research was sparked by the problem of autonomously docking an AUV. To simulate and predict the behavior of a REMUS vehicle when reducing speed and utilizing CTTs, 3DOF and 6DOF hydrodynamic models were developed. These models were then programmed and analyzed using Simulink and were tested and verified against real world REMUS missions conducted in Monterey Bay.

Both the 3DOF and 6DOF models provided "useful" models of the vehicle's behavior. The assumptions made in these models do not impact their fidelity dramatically and allow for a simulated prediction of the REMUS vehicle's behavior in the field. With the development of these models, a better understanding of the capabilities of a REMUS vehicle with CTTs has been accomplished. The models can simulate a REMUS vehicle's maneuvering behavior while using CTTs during docking missions, simulate the vehicle's depth control, simulate the vehicle's maneuverability at various propeller RPM, and can be consulted when designing future REMUS docking stations.

There were other unintended findings when developing the 3DOF and 6DOF models. The Cd was calculated and analyzed over the entire range of REMUS velocities. This study came to the conclusion that Cd of a REMUS vehicle can be assumed to be constant over nearly all the operational speeds. The creation of the models also provided the insight and catalyst for creating the pitch behavior parameter, M_{PB}. This parameter insures that the righting force acting in the pitch direction is always large enough to stabilize the vehicle's pitch behavior. Observation in the field of the REMUS vehicle strongly supports the argument that there is a strong righting force due to the moment arm created by the center of gravity and center of buoyancy.

Unexplored hydrodynamic phenomenons were also uncovered during the verification process. The suspected reduction of vehicle velocity when operating CTTs due to parasitic drag is worthy of further study. More analysis and comparison between the model and the REMUS vehicle's behavior can further justify that this phenomenon exists. Also tow tank analysis and computational fluid dynamics may provide a more concrete explanation for this parasitic drag witnessed in the initial comparisons between the model and the REMUS vehicle.

10.2 Future Work

The following goals can be pursued in future work:

1. Calculation and verification of the minor coefficients used in the models need to be further analyzed. A more in-depth study of these coefficients may uncover further phenomenon and create a higher fidelity model of an AUV.
2. Further development of a model that can accept environmental inputs such as wave action and currents will provide a needed capability for critiquing the feasibility of certain missions. Currents for a real world Monterey Bay mission are seen in Figure 10.1. The currents in Monterey Bay during the experiments were minimal, however their impact on the vehicle was still significant. Modeling and implementing environmental conditions would be a significant improvement in providing a higher fidelity and "useful" model.
3. Revising the design and implementation of controllers to minimize the REMUS vehicle's behavioral errors, such as the errors witnessed during the initialization period of the 3DOF model, would increase the model's fidelity. A model that does not have this initialization period would provide a more accurate and faster prediction of the vehicle's behavior, which would make it a better candidate for model based adaptive control.
4. Integration of the 6DOF model into the REMUS vehicle's secondary controller could provide a faster than real-time model to the controller, which may open more control options and provide an opportunity to test optimal trajectories prior to the execution of a maneuver.
5. Development of a waypoint controller for the 6DOF model has already begun. Figure 10.3 shows a mock waypoint mission, which utilized the 6DOF model developed in

this research interacting with a Latitude, Longitude, and Altitude controller, illustrated in Figure 10.2. This waypoint mission program was created to provide a top level mission simulation that accepted latitude, logitude, and depth commands and output overall vehicle behavior in the LLA reference frame. Model output is portrayed in Figures 10.4 and 10.5. This output allows for mission planning in LLA coordinates. The program provided a simulation of the vehicle's trajectory in the mission area and an approximate time of completion for the mission. The actual REMUS also is programmed to achieve waypoints geolocated by latitude and longitude. Futhering this LLA capability and waypoint controller will provide useful tools for overall mission planning and asset allocation considerations.

6. Implementation of a neural network into the 6DOF model to learn and predict the REMUS vehicle's behavior and to adjust coefficients for different payloads may provide a higher fidelity model for more than one vehicles' configuration.

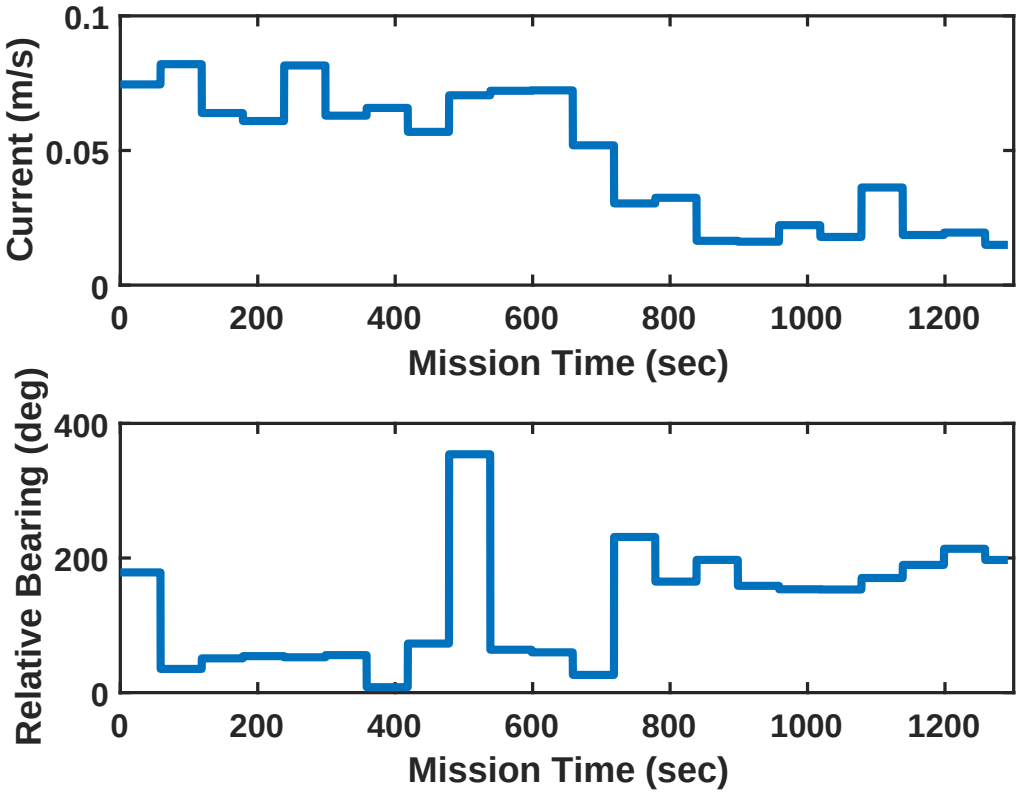

Figure 10.1. ADCP Estimated Currents During a REMUS Mission

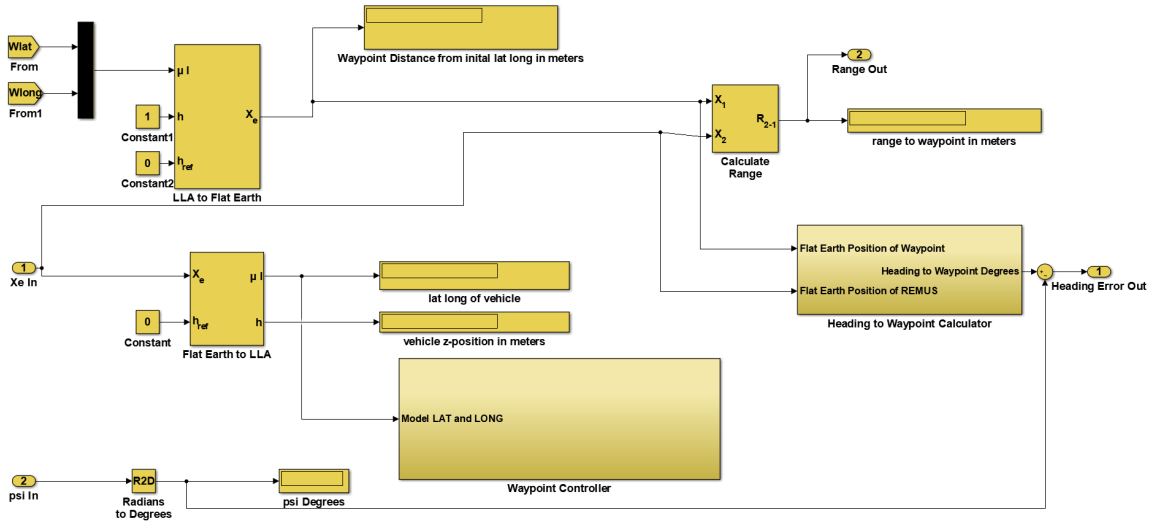

Figure 10.2. LLA Waypoint Program For Enhanced Use Of 6DOF Model

Figure 10.3. Four Navigational LLA Waypoints Given To Enhanced 6DOF Model

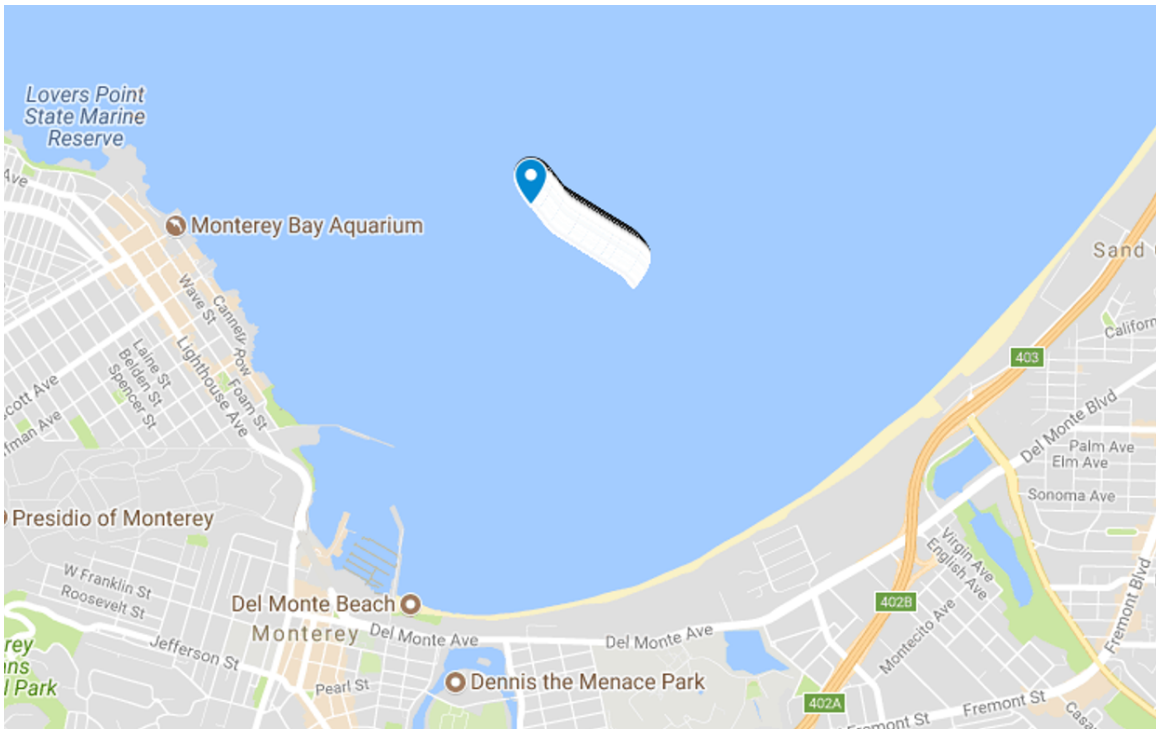

Figure 10.4. Modeled REMUS Vehicle's Path Through the Mission Environment

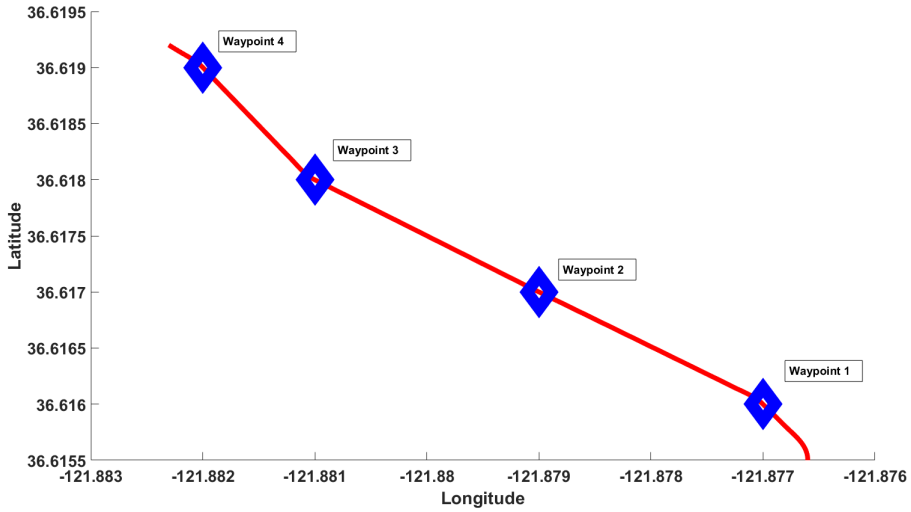

Figure 10.5. Plot of the Vehicle's and Waypoint's Latitude and Longitude

THIS PAGE INTENTIONALLY LEFT BLANK

APPENDIX: Important Values

A.1 Vehicle Parameters

Table A.1. Vehicle Parameters

Vehicle Parameter	Value	Units
Weight (W)	52.5	kg
Buoyancy (B)	55.8362	N
Length (L)	2.26	m
Hull Frontal Area (A_f)	$2.85 * 10^{-2}$	m^2
Hull Projected Area (A_p)	0.430512	m^2
Diameter of REMUS (D)	0.190492	m
Fin Taper Ratio (t)	0.654	
Fin Platform Area (S_fin)	$6.65 * 10^{-3}$	m^2
Moment Arm ($x_{finpost}$) [3]	-1.0475	m
Fin Lift Slope ($c_L\alpha$)	3.12	
Pitch Behavior Parameter (M_{PB})	50	

A.2 Environmental Variables

Table A.2. Environmental Variables

Environmental Parameter	Value	Units
Sea Water Density(ρ)	1030	kg/m^3
Sea Water Viscosity (μ)[4]	0.00141	$kg/(m \cdot s)$

[1]Origin at Center of Buoyancy (CB)
[2]At 10°C

A.3 Vehicle Hydrodynamic Coefficients

Table A.3. 3DOF REMUS Model-Vehicle's Hydrodynamic Coefficients

Vehicle Hydrodynamic Coefficients	Value	Units
$X_{u\|u\|}$	-12.4759	$\frac{kg}{m}$
$X_{\dot{u}}$	-0.930	kg
Z_{uw}	-28.6	$\frac{kg}{m}$
$Z_{w\|w\|}$	-185.621	$\frac{kg}{m}$
$Z_{uu\delta_s}$	-21.37	$\frac{kg}{m \cdot rad}$
$M_{\dot{w}}$	-4.16	$kg \cdot m$
M_{uw}	24.0	kg
M_{uq}	-10.00	$\frac{kg \cdot m}{rad}$
$M_{w\|w\|}$	4.00357	kg
$M_{uu\delta_s}$	-22.3855	$\frac{kg}{rad}$

Table A.4. 6DOF REMUS Model-Vehicle's XYZ Hydrodynamic Coefficients

Vehicle Hydrodynamic Coefficients	Value	Units
$X_{u\|u\|}$	-12.4759	$\frac{kg}{m}$
$X_{\dot{u}}$	-0.930	kg
X_{wq}	-77.8	$\frac{kg}{rad}$
X_{qq}	-1.93	$\frac{kg \cdot m}{rad}$
X_{vr}	35.5	$\frac{kg}{rad}$
X_{rr}	-1.93	$\frac{kg \cdot m}{rad}$
Y_{uv}	-28.6	$\frac{kg}{m}$
$Y_{v\|v\|}$	-2850	$\frac{kg}{m}$
$Y_{r\|r\|}$	0.632	$\frac{kg \cdot m}{rad^2}$
$Y_{\dot{v}}$	-77.8	kg
$Y_{\dot{r}}$	4.16	$\frac{kg \cdot m}{rad}$
Y_{ur}	5.22	$\frac{kg}{rad}$
$Y_{uu\delta_r}$	9.64	$\frac{kg}{m \cdot rad}$
$Z_{\dot{w}}$	-77.8	kg
$Z_{\dot{q}}$	-4.16	$\frac{kg \cdot m}{rad}$
Z_{uq}	-12.22	$\frac{kg}{rad}$
$Z_{q\|q\|}$	-0.632	$\frac{kg \cdot m}{rad^2}$
Z_{uw}	-28.6	$\frac{kg}{m}$
$Z_{w\|w\|}$	-185.621	$\frac{kg}{m}$
$Z_{uu\delta_s}$	-21.37	$\frac{kg}{m \cdot rad}$

Table A.5. 6DOF REMUS Model-Vehicle's MN Hydrodynamic Coefficients

Vehicle Hydrodynamic Coefficients	Value	Units
$M_{\dot{q}}$	-30	$\frac{kg \cdot m^2}{rad}$
$M_{q\|q\|}$	-188	$\frac{kg \cdot m^2}{rad^2}$
$M_{\dot{w}}$	-4.16	$kg \cdot m$
M_{uw}	24.0	kg
M_{uq}	-10.00	$\frac{kg \cdot m}{rad}$
$M_{w\|w\|}$	3.18	kg
$M_{uu\delta_s}$	-22.3855	$\frac{kg}{rad}$
$N_{\dot{v}}$	4.16	$kg \cdot m$
$N_{\dot{r}}$	4.88	$\frac{kg \cdot m^2}{rad}$
N_{uv}	-24	kg
N_{ur}	-2	$\frac{kg \cdot m}{rad}$
$N_{v\|v\|}$	-3.18	kg
$N_{r\|r\|}$	-245	$\frac{kg \cdot m^2}{rad^2}$
$N_{uu\delta_r}$	-22.3855	$\frac{kg}{rad}$

List of References

[1] E. B. Bermudez, "Terminal homing for autonomous underwater vehicle docking," Master's thesis, Dept. Mech. Eng., NPS, Monterey, CA, 2016.

[2] T. I. Fossen, *Marine Control Systems: Guidance, Navigation and Control of Ships, Rigs and Underwater Vehicles*, 1st ed. Thondheim, Norway: Marine Cybernetics, 2002.

[3] A. Palmer, G. E. Hearn, and P. Stevenson, "Modelling tunnel thrusters for autonomous underwater vehicles," *IFAC Proceedings Volumes*, vol. 41, no. 1, pp. 91–96, 2008.

[4] A. J. Healey, S. Rock, S. Cody, D. Miles, and J. Brown, "Toward an improved understanding of thruster dynamics for underwater vehicles," in *Autonomous Underwater Vehicle Technology, 1994. AUV'94., Proceedings of the 1994 Symposium on*. IEEE, 1994, pp. 340–352.

[5] X. Chen, D. Marco, S. Smith, E. An, K. Ganesan, and T. Healey, "6 DOF nonlinear AUV simulation toolbox," in *OCEANS'97. MTS/IEEE Conference Proceedings*. IEEE, 1997, vol. 2, pp. 1070–1074.

[6] D. Brutzman, T. Healey, D. Marco, and B. McGhee, "The phoenix autonomous underwater vehicle," in *AI-Based Mobile Robots*, 1st ed. Cambridge, MA: MIT/AAAI Press, 1998.

[7] T. T. J. Prestero, "Verification of a six-degree of freedom simulation model for the remus autonomous underwater vehicle," Master's thesis, Dept. Mech. Eng. and Ocean Eng., MIT, Cambridge, MA, 2001.

[8] D. E. Sgarioto, "Control system design and development for the REMUS autonomous underwater vehicle," Defence Technology Agency, Aukland, New Zealand, Tech. Rep., 2007.

[9] S. M. Doherty, "Cross body thruster control and modeling of a body of revolution autonomous underwater vehicle," Master's thesis, Dept. Mech. Eng., NPS, Monterey, CA, 2011.

[10] M. Blanke, K.-P. Lindegaard, and T. I. Fossen, "Dynamic model for thrust generation of marine propellers," *IFAC Proceedings Volumes*, vol. 33, no. 21, pp. 353–358, 2000.

[11] J. Carlton, *Marine Propellers and Propulsion*, 2nd ed. Waltham, Massachusetts: Butterworth-Heinemann, 2012.

[12] D. B. Marco and A. J. Healey, "Command, control, and navigation experimental results with the NPS ARIES AUV," *IEEE Journal of Oceanic Engineering*, vol. 26, no. 4, pp. 466–476, 2001.

[13] F. M. White, *Fluid Mechanics*, 7th ed. New York, NY: McGraw-Hill, 2011.

[14] L. F. Whicker and L. F. Fehlner, "Free-stream characteristics of a family of low-aspect-ratio, all-movable control surfaces for application to ship design," DTIC Document, Washington, DC, Tech. Rep., 1958.

[15] S. F. Hoerner, *Fluid-Dynamic Drag: Practical Information on Aerodynamic Drag and Hydrodynamic Resistance*, 1st ed. Midland Park, NJ: Hoerner Fluid Dynamics, 1965.

[16] S. W. Moore, H. Bohm, and V. Jensen, *Underwater Robotics: Science, Design & Fabrication*, 1st ed. Monterey, CA: Marine Advanced Technology Education (MATE) Center, 2010.

[17] O. Faltinsen, *Sea Loads on Ships and Offshore Structures*, 1st ed. New York, NY: Cambridge University Press, 1993, vol. 1.

Initial Distribution List

1. Defense Technical Information Center
   Ft. Belvoir, Virginia

2. Dudley Knox Library
   Naval Postgraduate School
   Monterey, California